Finite element modelling and experimental measurement of the mechanical properties of Nb_3Sn multi-filamentary composite superconducting wires

By

David Alan Harvey

A thesis submitted in partial fulfilment of the requirements of Oxford Brookes University for the degree of Doctor of Philosophy

June 2009

For my children,

Oliver and Lydia

Abstract

The most common superconductors used in medium and high field superconducting magnets are Nb_3Sn multi-filamentary composite wires. The mechanical properties of these wires can have a strong bearing on the capabilities of the magnets because their superconducting properties are strongly dependent on the strain state within the Nb_3Sn. The wires can be subjected to high levels of mechanical stress during fabrication and when the magnet is energised. The effect that this stress has on the Nb_3Sn strain state is dependent on the stress-strain behaviour of the wires.

A tensile testing procedure was developed and extensive measurements of stress-strain curves of particular superconducting wire were made at room temperature and 77 K. The effect of the reaction heat-treatment process on the stress-strain behaviour was investigated and this showed that it would not be possible to improve the mechanical properties, while at the same time maintaining satisfactory superconducting properties, by optimisation of the heat-treatment duration. The heat-treatment process changes the physical dimensions of wires and this can influence the stress and strain that the wires experience. A study of these dimensional changes was made and the implications were discussed.

Another part of the research was the development of a finite element model to predict the stress-strain behaviour of Nb_3Sn multi-filamentary composite wire. Considerable attention was paid to the accurate representation of the constituent material properties. A very good match between the F. E. and experimental results was obtained, although a number of aspects of the model remain uncertain. To provide further experimental data to validate the F. E. model, a novel experimental procedure was developed. This involved reducing the diameter of wires by etching in acid and measuring the effect on axial strain and stress-strain behaviour. This provided data that was directly related to the material within separate radial zones within the wire cross-section. Axial residual stresses were obtained as well as stress-strain curves for the material within the individual radial zones. In general, the results showed that the F. E. model provides a good representation of the wire.

Acknowledgements

EPSRC (Engineering and Physical Sciences Research Council) for funding the research.

The industrial partner, Oxford Instruments Superconductivity Ltd., for funding the research, supplying materials and giving direction.

I would like to thank my supervisors Dr Neil Fellows and Dr John Durodola for their support during the project and especially for their trust in allowing me to guide the direction myself.

I am eternally grateful to laboratory wizard Michael Hartman for his invaluable help and guidance in all the practical areas of the project. I would also like to thank fellow students Memo and Popo (otherwise known as Guillermo Urriolagoitia-Sosa and Adolfo Lopez-Castro) for training me how to use Ansys and helping me around its idiosyncrasies.

My greatest thanks are reserved for my friends at the university who made my time there an enjoyable experience. These include Mike, Memo and Popo as well as Jeff (Jean-Francois Jouin) and Shpend Gerguri. I will always remember our regular coffee meetings and the happy days playing squash and chess.

Last, but not least, I would like to thank my wife, Gom, for allowing all this.

TABLE OF CONTENTS

List of figures

List of tables

CHAPTER 1

Introduction

1.1 Introduction

Many of the world's most technologically advanced machines, such as MRI body scanners, nuclear fusion reactors and magnetic levitation trains, have superconducting magnets at their heart. These machines all utilise the high magnetic fields that can be generated by superconducting magnets, typically 1000 times higher than generated by normal electromagnets of similar size. Superconducting magnets are similar in construction to normal electromagnets, except instead of the windings being made from copper wire, they are wound with a superconducting material, usually in the form of a multi-filamentary composite wire. This wire can experience high levels of mechanical stress during fabrication and operation of the magnet. The mechanical properties of the wire will have a strong bearing on the level of this stress and on the associated strain. The stress and strain in the wire strongly affects the superconducting current carrying capacity and therefore the magnetic field that the magnet is able to generate. Thus, the mechanical properties can have a strong bearing on a superconducting magnet's capabilities. Until recently, however, the majority of research has been focussed on improving the superconducting properties of wires without much consideration of the mechanical properties. With the development of evermore larger and powerful superconducting magnets, the need has increased for accurate data on the mechanical properties as well as understanding about how these properties are affected by wire structure and manufacture.

This thesis presents comprehensive experimental data of the mechanical properties of one particular superconducting wire and how they vary with heat-treatment, and also a

finite element model of the wire for modelling the mechanical properties. The F. E. model is validated against a range of experimental data.

1.2 Aims and objectives of the thesis

Obtaining accurate measurements of the mechanical properties of superconducting wires (primarily elastic modulus, yield strength and stress-strain curve) presents a considerable experimental challenge. The difficulties are explained in detail in Chapter 5, but are mostly a result of the small diameter of superconducting wires (typically 0.4 to 1.5mm) and the requirement of testing at cryogenic temperatures. One aim of this thesis is to present an experimental method for the accurate measurement of the mechanical properties of superconducting wires at room temperature and 77 K. The method will be used to produce a comprehensive set of data for the mechanical properties of the particular superconducting wire investigated for this thesis.

A key stage of Nb_3Sn superconducting wire manufacture is the reaction heat-treatment process, which converts the niobium filaments into the Nb_3Sn compound. This reaction heat-treatment process is generally optimised to obtain the best possible superconducting properties. The effect on the mechanical properties, however, is not well documented in the literature. Therefore, another aim is to investigate the effect of the heat-treatment process on the mechanical properties. The heat-treatment process also causes the dimensions of superconducting wires to change. These dimensional changes will affect the stresses acting on the wires as the heat-treatment process

generally takes place after the wire is wound onto the magnet former. Another aim of the thesis is investigate the effect of the heat-treatment on wire dimensions.

Modelling techniques are often used in the design and development of superconducting magnets and superconducting wires. There is considerable difficulty in producing accurate models, however. One problem is that there is uncertainty about the material properties of the constituent materials. This is partly because it is necessary to know the properties over a wide temperature range, from the heat-treatment temperature of around 1000 K down to the magnet operating temperature of 4 K. Materials data over such a temperature range is generally very scarce. Also, the geometric constraints of the wire structure, which limits the grain size, and the extensive drawing operations of the manufacturing process mean that the constituent materials may not exist in the same form outside of the composite wire. Material testing is therefore very difficult. Another modelling problem is the complexity of the structure of the multi-filamentary composite wires. It is common for the number of filaments within wires to be tens of thousands or even more. To produce a finite element mesh to accurately represent such geometries would require such large numbers of elements that computational run times would be far beyond anything practical. Another problem has been the lack of reliable experimental data of mechanical properties with which to validate models. An aim of this thesis is to develop a finite element model of a superconducting wire and to validate it against the experimental measurements.

1.3 Outline of thesis

The thesis is divided into 8 chapters, the contents of which can be summarised as follows:

Chapter 2 presents background on the subject matter of the research and a detailed literature review. The background section begins with the discovery of superconductivity and the development of practical superconductors and goes on to describe the fabrication of Nb_3Sn multi-filamentary composite superconductors and the various applications of superconducting magnets. The literature review begins with the discovery that stress-strain state of Nb_3Sn superconductors has a significant influence on their superconducting properties. The influence on the superconducting properties of the thermal residual strain of the Nb_3Sn filaments resulting from cooling superconducting wires down from the heat-treatment temperature was another subject surveyed. Tensile testing methods and results were also subjects reviewed, as were the composition and material properties of the constituent materials. Finally, a detailed review of modelling of the mechanical properties of superconductors is presented.

Chapter 3 explains the reaction heat-treatment process and describes the apparatus and method used to heat-treat superconducting wire specimens used in the experimental part of the research. The range of different heat-treatments carried out is also detailed.

Chapter 4 is concerned with the dimensional changes in superconducting wires resulting from the reaction heat-treatment process. The causes and effects of these dimensional changes are discussed, the measurement methods are described and the results are presented.

Chapter 5 describes some of the problems associated with tensile testing superconducting wires as well as the apparatus and method used in this research. The data analysis techniques used are also described. The room temperature and 77 K tensile test results for wire specimens given a range of different heat-treatments are then presented and discussed. The effect of the strain rate used in the tensile tests and the effect of the cooling rate at the end of the heat-treatment process are also investigated in this chapter.

Chapter 6 presents the finite element modelling work undertaken to model the mechanical properties of the superconducting wire. A large part of the chapter is devoted to presenting the properties of the constituent materials used in the model and their sources. Where there are uncertainties about the material properties, these are discussed. The results of the F. E. modelling are presented and compared with the experimental results. The sensitivity of the model to the main uncertainties is investigated. Finally, the model is used to predict the thermal residual stresses in the constituent materials and to evaluate the evolution of stresses within them as axial strain is applied to the wire.

Chapter 7 describes a novel experimental method to measure thermal residual stresses, properties of the constituent materials and to provide more experimental data with which to validate the F. E. model presented in Chapter 6. The method involves etching concentric layers of material from the outside of superconducting wire specimens, measuring the axial strain that results from a redistribution of residual stresses and measuring the change in stress-strain behaviour. The experimental results are compared to those predicted by the F. E. model and the implications are discussed.

Chapter 8 presents the major findings of the thesis and also gives recommendations for future work.

1.4 Superconducting wire used in this research

All the experimental measurements for this research project were made on samples from a single spool of one particular superconducting wire. This wire was supplied by Oxford Instruments, the industrial sponsors of the project. It had been developed as a high field conductor and was a twisted multi-filamentary Nb_3Sn composite wire manufactured by the bronze-route process. The cross-section of the wire is shown in Figure 1.1 and details of the wire are given in Table 1.1. The volume fractions have been calculated using dimensions measured from images of the cross-section viewed under a microscope. The diameter to outside of barrier was 0.49mm, thickness of barrier was 0.013mm, average effective filament diameter was 0.0039mm pre-reaction and 0.0047mm post-reaction (heat-treatment as recommended by wire manufacturer) and the wire diameter was 1.5mm.

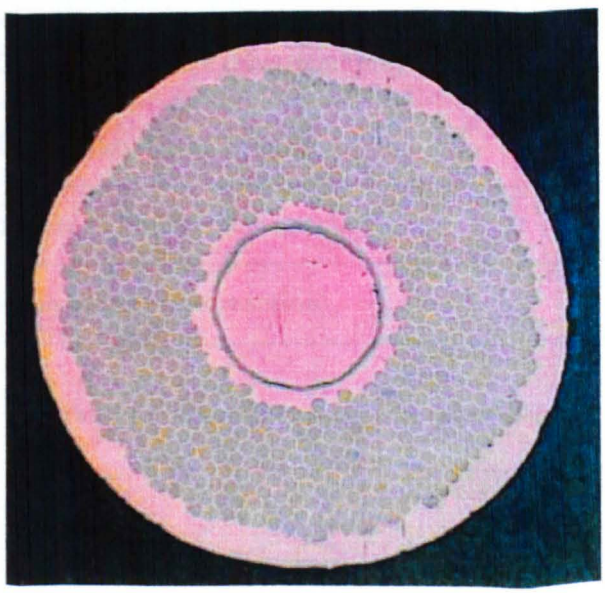

Figure 1.1 Cross-section of wire

The wire has 22866 niobium filaments of about 0.005mm diameter that are arranged in 618 bundles within a bronze matrix (Cu-13wt%Sn). The niobium contains a small amount of titanium (Nb-1wt%Ti). The titanium is added because it increases the growth rate of Nb_3Sn during the heat-treatment and because it improves the superconducting properties (Wada 1995). The bronze matrix is separated from the central core of copper by a double diffusion barrier layer consisting of niobium and tantalum.

Diameter	1.5 mm
Twist pitch	3 cm
Volume fraction of copper	9.6 %
Volume fraction of barrier	1.1 %
Volume fraction of filamentary Nb (pre-reaction)	15.5 %
Volume fraction of Nb_3Sn (post-reaction)	22.5 %
Volume fraction of bronze (pre-reaction)	73.9 %
Volume fraction of bronze (post-reaction)	66.9 %
Ratio of filamentary Nb to Bronze	1 : 4.8
Ratio of copper to Nb_3Sn (post-reaction)	1 : 2.3
Tin content in bronze (pre-reaction)	13 wt.%

Table 1.1 Superconducting wire specification

CHAPTER 2

Background and literature review

2.1 Introduction

This chapter gives some background to the research by describing the major developments from a historical perspective. Previous work pertaining to the mechanical properties of Nb_3Sn superconducting wire that has been published by other researchers is reviewed in the literature review.

2.2 Background

2.2.1 Discovery of superconductivity

When an electric current flows through a substance there is normally a resistance to the flow that gives rise to a voltage drop. The higher the resistance, the higher the voltage drop. This resistance causes electrical energy to be lost and heat to be generated in the substance. In 1911, while investigating the resistance of mercury at low temperatures, the phenomenon known as superconductivity was first discovered by Kammerlingh Onnes. He found that at 4 K the resistance falls to absolute zero. In a superconducting material, an electric current can flow with no resistance at all. There is no voltage drop and no energy is lost.

2.2.2 Development of practical superconductors

Superconductivity only occurs in a few materials and generally at very low temperatures. Also, it only occurs if the current density and magnetic field are below certain critical values. In the late 1950's and early 1960's new high-field superconducting alloys were discovered. These were made into practical superconductors with the development of new manufacturing methods in the 1960's

and 1970's. These had substantially higher critical current densities and critical fields than had been possible earlier. For the first time it became possible to build practical applications of superconductivity. One of the first superconducting materials to be used in practical superconductors was an alloy of niobium and titanium. This is still the most popular superconducting material. Another superconducting material, a compound of niobium and tin (Nb_3Sn) was also discovered around this time. This had superior superconducting properties to niobium titanium, but was much more difficult to make into practical superconductors because it is very brittle. Despite this, practical Nb_3Sn superconductors were soon produced and remain the most common superconductors used in middle and high field strength magnets.

In 1986, so called high temperature superconductors were discovered. Before then it was believed that superconductivity above 30K was impossible. Since then many more high temperature superconductors have been developed and although none of them are superconducting at room temperature, several are at liquid nitrogen temperature (-196°C). These superconductors can therefore operate when cooled with liquid nitrogen rather than liquid helium, which is required for niobium titanium and Nb_3Sn superconductors. Although the high temperature superconductors show great promise and are now being used in many applications, niobium titanium and Nb_3Sn remain the most commonly used superconductors.

2.2.3 Fabrication of Nb_3Sn superconductors

Although Nb_3Sn superconductors are made in other forms, such as tapes, the usual construction is in the form of twisted multi-filamentary composite wires. Fine filaments of Nb_3Sn are embedded in a matrix material of copper-tin alloy or bronze.

The filaments need to be fine, often around 0.005mm diameter, for optimum superconducting performance. The wires are twisted during manufacture so that the filaments form a spiral along the wire. This is also to optimise superconducting performance. The wires also contain copper that is separated from the matrix material by a thin barrier layer of niobium or tantalum. The copper provides protection from quenching. Quenching occurs when a local instability causes part of the wire to cease being superconducting and become resistive to the current. The heat generated by normal resistive conductivity spreads causing even more of the wire to cease being superconducting. The process then spreads to the whole magnet. The copper provides protection by having a low resistance for normal conductivity and so minimises the amount of heat produced. It is also a good conductor of heat and so quickly dissipates any local temperature rises. The barrier material prevents tin from the matrix diffusing into the copper during heat-treatment, which would raise its resistance and therefore its ability to protect against quenching.

Multi-filamentary Nb_3Sn composite wires were first made in the 1970's after the bronze-route manufacturing process was invented. A good review of manufacturing processes is given in Suenaga et al (1981). In the bronze-route process, rods of pure niobium are inserted into a billet of bronze. The stabilising copper is added either into the centre of the bronze billet or around the outside and is separated from the bronze with a barrier layer usually of niobium or tantalum. The whole assembly is then extruded and drawn down to form the wire. To obtain very large numbers of filaments, the process often involves restacking after partially drawing down the original billet assembly. Heat-treatments are required in between drawing operations

to anneal the bronze. A final high temperature heat-treatment is also required to form the Nb_3Sn compound by a solid state diffusion reaction.

Other manufacturing methods have also been developed, the most important being the internal tin method. It is similar to the bronze process except the bronze is replaced by copper and the tin comes from a tin rich alloy of copper and tin, which is added to the billet usually as a central rod. This method doesn't require the intermediate anneals that are required in the bronze process and has the capability to produce wires with a higher Nb_3Sn content and therefore higher critical current densities.

2.2.4 Applications

Almost all applications of superconductivity have been through the use of superconducting magnets. Two notable exceptions are SQUIDS (Superconducting Quantum Interference Device) - devices for detecting very small magnetic fields, and superconducting power transmission lines.

Superconducting magnets are used in a wide range of applications. The most widespread application is in Magnetic Resonance Imaging (MRI), which produces non-invasive internal images of the human body. MRI machines are now common place in hospitals.

Another application that uses similar technology to MRI is Nuclear Magnetic Resonance (NMR) machines. These are used in research establishments for the analysis of molecular structure. One area in which NMR machines are extensively used is in the development of new drugs.

Particle accelerators, such as the Large Hadron Collider (LHC) at CERN, make extensive use of superconducting magnets. They are used to accelerate particles to extremely high speeds, to contain the beam and to analyse the particles that are created when the beams collide.

Nuclear fusion reactors, such as those at Culham and the International Thermonuclear Experimental Reactor (ITER) being built in France, use superconducting magnets in the form of a toroidal ring to contain extremely hot plasma. If nuclear fusion can be controlled sufficiently to generate energy continuously, as opposed to only the short bursts that has currently been possible, the world will have an energy source that is virtually free, inexhaustible and pollution free.

Magnetic levitation trains use superconducting magnets to lift the train up off of the guideway as well as to propel them along. Only a few maglev trains have been built to date, most notably in Japan. They can operate at very high speeds, potentially much faster than normal trains, but the cost of building the guideways is very high and the strong magnetic fields can present a health risk (there is a serious risk for people with pace-makers, for example).

Superconducting magnets are also used in electric generators, energy storage and electric motors.

2.3 Literature review

2.3.1 Effect of stress and strain on superconducting properties

The mechanical properties of superconductors only became a topic of any real interest when Ekin (1976) discovered that stress has a significant effect on the critical current of Nb_3Sn multi-filamentary composite wire. Larbalestier et al. (1977) reported similar findings, albeit with the critical current degradation beginning at higher stresses and strains. They also showed that the degradation is completely recoverable up to a certain amount of strain. Beyond that strain, some degradation is permanent on the removal of the applied strain. Four papers, Ekin (1979), Rupp (1979), Luhman et al. (1979) and Easton and Kroeger (1979) that were published in the same journal, showed that the critical current actually increases with applied axial tensile strain before reaching a maximum and decreasing with further increases in strain. The term intrinsic strain was coined to mean the applied axial strain relative to the strain at which the maximum critical current occurs. The applied strain for maximum critical current was shown to be equal to the calculated residual compressive strain of the Nb_3Sn filaments, also referred to as the pre-strain in some of the literature. The maximum critical current was therefore concluded to occur at an applied tensile strain that cancelled out the residual compressive strain, resulting in a zero axial stress in the filaments. Rupp and Easton/Kroeger showed that the pre-strain decreases with increasing reaction (heat-treatment) time and increasing Nb_3Sn content. Ekin showed that the pre-strain was very different for wires manufactured by different methods. Luhman et al. showed how the pre-strain was related to the bronze/niobium ratio of the wire. They also presented SEM and optical observations of cracks in the Nb_3Sn filaments. Permanent degradation in critical current corresponded with the onset of

cracking. Ekin (1980) introduced his scaling law for predicting the effect of strain on the critical current in a wide range of superconductors including Nb_3Sn and Nb-Ti.

An explanation for the high sensitivity of the critical current of Nb_3Sn superconductors to stress was given by Flükiger et al. (1981). They used low temperature X-ray diffraction to show that the Nb_3Sn in multi-filamentary composite wires undergoes a stress induced cubic-tetragonal phase transformation. They suggested that stress affects the volume fraction and the c/a ratio (shape of unit cell) of the tetragonal phase and that this was the cause of the critical current dependence. Goldacker and Flükiger (1984) later revised that theory by showing that the volume fraction of the tetragonal phase was small and could therefore only be of secondary importance. They, as well as Roberge et al. (1985), presented evidence to conclude that the probable cause of the strain effect is the distortion of the cubic phase.

The effect of transverse stress on the critical current was first reported by Ekin (1987) and expanded on by Ekin et al. (1991). The effect was found to be approximately 7 times greater than the effect of axial stress. In Ekin (1995) bending strain was also shown to cause critical current degradation. This has importance because wires have to be bent when wound to form a magnet coil. Katagiri et al. (1996) investigated the effects of axial tensile strain and compressive transverse stress on high strength Nb_3Sn superconducting wires. These wires were developed to try to improve superconducting performance in high stress conditions. The conclusion was that high critical current density and strength is practical by using a copper-niobium alloy instead of pure copper as the stabilising material. The strain dependence was very

similar for the high strength and normal wires, but the critical current degradation was less for the high strength wires.

Markiewicz (2004) in two papers presents an elastic stiffness model to predict the strain dependence of the critical temperature of Nb_3Sn. The model uses the elastic constants for the cubic crystal structure. The results agree well with experiment suggesting that the strain dependence can be explained by the behaviour of the cubic crystal structure under strain, thus confirming the conclusions of Goldacker and Flükiger (1984) and Roberge et al. (1985). Flükiger et al. (2005) revisited earlier neutron and x-ray diffraction measurements and concluded that the asymmetry of the relationship between critical current and applied strain is connected to the asymmetric change in the 3D stress distribution in the filaments, which is responsible for the elastic tetragonal distortion.

Nishijima et al. (2005) investigated the effect of transverse compressive stress on Nb_3Sn superconducting wires reinforced by Cu-NbTi. It was shown that the Cu-NbTi provided reinforcement in the transverse as well as axial directions. It was also shown that the location of the Cu-NbTi reinforcement had a significant effect on its effectiveness. If the reinforcement is located in the centre of the wire, there is less deterioration in superconducting properties than if it is located around the outer part of the wire.

2.3.2 Thermal residual stresses

In the papers that first reported that superconducting properties improve with applied axial tensile strain before reaching a maximum and decreasing with further increases

in strain, it was suggested that the effect correlated with the strain in the Nb_3Sn filaments. In cooling from the heat-treatment temperature to the operating temperature of 4 K, axial thermal residual compressive stresses are produced within the Nb_3Sn filaments. This is because of differences in the thermal expansion coefficients between the Nb_3Sn and the bronze and copper. It was suggested that the superconducting properties reach a maximum when the applied axial strain cancels out the compressive residual strain. Easton et al. (1980) presented an analytical method to predict the axial thermal residual stresses and stress-strain curves of Nb_3Sn composite superconductors. The method only requires knowledge of the volume fractions and material properties of the constituent materials. The agreement between predicted and measured stress-strain curves is good. Watanabe et al. (1995) used the same method to calculate the residual strain in the Nb_3Sn filaments in Cu-Nb reinforced superconducting wires. This agreed well with the experimental measurements of the applied tensile strain required to maximise the critical current.

Hoard et al. (1980) calculated the 3 dimensional strain in Nb_3Sn filaments due to the thermal contraction and applied axial strain, and showed them to correlate well with results of critical current variation with strain. The strains were calculated using a computer program that solves the equations for a cylinder representing a single filament surrounded by its share of the matrix material. Lanteigne et al. (1981) used finite element modelling to try to explain the improved resistance to strain of in situ Nb_3Sn multifilamentary composites. The in situ wire fabrication method is an alternative to the bronze-route or internal tin method and produces short, non-continuous, very fine axially aligned filaments. The modelling was rudimentary and some of the assumptions about the material properties were inaccurate. The improved

resistance to strain was not explained by the model, however a hardening effect on the bronze matrix caused by the fine filament spacing was proffered as an explanation. A number of papers including Rupp (1981), Ochiai and Osamura (1992) and Awaji et al. (2005) investigated ways of modifying the residual stresses. Rupp showed how the residual strain is reduced following a loading cycle, but that it can be partially restored by reheating the wire to room temperature. Ochiai and Osamura showed how the critical current at 4 K is affected by applying cyclic loading at room temperature. Awaji et al. investigated how prebending treatments at room temperature affect the residual stress and the variation in superconducting properties with applied strain.

The finite element method was used by Murase et al. (2003) to calculate the 3 dimensional thermal residual strains. The model is much more realistic than that presented by Lanteigne et al. (1981). Although the results are not verified by experiment, they do show that the non-axial strains are significant and cannot be ignored. The thermal residual stress in the stabilising copper of a Nb_3Sn composite wire was investigated by Hojo et al. (2004). The copper, which was located around the outside of the wire, was removed by etching with nitric acid. A stress-strain curve for the copper layer was obtained by comparing the stress-strain curves of the wire before and after removing the copper. The analysis, however, only considers axial stresses, i.e. it assumes that radial stresses and hoop stresses are zero. The method also required the change in length of the wire caused by the removal of the copper. However, this was not measured, but calculated using an assumed value for the yield stress of the copper. The calculated residual stress in the copper was in the plastic zone at around 70 MPa, although for the reasons stated above this can only be treated as a first order approximation. Ekin et al. (2005) showed that the 0.1% to 0.2% pre-strain (the

residual compressive strain in the Nb_3Sn filaments) of high niobium fraction superconductors (niobium fraction of 20% to 30%) was lower than the pre-strain of traditional bronze-route wires (niobium fraction 10% to 15%). However, by including dispersion-strengthened copper in the matrix, the pre-strain could be restored to the more normal levels of 0.2% to 0.4%, which are more practical for magnet design.

Awaji et al. (2006) presented the results of a neutron diffraction study of the effect of pre-bending treatments at room temperature. The residual strain in the Nb_3Sn filaments was measured in the axial and lateral directions. Stress free lattice parameters were obtained by X-ray diffraction in the filaments after etching away the matrix. Lattice parameters of the filaments within the wire were obtained by neutron diffraction and averaging the results over a few diffraction peaks. The results were in agreement with calculations of the residual stress using the method first used by Easton et al. (1980).

2.3.3 Tensile testing method

A tensile testing method for Nb_3Sn multi-filamentary composite wires was first described by Larbalestier et al. (1977). The method involved using a servo-hydraulic materials testing machine equipped for testing at liquid helium temperature and clip on extensometers for the strain measurement. Some of the difficulties in obtaining accurate results were discussed, including the necessity to produce straight reacted samples. They achieved this by reacting samples in straight channels. The poor repeatability of the stress-strain curves obtained, particularly at the beginning of the curves (strain $< \sim 0.2\%$), is indicative of the experimental difficulty. Luhman et al. (1979) used a calibrated strain gauge soldered directly onto the wire specimens to

measure the strain. Stress and strain were measured along with critical current in the apparatus used to investigate the effect of strain on the critical current. A stress-strain graph is shown with several hysteresis loops produced with unloading and reloading cycles, the stress increasing on each cycle. This graph shows an increasing slope of the curve during the loading cycles. This is evidence of strain measurement error, as the slope should decrease as plastic deformation occurs. Sakai et al. (1996) describe a standardised method for the tensile testing of niobium-titanium composite superconducting wires. Prior to standardisation, proof stress and elastic modulus measurements showed a lot of variation. This variation was reduced considerably by using the standardised method. The main feature of the method was the use of a specially developed lightweight extensometer. The method used to obtain the elastic modulus was to measure the slope of the stress-strain curve at the linear region at the start of unloading cycles. This reduces the errors associated with using the loading parts of the curve; at the start of the loading cycles, the load is still quite low and not sufficient to fully straighten the wire samples.

A tensile testing method for Nb_3Sn superconducting wires at room temperature was presented by Katagiri et al. (2001). They used lightweight extensometers as recommended by Sakai et al. (1996) and also used the unloading curve to obtain a reliable elastic modulus. Significant variation in the stress-strain curves was found for low stress levels up to about 80 MPa, but beyond that the curves obtained were very consistent. Pre-loading the samples with 40 MPa prior to testing was shown to be effective in reducing the variation at low stress levels. Another method of reducing the variation was to fit a simple exponential function to the curve excluding the variable initial part. This function could then be extrapolated back to determine the zero strain

position of the curves. Nyilas (2005) discusses strain sensing systems tailored for fragile Nb_3Sn composite superconducting wires. New ultra-light extensometer were developed and compared to a double-extensometer system. Both gave good results, but the ultra-lightweight extensometer was said to be less affected by small irregularities in the straightness of the wire samples. A non-contacting laser extensometer system was also tested, but this produced strain measurements with a lot of scatter. Van der Eijnden et al. (2005) present results of tensile stress-strain characterisation on a range of Nb_3Sn wire types. The testing apparatus and method that was used, as well as the sample preparation, are described in some detail. The testing apparatus was one developed for measuring the strain dependence of the critical current, but it was used with no transport current through the wire specimens. The double-extensometer system tested by Nyilas (2005) was used for the strain measurement.

Osamura et al. (2008) presented the results of tensile tests carried out by 11 research groups worldwide on the same batches of 6 different types of Nb_3Sn multi-filamentary composite wire. The objective was to establish a standard best practice test method. The scatter of the measured values was analysed to see how the experimental conditions influence the determination of the physical quantities (elastic modulus, proof stress, etc.) The most important finding was that there was a lot of scatter in the initial slope of the curves caused by the low elastic limit.

2.3.4 Mechanical properties of Nb3Sn superconducting wires

McDougal (1975) appears to have been the first to measure the mechanical properties of Nb_3Sn superconducting wires. The experimental procedure, however, was not

described. Stress-strain curves at room temperature and 4 K of several wires with different heat-treatments are shown, albeit on a very small graph. Stress-strain curves of one particular type of Nb_3Sn superconducting wire at 4 K were published by Larbalestier et al. (1977). The curves showed significant variation, some of which is undoubtedly specimen variation, but some is also measurement error. Measurements of elastic modulus, proof stress and failure stress and strain were tabulated. Luhman et al. (1979) present a single stress-strain curve with hysteresis loops of a mono-filament wire at 4 K. Stress-strain curves for internal tin Nb_3Sn wires were measured at 4 K by Cogan et al. (1983), although only two curves are shown, each for wires given different heat-treatments.

Ochiai, Osamura and Uehara (1986) investigated the failure modes of bronze-route Nb_3Sn wires under tensile stress at room temperature. The Nb_3Sn filaments exhibited multiple fracturing and the strength of the Nb_3Sn showed a tendency to decrease with increasing heat-treatment temperature and duration. In Ochiai, Uehara, Hojo and Osamura (1986) and Ochiai et al. (1987), the strength of the Nb_3Sn was shown to be a function of the grain size in a Hall-Petch type relationship. Ochiai et al. (1988) and Ochiai et al. (1991) showed the same findings for wires that had a small amount of titanium added to the bronze, a practice employed to improve the superconducting properties. The strength of the Nb_3Sn for a given grain size was found to be reduced by the addition of titanium, although, depending on the heat-treatment temperature, the titanium also affects the Nb_3Sn grain size. In Ochiai et al. (1993), Ochiai et al. (1994) and Ochiai et al. (1995) the distribution of the Nb_3Sn filament strength was estimated for a range of wires and heat-treatments. This was done by analysing the change in critical current caused by preloading treatments at room temperature.

Vorobiova et al. (1996) measured the ultimate tensile strength, yield strength and elongation on a range of bronze-route Nb_3Sn composite wires for a range of heat-treatment durations. They show that the location of the copper stabiliser (internal or external) can affect the mechanical properties. A lot of their results, however, are for wires given short heat-treatments designed to anneal the bronze, and therefore with very little Nb_3Sn.

Iwaki et al. (2000) compare the mechanical properties of a high strength reinforced Nb_3Sn composite wire with a reference wire. The reinforced wire used a Nb/Cu composite material as a substitute for the stabilising copper in the reference wire. Stress-strain curves, proof stress and rupture stress are given for room temperature and 4 K. The reinforced wire was shown to have considerably higher proof stress and rupture stress. The room temperature results are the average of two tests, although the variation between them is not given, and only single tests were done at 4 K. The repeatability of the results is therefore not evident. Another version of this kind of reinforced wire was tested by Sakamoto et al. (2002) and by Awaji et al. (2003), but again only a single stress-strain graph is presented. Another type of reinforced wire was tested by Kondoh et al. (2001). The reinforcement in these wires was a tantalum core at the centre of each Nb_3Sn filament. The proof stress of these wires was considerably higher than even the Cu/Nb composite reinforced wires. The critical current was reported to be poor, however, and this was attributed to the high lateral residual stresses in the Nb_3Sn caused by the tantalum core. The same kind of wire, but with a different configuration and a lower tantalum volume fraction, was tested by Iwaki et al. (2002). The new configuration produced high proof stress combined with reasonable critical current values. Jewell et al. (2003) investigated the influence of

Nb_3Sn wire geometry on filament breakage under bending strain. Four different wire geometries were studied including bronze-route, internal tin and powder in tube (PIT) wires. In all but the PIT wire, significant cracking was found with a bending strain of 0.5%. However, at 0.6% bending strain, cracks were found in the PIT wire as well. Nyilas et al. (2003) report the results of tensile testing of a multi-filamentary Nb_3Sn composite wire at room temperature and 7 K. They show the importance of minimising any pre-loading of the wire prior to testing. Pre-loading was shown to change the initial slope of the stress-strain curve by a factor of 3.

Perhaps the most comprehensive set of stress-strain curves is presented by van den Eijnden et al. (2005). They tested 48 specimens in all, from 4 different wire types; 2 bronze-route, 1 internal tin and 1 PIT wire. Tensile tests were carried out at 4 K, 77 K and 293 K and for reacted and unreacted wires. The results show some quite a lot of specimen to specimen variability, particularly at the start of the curves.

2.3.5 Composition and constituent material properties

Any calculation or model used to determine the mechanical properties of a composite superconducting wire requires knowledge of the composition and material properties of the constituent materials. Cogan et al. (1979) investigated the texturing (crystalograhic alignment) within the constituent materials of a number of Nb_3Sn composite wires. They found significant texturing both before and after the reaction heat-treatment process. This could have a significant effect on the material properties. For example, the elastic modulus of copper grains differs by a factor of 3 depending on the orientation. The temperature and duration of the reaction heat-treatment process determines how much Nb_3Sn is formed and on how much tin is left in the bronze. This

was investigated by Tang et al. (1981) on two types of bronze-route wires. The Nb_3Sn layer thickness and the tin content in the bronze could be expressed with power laws with respect to time. McDonald et al. (1983) found significant variation in the tin content of both the bronze matrix and the Nb_3Sn filaments in a multi-filamentary composite wire. It varied by a factor of about 2 within the bronze, with the highest levels being in the regions where there were no filaments and the lowest being in amongst the filaments. The tin content of the Nb_3Sn varied from 20 at.% (at.% meaning the percentage of atoms) to the stoichiometric 25 at.%. Similar results were also reported by Tan et al. (2004).

Bussière et al. (1980) determined the Young's modulus of polycrystalline Nb_3Sn between 4 K and 300 K, by measuring the static deflection of Nb_3Sn-Nb-Nb_3Sn composite strips. The Young's modulus of polycrystalline Nb_3Sn was found to soften by a factor of about 2 between room temperature and 4 K, though this is not as much as expected by a polycrystalline average of the single crystal elastic constants, which soften dramatically at the martensitic transformation temperature of around 50 K. The room temperature value of 132 GPa for the Young's modulus, however, was close to the polycrystalline average of the single crystal elastic constants (137 GPa). It was assumed that the distribution of grain orientation in the composite strips was random. However, there was no evidence of this. Moreover, because rolled sheets were used in the preparation of the composite strips, some degree of preferred orientation was likely. Bussière et al. (1981) used a vibrating reed technique to investigate the softening of polycrystalline Nb_3Sn further. It was found that compressive residual strains substantially reduces the softening of the Young's modulus on cooling from 300 K to 6 K. This indicates that elastic deformation of Nb_3Sn is highly non-linear at

low temperatures. Bussière et al. (1982) used the same technique to investigate the effects of ternary additions on the Young's modulus of Nb_3Sn. Tantalum, titanium and zirconium were added to the niobium that was used to form Nb_3Sn. It was found that all three additions suppressed the martensitic phase transformation that occurs at around 50 K. The softening of Young's modulus was also suppressed as a result. The Young's modulus of Nb_3Sn at low temperatures was shown to be strongly dependent on the type and quantity of the additions. LeHuy et al. (1983) found that hydrogen, which was introduced by heat-treating in hydrogen gas, has a similar effect of suppressing martensitic phase transformation and softening Young's modulus of Nb_3Sn. Disorder in the crystal structure was also shown to have a similar effect in Snead et al. (1983). Higher degrees of disorder were introduced by irradiating samples with neutrons.

Flükiger (1982) investigated the crystal structure of Nb_3Sn filaments in multi-filamentary wires by neutron diffraction in the temperature range 4 to 800 K. Three different tetragonal phases were observed (denoted T1, T2 and T3). T1 is the tetragonal phase that the cubic phase transforms into in stress free Nb_3Sn below the transition temperature of 43 K. This transition is suppressed by stress and ternary additions, and only occurs in Nb_3Sn with a composition close to stoichiometry. T2 is the stress induced tetragonal distortion of the cubic phase, which was observed below 800 K. This observation provides evidence that residual stresses build up from at least 800 K during cool-down following heat-treatment. It is unclear from the paper, however, how quickly the samples were cooled and this could have had a significant effect on how much stress relief took place. T3 is another stress induced phase that occurs below about 100 K and has been shown to be different from the T1 phase.

Unlike T1, T3 occurs over a wide range of composition of Nb_3Sn, from at least 22 to 25 at.%Sn. The structure of T3, however, had not been resolved at the time of publication. With the possibility of Nb_3Sn being composed of 3 different phases, the proportions of each being strongly dependent on composition and stress, it is clear that obtaining accurate material property data is fraught with complexity. Goldacker and Flükiger (1984) used X-ray diffraction to measure the effect of applied axial strain on phases T2 and T3. The T2 phase (tetraganonal distortion of cubic phase) was shown to undergo an elastic volume change as well as shape distortion. In contrast, the T3 phase shows a change in volume fraction rather than any lattice distortion.

Poirier et al. (1984) measured the Young's modulus, shear modulus and Poisson's ratio of polycrystalline Nb_3Sn between 4 and 300 K using an ultrasonic pulse method. The results for Young's modulus agree well with Bussière et al. (1979 and 1981), but there is some doubt about the accuracy of the Poisson's ratio measurements because they don't agree with the polycrystalline average of single crystal data. Using the ultrasonic pulse method again, Poirier et al. (1985) showed that uniaxial stress stiffens both the Young's modulus and shear modulus below 90 K. This is a similar finding to Bussière et al. (1981) and again suggests that the elastic stress-strain relationship is non-linear at low temperatures. Building on the work by Bussière et al. (1982), Kumakura et al. (1985) investigated the effect of alloying additions to Nb_3Sn on the material properties. Titanium, tantalum, zirconium and Hafnium additions all reduced the softening of Young's modulus. Balankin (1988) compared theoretical calculations of Poisson's ratio of six compounds with A15 type crystal structure, one being Nb_3Sn, with experimental data. The calculation was based on the electron-phonon interaction constant and used no empirical parameters. The agreement was generally good,

although for Nb_3Sn the agreement is only good below about 50 K. At room temperature, the calculated value is 0.29 whilst the experimental value quoted is 0.2, although this has been taken from Poirier et al. (1984) where the accuracy of the measurement was said to be in doubt. The calculated values do however agree quite well with the polycrystalline average of single crystal data.

Wright and Dixon (1988) measured the Young's modulus and flow stress of Nb_3Sn at high temperatures. They found that the Young's modulus is approximately constant above room temperature. Bray et al. (1997) were the first to use tensile test data to measure the Young's modulus of Nb_3Sn. The Young's modulus was obtained by extrapolating data obtained from niobium and Nb/Nb_3Sn tapes. The results (150 GPa at room temperature, 65 GPa at 4 K) are consistent with earlier data from ultrasonic, vibrating reed and static beam deflection measurements. Markiewicz and Goddard (2002) used energy dispersive X-ray spectroscopy (EDS) to measure the post-reaction grain size and residual tin content of the bronze in five different types of Nb_3Sn superconducting wire. The tin content varied between 2 and 7 wt%, depending on the location within the wires. Grains were not elongated in any direction and their size was found to be dependent on the space available in the particular region of bronze. There was therefore a lot of variation within the wires, i.e. small grains in and around the filaments, larger grains elsewhere. For modelling the mechanical properties, knowledge of the tin content and grain size is important because they have a big influence on the bronze yield stress. Hojo et al. (2004) obtained the Young's modulus and the plastic zone part of the stress-strain curve for the copper in an externally stabilised Nb_3Sn superconducting wire. This was done by comparing the stress-strain curves of wires before and after having the copper layer etched away. The Young's

modulus obtained was 116 GPa, which is slightly lower than the isotropic value of 125 GPa. This was attributed to texturing of the copper grains. The analysis only considered the axial direction, however, and so suffers from some inaccuracy because the lateral stresses are likely to be significant. Goddard et al. ((2005) studied the variation in filament area along the length of the wire as well as within the cross-section. Large variations were found, although the total filament area was found to be relatively uniform along the wire length. Hojo et al. (2006) made a direct measurement of the elastic modulus of Nb_3Sn by extracting filaments from superconducting wire. The filaments were extracted by etching away the other materials with nitric and hydrofluoric acid. The filaments were then impregnated with epoxy resin to form a simple filament bundle composite rods. The value obtained for the elastic modulus was 127 GPa, although the accuracy of the measurement is questionable because it is dependent on the approximate measurements of the number of filaments in the bundles and the amount of unreacted Nb in the core of the filaments.

2.3.6 Modelling of mechanical properties

Easton et al. (1980) presented an analytical method to predict the axial thermal residual stresses and stress-strain curves of Nb_3Sn composite superconductors. The method only requires knowledge of the volume fractions and material properties of the constituent materials. Although non-axial stresses are ignored in the analysis, the agreement between predicted and measured stress-strain curves is good. More precise modelling than that given by their method was said to be very difficult for a number of reasons: Kirkendall voids at filament/matrix interface, non-uniformity of Nb_3Sn layer, anisotropy, uncertainties in the grain size, hardening of matrix due to filaments. The

strain within the Nb_3Sn filaments of superconducting wire was modelled using a computer program developed by Hoard et al. (1980). The model analysed a single filament surrounded by its share of the matrix material. Good agreement was found between the predictions of applied strain at which maximum critical current occurs and experimental data.

Finite Element Modelling (FEM) was used by Murase et al. (2003) to analyse the 3 dimensional thermal residual strains in Nb_3Sn composite superconductors as well as in oxide high temperature superconductors. Very similar modelling was also used in Murase and Okamoto (2004) to analyse the 3 dimensional strain states under applied tensile stress for various composite conductors, including Nb_3Sn composite wires. Models with 16 and 36 filaments within the cross-section were analysed. The model employed symmetry such that, for example, the 36 filament model only required a mesh representing a 15° sector of the wire cross-section. Some of the material properties used in the models were simplifications; for example, the Young's modulii and coefficients of thermal expansion were assumed to be independent of temperature. No comparison is given with experimental results, but the analyses showed that the radial and tangential strains are significant and depend strongly on wire structure. FEM was also used by Peng et al. (2005). Their analysis, however, was concerned with the drawing of multi-filamentary wires and the residual stresses produced.

Mitchell (2005) used a 1 dimensional FE model to predict the mechanical properties of Nb_3Sn superconductors. The model used strut elements joined in parallel with each element representing a different constituent material. The models were verified against experimental data for the mechanical properties, although only qualitatively

because data on known wire configurations was not available. In an appendix, the paper provides a very good collection of materials data recommended for use in elasto-plastic finite element modelling of Nb_3Sn superconducting wires. In another paper, Mitchell (2005) built on his earlier work by modelling the cross-section of a Nb_3Sn superconducting wire with a 3D finite element mesh, similar to that used by Murase et al. (2003). Mitchell used element birth and death options to simulate the effects of the reaction heat-treatment; annealing, stress-relief, tin depletion in bronze, swelling and property changes associated with Nb_3Sn formation. Variations in the basic model were used to investigate differences between bronze-route and internal tin wires. A steel jacket was also added to the outside of the mesh to simulate cabling, the practice of enclosing several superconducting wires in a steel conduit. The paper analyses the 3D stresses and strains that result from the heat-treatment temperature and the cool-down to 4 K as well as how they change with applied axial tensile stress. The results are not verified against any experimental data, however.

To model an entire superconducting coil, it is not practical to have a fine enough mesh to accurately represent the true structure of the composite superconducting wire, but if the wire can be represented as a single homogeneous material, accurate modelling of the strains in the wire that result from cooling the coil from the heat-treatment temperature down to 4 K would be possible. In Boso et al. (2005) and Boso et al. (2006) methods to enable Nb_3Sn superconducting wire to be modelled as a single homogeneous material are explored.

Farinon et al. (2007) used FEM to evaluate the effect of deformation caused by cabling, the process where several superconducting wires are enclosed in an outer

normally stainless steel jacket or conduit. To simulate cabling, an initially round wire is flattened in the model to an approximately rectangular shape. The model revealed areas of high elongation relative to elongation at fracture and therefore areas where breakages could occur. The 2D model used the plane strain assumption, where the axial strain is assumed to be zero. Although it was conceded that plane strain would give inaccurate results, the results were compared with those obtained when the generalised plane strain assumption was applied instead. Generalised plane strain is where the axial strain is finite but uniform across the cross-section. This would be the correct assumption to make, but the results were not sufficiently different from those obtained with the plane strain option to justify the much longer times required for the computer to run the analyses. Alsharo'a et al. (2008) used similar modelling techniques in the optimisation of Nb_3Sn superconducting wires used in cables. Sub-element (filaments bundle) shape, number of sub-elements and the spacing between sub-elements were investigated. Results were verified with experiment by visually comparing the FE results of the deformed shape with microscope images taken of deformed wire cross-sections.

Zanino et al. (2008) produced a 3 dimensional F.E. model representing a 5mm length of a Nb_3Sn superconducting wire in order to investigate the critical current degradation caused by bending that can occur inside cabled conductors. To verify the model, the residual strain in the Nb_3Sn filaments was compared to the applied axial strain at which maximum critical current occurred. A possible explanation for the significant discrepancy was suggested as being uncertainties in thermal expansion properties. However, the modelling did not allow for any stress relief during the cool-down after heat-treatment. This would also provide an explanation for the

discrepancy. Results of axial tensile tests were also compared with experimental data. A reasonable match was achieved by assuming a tin content in the bronze of 1 wt.% (percentage by weight), however, this is considerably lower than has been reported by Markiewicz and Goddard (2002). They measured the tin content to be between 2 and 7 wt.% depending on the location within the wire.

Ahoranta et al. (2008) proposed simple methods for dealing with two of the common problems associated with modelling Nb_3Sn superconducting wires. The first problem is how to model the large numbers of filaments with sufficient detail and keep the computer run time down to reasonable levels. In the paper, it is stated that the homogenisation approach as reported by Boso et al. (2005 and 2006) may not adequately describe the complex behaviour. The approach suggested by Ahoranta et al. is based on dividing the problem into auxiliary models, which focus on finding an accurate solution for one region within the cross-section at a time. The mesh in the auxiliary models is detailed in a small region, for example, a filament bundle, but the geometry is simplified in the rest of the model. The overall picture of the wire behaviour is obtained when the results of the different auxiliary models are combined, although how this is done is not explained. The second problem is how to model the stress relief and annealing that occurs at the high temperatures during heat-treatment. The method proposed by Ahoranta et al. is to start the analysis at the heat-treatment temperature, at which the wire is assumed to be stress-free. As the wire is cooled, deviatoric stresses in the copper and bronze are forced to zero, as if stress relaxation was infinitely fast. Below a certain temperature, somewhere between the heat-treatment temperature and room temperature, thermal stresses are allowed to develop with no relaxation. By using a limit temperature for stress relaxation of 450 – 500 K a

match was obtained between the axial thermal residual strain in the Nb_3Sn filaments and the experimentally determined axial strain at which maximum critical current occurred. The stress-strain curve predicted by the model is compared with experiment and a good match is obtained up to 0.5% strain. However, the slopes of the curves seem to be diverting at 0.5% strain suggesting that the match is not so good at higher strains.

CHAPTER 3

Heat-treatment of superconducting wires

3.1 Introduction

The mechanical properties that were investigated for this thesis were those of a particular multi-filamentary Nb_3Sn composite superconducting wire manufactured by the bronze route method. This wire requires heat-treatment to form the superconducting Nb_3Sn compound. The heat-treatment process and its effect on the composition, dimensions and residual stresses are described in this chapter. Special apparatus had to be designed and built in order to carry out the inert atmosphere heat-treatments on wire samples. This apparatus and the heat-treatment procedure are also presented here. Finally, the different heat-treatments that were given to different batches of wire samples are described.

3.2 The heat-treatment process

The two most common manufacturing methods of making superconducting wires containing Nb_3Sn, namely the bronze route and the internal tin method, require a heat-treatment process. The wires are manufactured using pure niobium, which gets converted into Nb_3Sn during the heat-treatment by a diffusion reaction process. Tin (Sn) diffuses from the tin sources in the wire into the niobium (Nb) filaments where it reacts with the niobium to form the Nb_3Sn compound. In the case of bronze-route wires, tin diffuses out of the bronze matrix (bronze being an alloy of copper and tin). In the case of internal tin wires, the tin comes from pure tin (or tin rich alloy) reservoirs within the wire. A Nb_3Sn layer grows at the interface between the niobium and the diffusing tin. As the heat-treatment proceeds, the layer gets thicker until all the niobium has been converted or until the reaction effectively stops due to a deficiency of tin at the interface.

The optimum heat-treatment regime varies depending on the precise composition of the wire. Often there are two stages or more. It is during the final stage, which is carried out at the highest temperature, that the majority of the Nb_3Sn is formed. For bronze route wires, the earlier stages, which are carried out at lower temperatures, have the purpose of seeding small Nb_3Sn grains (Schelb 1981, Taillard et al. 1997). This has the effect of producing a grain size at the end of the heat-treatment regime that is smaller than it is for a heat-treatment where the low temperature stages are omitted. For internal tin wires, the earlier stages prevent the tin sources from melting (Naus et al. 2000). The temperature at which these heat-treatment stages are carried out is below the melting point of tin. During these low temperature stages, different phases of copper-tin form as tin diffuses into the copper matrix. The temperature of the final stage is high enough to melt tin, but not the copper-tin phases that are formed during the low temperature stages. Melting is to be avoided because the filaments can move within the liquid phase causing them to coalesce. The superconducting properties are seriously affected if this occurs.

The optimum temperature for the final stage of the heat-treatment, in which most of the Nb_3Sn is formed, is a compromise between obtaining a fast reaction and minimising the final grain size of the Nb_3Sn (Schauer and Schelb 1981, Bruzek et al. 1997). The higher the temperature, the faster the reaction takes place. The duration of the heat-treatment can be several days or even weeks, so a fast reaction rate is desirable to minimise production time. However, a higher temperature also results in a larger Nb_3Sn grain size and the larger the grain size, the worse the superconducting properties (West and Rawlings 1977, Tang et al. 1981). This is because the grain boundaries act as pinning centres for magnetic flux and the greater the pinning force

the higher the critical current (Scanlon et al. 1975). In practice, the temperature of the final heat-treatment stage is around 650°C to 750°C.

The optimum duration of the heat-treatment is also a compromise (Hense et al. 2003). Unless all of the niobium in the filaments has been converted to Nb_3Sn, increasing the duration will produce more Nb_3Sn within the wire. Another positive effect of increasing the duration is that the Nb_3Sn composition gets closer to stoichiometry (Larbalestier et al. 1975, Tang et al. 1981, Fillunger et al. 2002). Nb_3Sn has a distinct chemical composition, 3 atoms of niobium to 1 of tin, i.e. 25% tin. However, the crystal structure is not perfect and so the actual composition may be slightly different. In practice, when the Nb_3Sn first forms the composition is deficient in tin at around 18%. As the reaction proceeds the tin content generally increases up to a maximum close to the stoichiometric 25%. The tin content has an effect on the superconducting properties of the Nb_3Sn, the closer it is to stoichiometry the better the properties. On the negative side, the size of the Nb_3Sn grains increases with increasing heat-treatment duration (West and Rawlings 1977, Tang et al. 1981, Fillunger et al. 2002). Thus, the optimum duration is that at which the positive effects of more Nb_3Sn being formed and a closer to stoichiometry composition are outweighed by the negative effect of increasing Nb_3Sn grain size. Generally, the larger the filament size the greater the heat-treatment duration that is required. This is because tin has to diffuse through the Nb_3Sn layer, which has formed around the outside of the filaments, before new Nb_3Sn can be formed at the niobium/Nb_3Sn interface. In practice, the duration of the final heat-treatment stage is anything from a few hours to several days.

For superconducting magnets containing Nb_3Sn wires, the heat-treatment process is normally carried out after the wire has been wound onto the coil. This is refereed to as the "wind and react" process. Alternatively, there is the "react and wind" process where the wire is heat-treated prior to winding onto the coil. The "wind and react" process is the more common because the reacted wire is very brittle and can easily be damaged during winding.

To prevent the surfaces of the wires from oxidising, the heat-treatment must be carried out in a vacuum or an inert atmosphere. At the heat-treatment temperature, the surface material of bronze or copper readily oxidises in the presence of oxygen or CO_2 and because the heat-treatment duration is so long, the oxidation is severe unless steps are taken to dramatically reduce the levels of these gases. Most superconducting magnet coils of the Nb_3Sn "wind and react" kind are heat-treated in a vacuum furnace with a vacuum of around 10^{-9} bar.

3.3 Heat-treatment apparatus

To investigate how the mechanical properties are affected by the heat-treatment it was necessary to prepare wire samples for tensile testing. These were cut from the spool of wire supplied by Oxford Instruments Superconductivity. The spool of wire was in a pre-reacted condition and therefore it was necessary to heat-treat the wire samples to convert the niobium filaments into Nb_3Sn. Another requirement was to produce straight wire samples. This was because bent samples would fracture prematurely during tensile testing due to high bending strains as they straighten out. Also, strain

measurement by extensometers, the method used in this research, will produce errors with bent samples.

Initially it was intended that the inert atmosphere heat-treatment apparatus already in possession of the Department would be used, a vacuum furnace not being available. The apparatus in question was the Snijstaal gas grid system for a Nabertherm furnace. This consists of a steel bag 300 x 150 x 100mm in size that is fitted onto a supporting frame. The end of the bag fits over a tapered plug through which inert gas is fed. The inert gas is distributed throughout the bag by means of a feed pipe with several bleed holes. The outlet for the gas is through the gap between the end of the bag and the tapered plug. A schematic is shown in Figure 3.1.

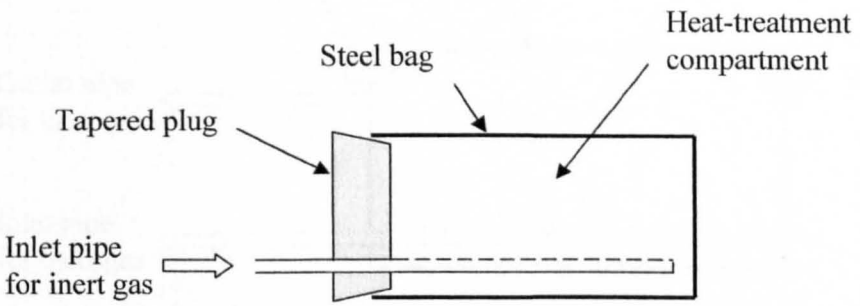

Figure 3.1 Snijstaal gas grid system for inert atmosphere heat-treatment

It was not possible, however, to obtain oxidation free wire samples using this apparatus. It was felt that the main problem was oxygen getting into the heat-treatment compartment between the plug and the end of the bag. The severity of oxidation was reduced by increasing the flow rate of the inert gas (argon), but even at a high flow rate of 10 litres/min it was unacceptable. Maintaining a flow rate of 10 litres/min or

more for the duration of the heat-treatment was impractical because of cost of the gas that would be used. Alternative apparatus was therefore investigated. To prevent oxidation, other researchers have sealed wire specimens within quartz glass tubes. This was not considered practical for this research because of the large numbers of specimens required and the lack of a glass blowing facility in the University.

Instead, apparatus similar to the Snijstaal gas grid system was purchased. This was a sealed Snijstaal container, which consists of a steel box with a lid. The inlet for the inert gas is similar to the first apparatus, but the outlet is via a pipe positioned close to the top of the box. A schematic is shown in Figure 3.2.

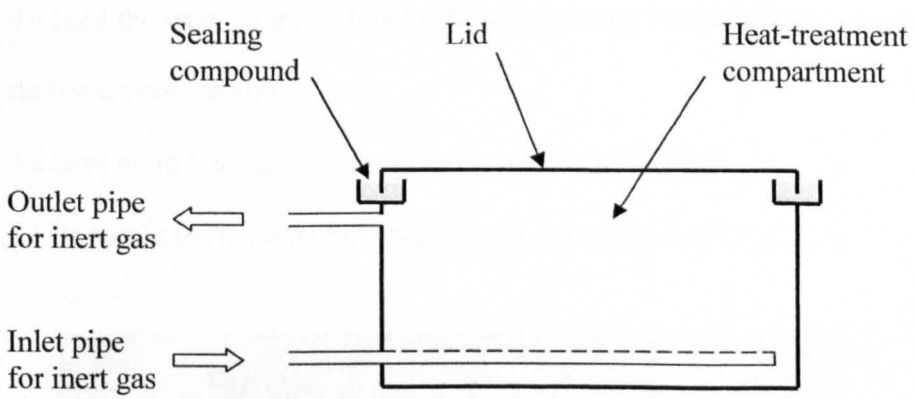

Figure 3.2 Sealed Snijstaal container for inert atmosphere heat-treatment

With this type of apparatus sand is often used as the sealing compound, but as sand is very porous, a high temperature sealing cement was used to seal the lid. Applied as a paste, the water based compound sets hard as it dries out providing a good seal. Despite the use of the sealing cement, there was little if any improvement over the sealed Snijstaal container. Oxidation was still unacceptable.

Copper sheets were placed in the heat-treatment compartment with the wire samples, to act as getters (i.e. any oxygen present would oxidise the sheets, depleting the oxygen in the compartment). This also failed to provide any improvement. It was concluded that the main problem with the apparatus was that it was not possible to thoroughly purge the heat-treatment compartment because of its large volume and shape. It was therefore decided to design and build apparatus specifically for the heat-treatment of superconducting wires.

The design had the following objectives:

- To minimise the volume (for purgability)
- To have no dead zones (so that all the volume would be purged)
- To hold the wire samples straight (bent specimens would fracture prematurely during tensile testing)
- To have good sealing (to prevent oxygen from getting in)
- To fit within the department's Nabertherm box furnace (Figure 3.3)

Figure 3.3 Nabertherm furnace

The Ellingham diagram (Ellingham 1944) shown in Appendix A indicates that for copper not to oxidise at 700 °C, the partial pressure of oxygen must be below about 10^{-11} to 10^{-12} bar (as indicated by the red lines on the figure in the appendix). This implies that oxidation does take place during the heat-treatment in a vacuum of 10^{-9} bar, i.e. standard heat-treatment of Nb_3Sn superconducting coils. The rate of the reaction, however, must be very slow. A private communication with Jeff Parrell PhD, a senior scientist at Oxford Instruments Superconducting Technology in the USA, suggested that oxidation rates would be sufficiently low with an oxygen level of 5ppm or less in the inert gas when heat-treating at atmospheric pressure.

A schematic of the final design is shown in Figure 3.4 and a photo of the apparatus prior to assembly is shown in Figure 3.5. Engineering drawings are shown in Appendix C.

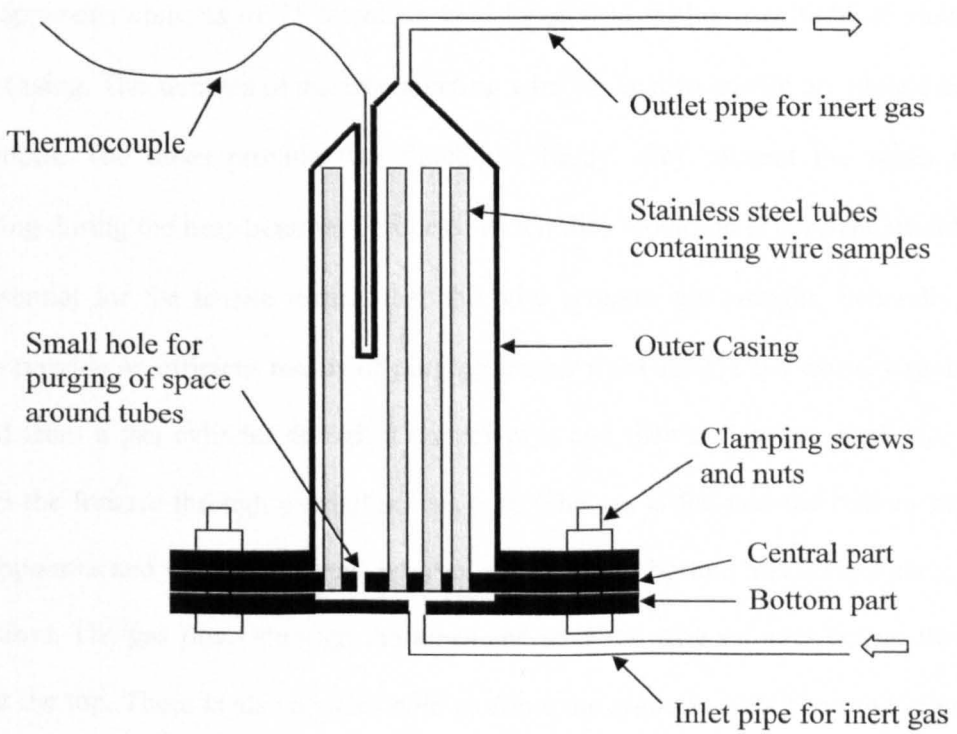

Figure 3.4 Schematic of heat-treatment apparatus

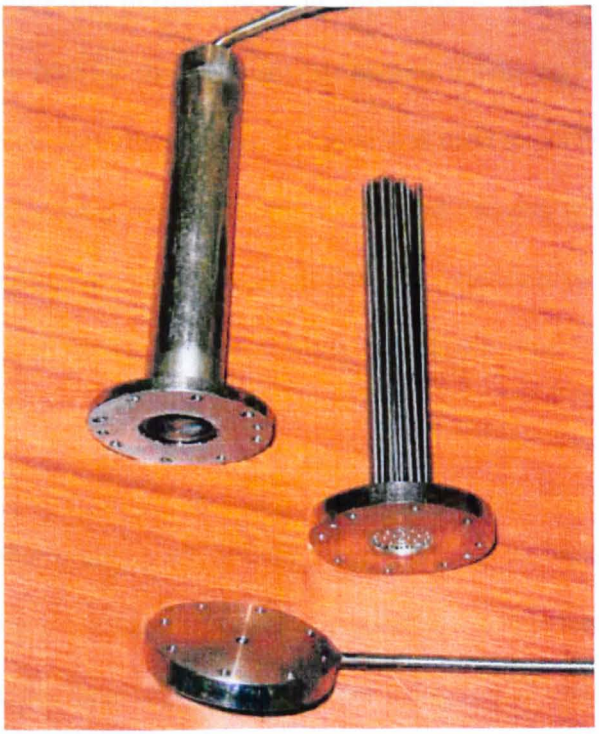

Figure 3.5 Heat-treatment apparatus

The apparatus consists of 25 stainless steel tubes held within a cylindrical stainless steel casing. The samples of superconducting wire for heat-treatment are placed inside the tubes. The tubes provide two functions; firstly, they prevent the wires from bending during the heat-treatment process, which they would do if not held straight. It is essential for the tensile testing that the wire samples are straight. Secondly, the tubes provide an efficient means of purging the air from around the wires. Argon gas is fed from a gas cylinder though a copper pipe and then a stainless steel pipe that enters the furnace through a small access hole. The gas is fed into the bottom part of the apparatus and then, via a small reservoir between the bottom and central parts, into the tubes. The gas flows through the tubes and over the wire samples before flowing out at the top. There is also a small hole to allow the argon to flow from the reservoir directly into the main cavity. The top of the apparatus is cone shaped to minimise the

dead space to improve the purgability. The apparatus is stood vertically as shown because, as argon is heavier than air, any air within it will rise to the top and exit through the outlet pipe. Initially a plastic gas pipe was used to connect the gas cylinder to the stainless steel inlet pipe, but it was found that oxygen was able to permeate through this at a sufficient rate to cause noticeable oxidation on the surface of the wires. No such oxidation was apparent when the plastic pipe was replaced by the copper one.

Eight screws are used to clamp the bottom plate, the outer casing and the central part together. The mating faces need to provide a good seal to prevent air getting in. To produce a good seal the faces are lapped together using fine diamond lapping paste. A thermocouple is fitted into a tube that is sealed at the end and welded to the inside of the outer casing. On assembly, this tube sits amongst the other tubes that contain the wire specimens. The outlet pipe is fed out of the furnace and into the top of a clear plastic bottle containing water. The flow rate of the inert gas can thus be observed as a stream of bubbles. A tap in the outlet pipe enables the gas flow to be controlled. A pressure regulator on the gas cylinder controls the pressure within the apparatus.

The superconducting wire samples that were investigated for this research project were heat-treated using this specially designed and built apparatus. By doing so it was possible to produce heat-treated samples that were completely free of surface oxidation. The mating surfaces of the apparatus proved to provide a good seal as is shown in Figure 3.6. The figure shows the condition of two of the surfaces after the completion of a heat-treatment. Although some oxidation is apparent around the

outside, the surfaces close to the interior cavity remain bright, indicating that no oxidation occurred and that no air was able to get in.

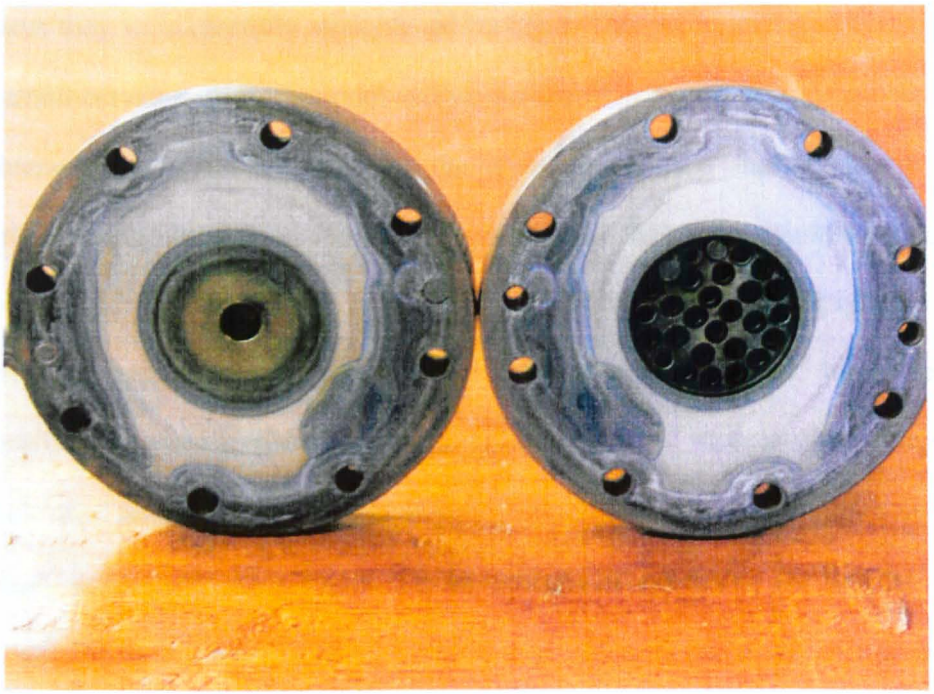

Figure 3.6 Mating surfaces after completion of a heat-treatment

3.4 Heat-treatment procedure

The procedure for heat-treating the superconducting wire samples can be broken down into the following steps:

i) Preparation of wire samples

Approximately 500 lengths of approximately 175mm were cut from the spool of wire supplied by Oxford Instruments Superconductivity. These wire samples were mixed up to provide a randomised source from which samples for each heat-treatment batch could be taken. This was done so that the variation in wire composition along the length of the spool would not influence the results when averaged over all the wires in

a heat-treatment batch. It was necessary to do this because significant variation was observed between different parts of the spool. 25 wires were taken from the common supply for each heat-treatment batch. Before they were inserted into the heat-treatment apparatus they were carefully straightened by hand. This was necessary because they had a small curvature from the spool and would not fit in the tubes without first being straightened. The act of straightening the wires would have changed the material properties by introducing some cold work and also changing the residual stresses. It was considered that this change in properties would have a negligible effect on the properties of the heat-treated wires because the heat-treatment would largely anneal the constituent materials of the wire and relieve the residual stresses while being held at the elevated temperatures. As well as being straightened, the wire samples also had their ends squared off. This was to aid the process of measuring the lengths of the wires, which was required to determine the change in length due to the heat-treatment. Square, or in practice slightly rounded ends, would produce more reliable change in length measurements than rough ends. Diffusion during the heat-treatment would tend to round off any sharp points and thus give misleading results of change in length. The ends were squared off using a grinding wheel and a hand file to remove the burrs. During the grinding care was taken not to heat the wires too much. Between short spells of grinding, the wires were immersed in cold water to cool them.

ii) Lapping the mating surfaces of the heat-treatment apparatus together

Before each use of the heat-treatment apparatus, the mating surfaces had to be lapped together to provide a good seal. Without a good seal there was the likelihood that air would penetrate into the heat-treatment cavity and result in oxidation on the surface of the wires. The lapping process was done by slowly rotating one of the parts in a lathe whilst holding the other part against it. Diamond lapping paste of various grades was

used to lap the two surfaces together. For the initial preparation of the surfaces, coarse grade compound was first used with finer grades being used in stages to improve the surface finish. The final grade was 0.25 micron. Between each heat-treatment batch it was necessary to lap the mating surfaces together for a couple of minutes using the 0.25 micron grade paste to remove the small amount of oxide that would prevent good sealing on reassembly.

iii) Assembling the apparatus

The 25 wire samples were placed inside the stainless steel tubes of the apparatus and the three parts were clamped together using 8 stainless steel cap head screws and nuts. Care was taken to tighten the screws up progressively to obtain an even pressure on the mating surfaces. To test for leaks the apparatus could be immersed in water and pressurised using the argon gas supply. This was not necessary once confidence in the lapping process was achieved. The apparatus was placed vertically in the Nabertherm furnace with the outlet pipe at the top. The inlet and outlet pipes for the argon gas fitted through a small hole by the top of the furnace door. The thermocouple wire also was fed through this hole. The inlet pipe was connected to the argon gas supply and the oulet pipe to the device for measuring the flow rate (a clear plastic bottle filled with water).

iv) Providing the inert atmosphere

The argon gas used to provide the inert atmosphere was Zero-Grade argon supplied by BOC. This has a maximum level of oxygen of 2ppm. The pressure regulator on the cylinder was set to 1 bar. This was sufficient to provide more than enough flow rate for purging and high enough to ensure that the flow of gas through any slight leak in the apparatus would be from inside to out. To purge the air within the apparatus with

the inert argon gas, a high flow rate was used for about 15 minutes. The flow rate was adjusted by using the tap on the outlet pipe. After initial purging the flow was reduced to a very low level (1 or 2 bubbles per second), required to prevent the build up of any volatiles and to remove any trace levels of air. As the temperature changed during different stages of the heat-treatment it was necessary to make small adjustments to the tap restricting the gas flow rate in order to maintain the desired flow rate. The flow of argon was maintained throughout the heat-treatment, including ramping up to temperature and cooling down. Only when the temperature had fallen below about 100°C was it considered safe to turn off the flow.

v) Heat-Treatment

An electronic controller on the Nabertherm furnace was used to set the heat-treatment schedules. The temperature, the dwell time at that temperature, and the time to heat up to that temperature could all be programmed in. The temperature that was controlled was the furnace temperature not the actual temperature within the apparatus that was monitored separately. A small difference of a few degrees between the two was observed, so the set temperature was adjusted to give the desired temperature in the apparatus. The furnace controller did not allow for the cooling rate to be controlled. So for the cooling stage of the heat-treatment schedule the furnace was obtained by allowing the furnace to cool down naturally when the heating elements were switched off. The cooling rate was approximately 100°C/hour, a value comparable to what practical superconducting wires would experience during the heat-treatment of a magnet coil. One batch of wire samples was cooled much faster in order to investigate the effect. This high cooling rate was obtained by removing the heat-treatment apparatus from the furnace and immersing it in oil. This produced a cooling rate that was approximately 100 times faster than the natural cooling rate.

3.5 Details of different heat-treatments given to wire samples

The wire manufacturer, Oxford Instruments, recommended that the full heat-treatment for the wire should be 144 hours at 570°C followed by 96 hours at 695°C, with ramp rates of 150°C/hour. Table 3.1 shows the different heat-treatment regimes that were applied to batches of 25 wire samples. The batch number shows the randomised order in which the heat-treatments took place. The heat-treatment duration was different for each regime (shortest at the top of the table, longest at the bottom), but all the regimes followed the same temperature profile. Batches 3 and 10 were heat-treated according to the recommended regime (regime 8). For regime 9, the heat-treatment duration was longer than recommended, for all the other regimes it was as recommended or shorter. The cooling rate at the end of the heat-treatment was the same for all regimes, except regime 8a, and was the natural cooling rate of the furnace when the heating elements were switched off (approximately 100°C/hour). The rapid cooling rate of regime 8a was obtained by immersing the heat-treatment apparatus in oil. The cooling rate was measured using the thermocouple inserted into the outer casing of the heat-treatment apparatus. The cooling curves are shown in Figure 3.7. Heat-treatment regimes 1 to 5 would not be sufficient to achieve acceptable superconducting properties, but have been considered here to investigate the causes of changes in mechanical properties. This knowledge may help in the design of new superconducting wires and manufacturing methods to give improved mechanical properties.

Regime Number	Batch Number	Heat-Treatment Schedule
0		No heat-treatment
1	9	Ramp to 570°C, no dwell
2	1	95hrs@570°C
3	2	144hrs@570°C
4	7	144hrs@570°C + ramp to 695°C no dwell
5	8	144hrs@570°C + 6hrs@695°C
6	5	144hrs@570°C + 24hrs@695°C
7	4	144hrs@570°C + 48hrs@695°C
8	3 and 10	144hrs@570°C + 96hrs@695°C
8a	11	Same as Regime 8, but with rapid cooling
9	6	144hrs@570°C + 144hrs@695°C

Table 3.1 Heat–treatment schedules

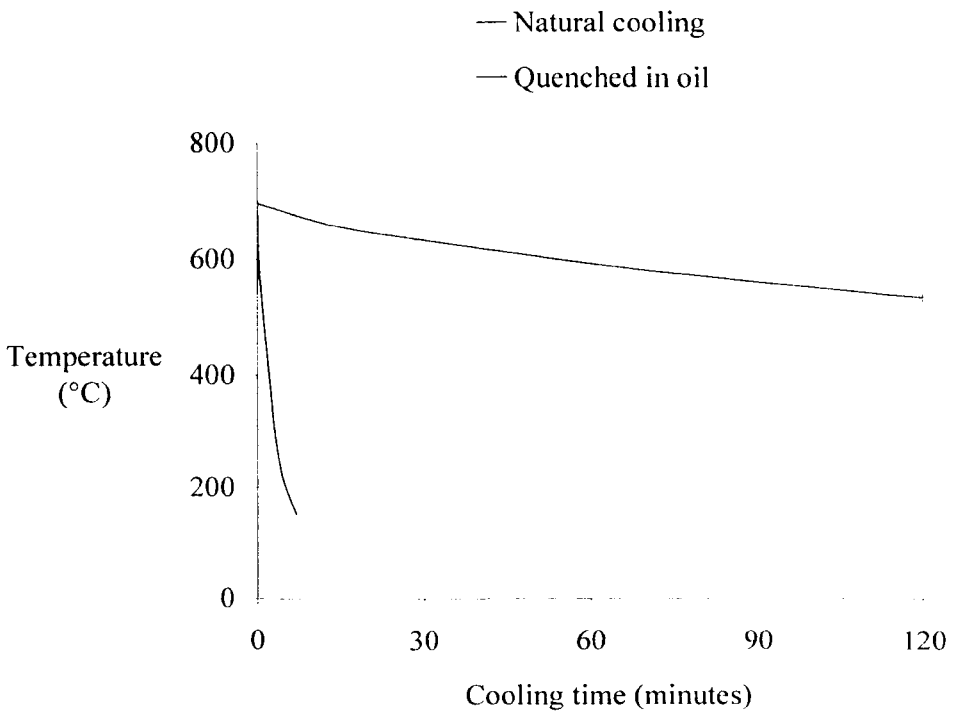

Figure 3.7 Comparison of different cooling rates

CHAPTER 4

Dimensional changes caused by heat-treatment

4.1 Introduction

The heat-treatment given to Nb_3Sn superconducting wires results in significant changes to the wire dimensions. This has important consequences for the manufacture of superconducting magnets. These consequences and the causes for the dimensional changes are discussed in this chapter. The literature on the dimensional changes is very scarce and the data that has been published is somewhat contradictory (Easton and Kroeger 1979, Cave and Weir 1983, Andreev et al. 2002, Goddard et al. 2005). Experimental data was obtained for this thesis by measuring the length and volume of wires before and after each of the heat-treatments detailed in Chapter 3. With a simple calculation, the wire diameter was also obtained. For each heat-treated batch, the size of the Nb/ Nb_3Sn filaments was also measured. (The weights of the wires were also measured before and after heat-treatment, but no change was found within the measurement accuracy of ±0.15%). The measurement methods are described in detail and the results presented. Finally, the implications of the results are discussed. Some of the content of this chapter has been published previously in Harvey et al. (2005) and Harvey et al. (2006).

4.2 Causes of dimensional changes

During the heat-treatment, the niobium within the filaments is slowly converted into Nb_3Sn. The change in volume associated with the conversion is approximately 37% (Cave and Weir 1983). However, this increase in volume is counteracted by a decrease in volume of the bronze caused by the depletion of the tin as it diffuses into the filaments to form the Nb_3Sn. It is the combination of these two effects that determines the overall change in volume.

Another mechanism that influences the change in dimensions is creep. Creep is slow deformation that occurs at stresses below the yield stress. The rate of the creep deformation depends on the temperature as well as the magnitude of the stress. The higher the temperature, the higher the creep rate. For metals, the creep rate is negligible when the temperature is below about 0.3 to 0.4 of the melting point (Ashby and Jones 1980). This approximate creep threshold temperature for the constituent materials of the superconducting wire investigated is given in Table 4.1.

Material	0.3 to 0.4 of Melting Point (°C)
Copper	134 to 269
Tin	-121 to -71
Niobium	552 to 827
Nb_3Sn	349 to 556
Tantalum	714 to 1043

Table 4.1 Approximate creep threshold temperatures

Residual stresses exist within the wire prior to heat-treatment as a result of the drawing process during manufacture (Peng et al. 2005). Thermal stresses caused by differences in the thermal expansion coefficients of the different constituent materials within the wire, add to the residual stresses as the temperature rises during the heat-treatment. Creep, primarily of the bronze matrix, during the heat-treatment almost certainly results in these stresses being relieved, at least partially. During the cool down at the end of the heat-treatment, residual stresses are again developed as a result of differences in the thermal contraction coefficients (Luhman et al. 1979, Goldacker and Flükiger 1985). Creep will partially relieve these stresses, at least while the temperature is high. The dimensions of the heat-treated wires are thus influenced by the creep strains and the residual strains associated with the residual stresses.

Another factor that could potentially have a significant effect on the dimensions is the possible formation of voids within the wire. It has been shown (Easton and Kroeger 1979)) that Kirkendall voids can form during the heat-treatment. These voids are created as the tin in the matrix diffuses into the niobium and will obviously cause a significant increase in volume.

4.3 Consequences of dimensional changes

Superconducting magnets using Nb_3Sn wire are usually manufactured using the "wind and react" process. The superconducting wire is wound onto a former prior to heat-treating. Changes in the dimensions of the wire during the heat-treatment and cool-down clearly have an effect on the stresses acting on the wire. No information about this, however, could be found in the literature. Consideration of the consequences is felt to be important and so some consideration is given here, although it is conjecture and not supported by any direct scientific evidence.

One possible consequence of dimensional changes in the wire is that the wire could become loose. Magnet quenches can be initiated if the superconducting wires are able to move during magnet operation. (Quenches occur when a part of the coil undergoes a superconducting to normal-conducting transition. The resistive heat that is generated causes more of the coil to become normal-conducting generating more heat until the whole magnet becomes normal-conducting). Coils are impregnated with resin after the heat-treatment process in order to prevent the wire from moving during magnet operation. It would still be desirable, however, to prevent the wires becoming loose during the heat-treatment to maintain the position and alignment of the strands.

The winding tension produces a tightly wound coil, with axial tensile and transverse compressive forces acting on the wire. The heat-treatment will affect these stresses in a complex way. Initially, the stresses will be affected by the relative expansion rates of the former onto which the wire is wound and the wire itself. This will depend on the thermal expansion coefficients of the former material and the wire and also on the thermal conductivity and ramp rate.

During Nb_3Sn formation, changes to the wire dimensions will affect the axial and transverse stresses acting on the wire. An increase in wire diameter will act to increase the transverse stresses between adjacent contacting wires. Conversely, a reduction in wire diameter will reduce the contact stresses, possibly causing the wire to become loose. An increase in stress-free wire length (length with no applied stresses) will act to reduce the axial tension, possibly causing the wire to become loose. Conversely, a reduction in wire length will act to increase the axial tension. An increase in wire diameter could also push the strands further apart causing an increase in axial tension, particularly in the strands near the outside of the coil. However, the strands probably do not get pushed apart very much because this would mean that the outside diameter of the coil would increase and the axial strain in the strand on the outside of the coil would be large. This would require the strand to yield plastically in the axial direction. The stresses probably do not get anywhere near that required to cause plastic axial yield. The reason for this is that the bronze and copper within the wire creep at the high heat-treatment temperature. Creep will cause the wire cross-section to change; material will creep away from the points of contact between the wires. The wires will not creep in their axial direction because the tantalum (and possibly the niobium) in the barrier does not creep at the heat-treatment temperature. Thus any increase in wire

volume probably doesn't increase the volume occupied by the coil, but rather fills some of the space between the wires within the coil.

During the cool down phase of the heat-treatment process, stresses will again be affected by the relative contraction rates of the former and the wire. This will depend on the thermal expansion coefficients of the former material and the wire and also on the thermal conductivity and ramp rate.

The tightness of the coil after it has been cooled to its operating temperature of around 4K will not only affect the likelihood of quenches occurring, but will also influence the superconducting properties. It is well known that the superconducting properties of Nb_3Sn are strongly influenced by its stress state. Therefore, if the dimensional changes influence the axial and transverse stresses acting on the wire, they therefore also influence the superconducting properties.

4.4 Measurement method

4.4.1 Length

The lengths of the wire samples were measured using a set of long length vernier callipers. To ensure accuracy of measurement the wires were prepared with square ends (refer to Section 3.4). To hold the wires straight and square to the callipers they were held in a groove machined onto the top surface of a rectangular metal plate and held down by another plate placed on top. Only small lengths of wire protruded from the ends of the plates to enable measurement. A schematic is shown in Figure 4.1. The edge of the plate with the groove was held against the callipers to ensure that the wire

was held square to the calipers. The callipers had a ratchet device that enabled them to be closed onto the ends of the wires with a consistent pressure. This was important because the wires were relatively flexible and any variation in the pressure would have caused a variation in the length measurement obtained.

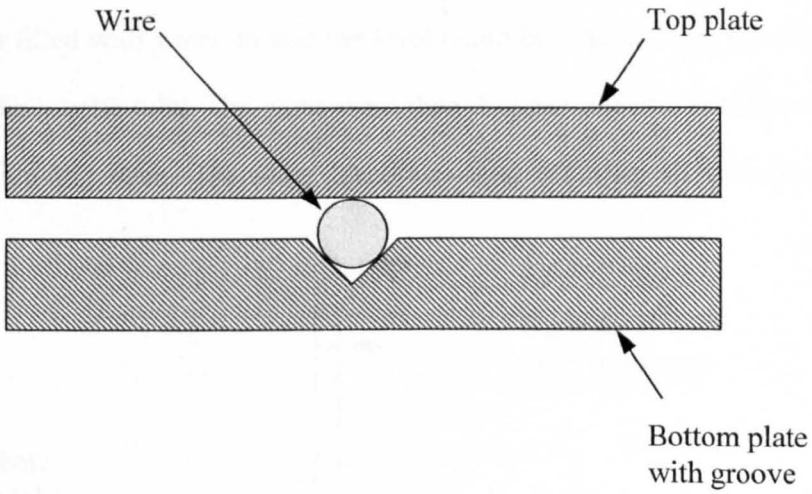

Figure 4.1 Method for holding wires straight for length measurement

The measurement accuracy was investigated by repeating measurements on a batch of 25 wires. The lengths of the wires were around 175mm and each wire was measured to 2 decimal places. The average difference between the two measurements made on each wire was 0.0056mm and except for one wire where the difference was 0.02mm, the difference between the two measurements was either zero or 0.01mm. Thus the accuracy of the measurement of change in length of each specimen is approximately ±0.01mm or ±0.01% (rounded up) of the original length.

4.4.2 Volume

The total volume of the 25 wire samples within each heat-treatment batch was measured before and after heat-treatment. This was done by immersing the wires in water and measuring the displacement of the water level. The apparatus used consisted of a glass measuring flask with a small bore burette tube fitted into the neck. The flask was filled with water so that the level could be read close to the bottom of the scale on the burette tube. The wires were then dropped one at a time through the burette tube into the flask. The water level was read off after all the wires were

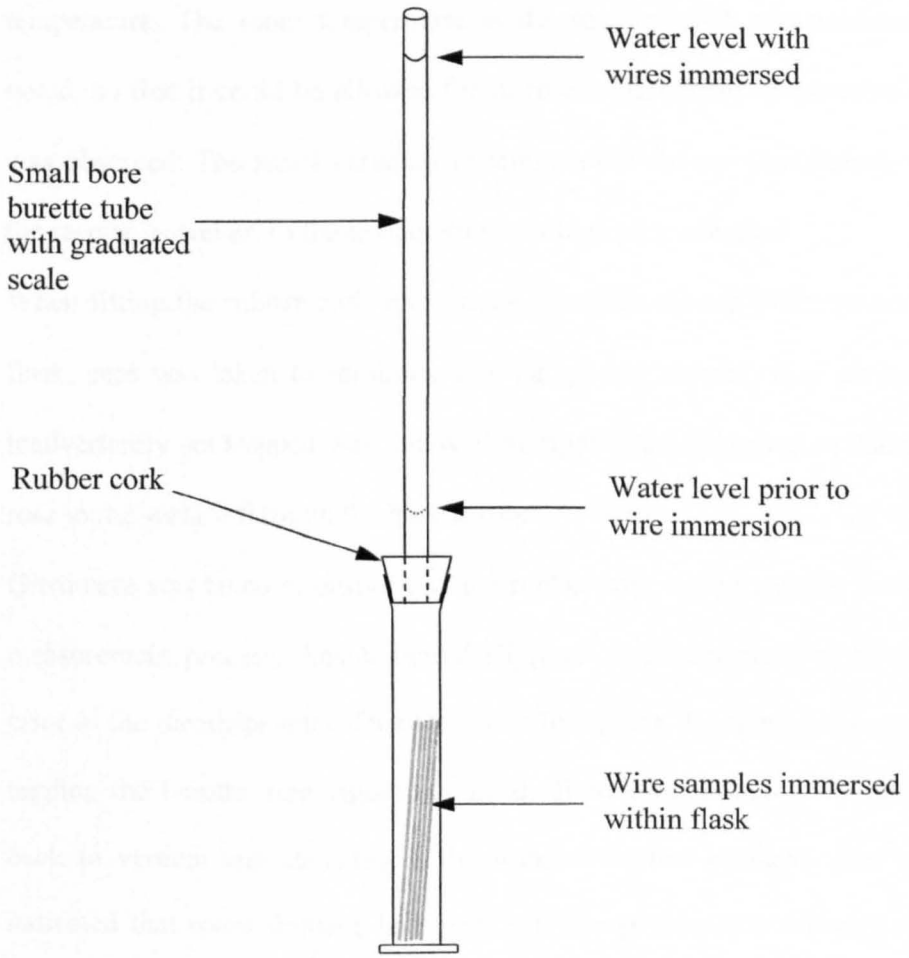

Figure 4.2 Schematic of volume measurement apparatus

immersed. The change in level corresponded to the volume of the wires. The small bore of the burette tube enabled an accurate measure to be obtained as the change in level was approximately 50cm. A schematic of the apparatus is shown in Figure 4.2.

To maximise the accuracy of the measurement a number of important strategies were deployed:

1. The measurement was carried out in a temperature stable room and the water used for the measurement was taken from bottle that was allowed to stand for at least 24 hours prior to use to enable its temperature to equalise with room temperature. The room temperature at the time of each measurement was noted, so that it could be allowed for in case a significant temperature effect was observed. The small variation in temperature did not significantly effect the results, however, so the temperature readings were not used.
2. When fitting the rubber cork and burette tube into the top of the water filled flask, care was taken to minimise any air getting trapped. Any air that did inadvertently get trapped was removed by tipping the apparatus so that the air rose to the surface through the burette tube.
3. Great care was taken to ensure that the rubber cork would not slip during the measurement process. Any potential slippage was encouraged to take place prior to the measurements. This was done by tipping the apparatus horizontal, tapping the burette tube vigorously in all directions, returning the apparatus back to vertical and checking if the water level had changed. Any change indicated that some slippage had occurred. The process was repeated several times until no more slippage took place.

4. To minimise the number of air bubbles being carried down into the flask or attaching themselves to the inside surface of the burette tube during the process of immersing the wires, the apparatus was tipped to an angle of approximately 30^{o} from horizontal for the purpose of inserting the wires. By sliding the wires slowly down the burette tube into the water very few air bubbles were produced. Any bubbles that attached themselves to the inside surface of the burette tube could be 'knocked off' by the insertion of the next wire. Once 'knocked off' the bubbles would rise to the surface, or at least rise part way to the surface before re-attaching to the burette wall once again.
5. After all the wires had been immersed in the flask, if there were any air bubbles in the flask or burette tube, an attempt was made to remove them. This was done by agitating the apparatus to free the bubbles and tipping it to enable the bubbles to pass up through the burette tube to the surface. If the bubbles could not be removed, the measurement was abandoned and the whole process began again.
6. During the handling of the apparatus, care was taken not to cause any warming with direct hand contact. Any small warming was found to cause an error by causing the water to expand. For a similar reason, the volume of the flask used was the minimum possible, as the greater the volume the greater the change in level in the burette tube that would result from any temperature change.
7. The measurement was repeated 3 times and if agreement wasn't within ±0.1% further measurements were made until 3 consecutive measurements were within the limit.

The repeatability of the measurement of volume was approximately ±0.09%. The change in volume was obtained from the difference between volume measurements and the accuracy is therefore approximately ±0.13%. (This was obtained by multiplying the accuracy of a volume measurement by 2 because the difference was obtained from 2 volume measurements, and dividing by $\sqrt{2}$. The division by $\sqrt{2}$ is because of probability; there is a low probability of the error being larger than ±0.13% because the individual errors of the two measurements would both have to be close to 0.09% and with opposite signs).

4.4.3 Filament diameter

A comprehensive study of the cross-sectional area and effective diameter of the filaments within the superconducting wires was undertaken. The effective diameter being defined here as the diameter of a circle which has the same cross-sectional area as the irregular shaped filament as illustrated in Figure 4.3.

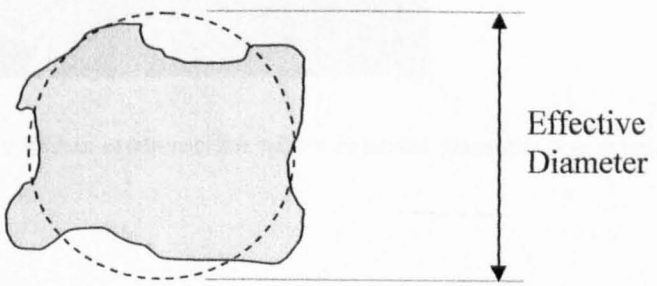

Figure 4.3 Effective diameter of a filament

Measurements were made with unreacted wire as well as all the batches of heat-treated wires. Because of the large variability in filament size, it was necessary to measure a large number of filaments from different regions within the wire cross-

sections of a number of different wires from each heat-treatment batch. For each of the 9 variables of wire (all the heat-treated batches plus the unreacted batch), 3 cross-sections were analysed, each from a different wire within the batch. For each cross-section, the filament diameters from 6 different regions were measured. The location of the 6 regions is shown in Figure 4.4. Two of the regions were from the outside of the filament/matrix ring, two from the inside and two from the central area.

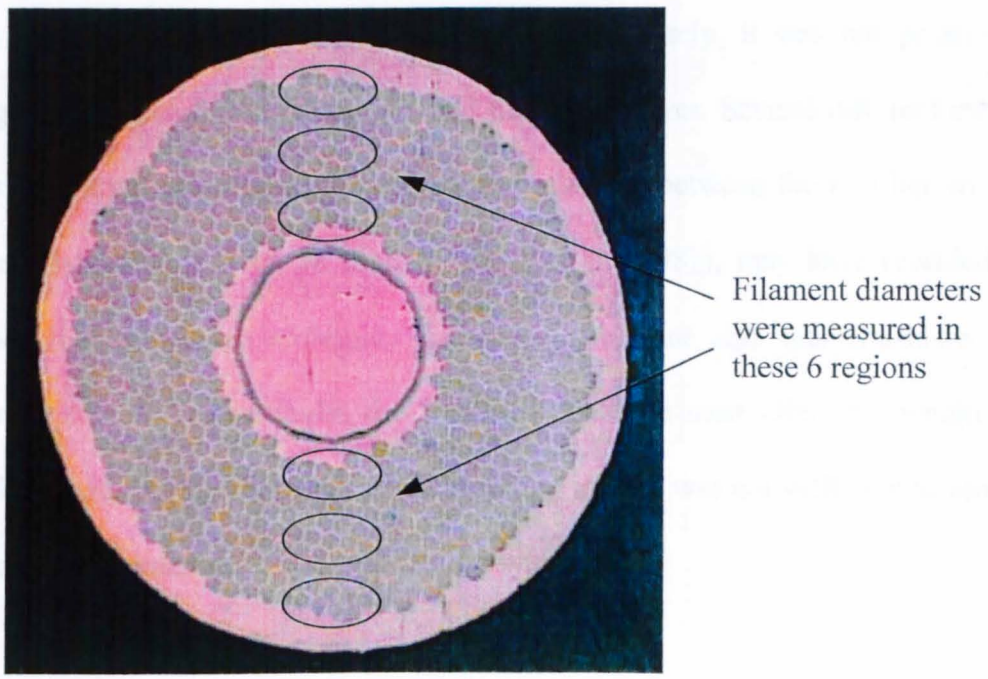

Figure 4.4 Regions within cross-section where filament diameter was measured

Within each region, the effective diameters of approximately 30 filaments were measured. Thus, the number of filaments measured was approximately 180 per cross-section, 540 per heat-treatment variable, and 4860 in total (a long and laborious task!).

The effective diameters were measured using a high magnification optical microscope. To prepare the micrograph samples, short sections of wire were encapsulated in potting compound using special clips to hold the wires perpendicular to the ends. A polishing regime involving four stages was employed to achieve the high quality finish required. The polishing regime used was that recommended by Metprep Ltd, a supplier of polishing materials and is given in Appendix B.

It was hoped that it would have been possible to measure the size of the niobium core at the centre of partially reacted filaments. Unfortunately, it was not possible to distinguish between the niobium core and the Nb_3Sn layer. Several different etching agents were tried in an attempt to reveal the interface between the two but with no success. Hydrofluoric acid, as used by Tang et al. (1981), may have revealed the interface, but this is an extremely hazardous substance and was considered too dangerous to use. Interestingly, the interface could be seen after the penultimate polishing stage, but the sharpness of the resulting images was not sufficient to provide accurate measurements.

An Olympus BX51 microscope was used to view the polished samples. This had a maximum magnification of 1000 and was fitted with a digital image grabber. *Aquinto a4i Docu* software by Aquinto AG, Berlin, Germany was used to analyse the images. The circular measurement tool within the software was used to draw circles over the filaments within the 1000x magnified image. The position and size of the circles were adjusted to cover the actual filaments such that the areas of the circles and the filaments were visually equal. An example of one of the 162 images analysed is shown in Figure 4.5.

Note, however, that the analysis software gives the effective radii of the filaments rather than the diameter. The image in the figure is of a wire from heat-treatment regime 8 (i.e. a fully reacted wire), although all the cross-sections analysed produced similar images.

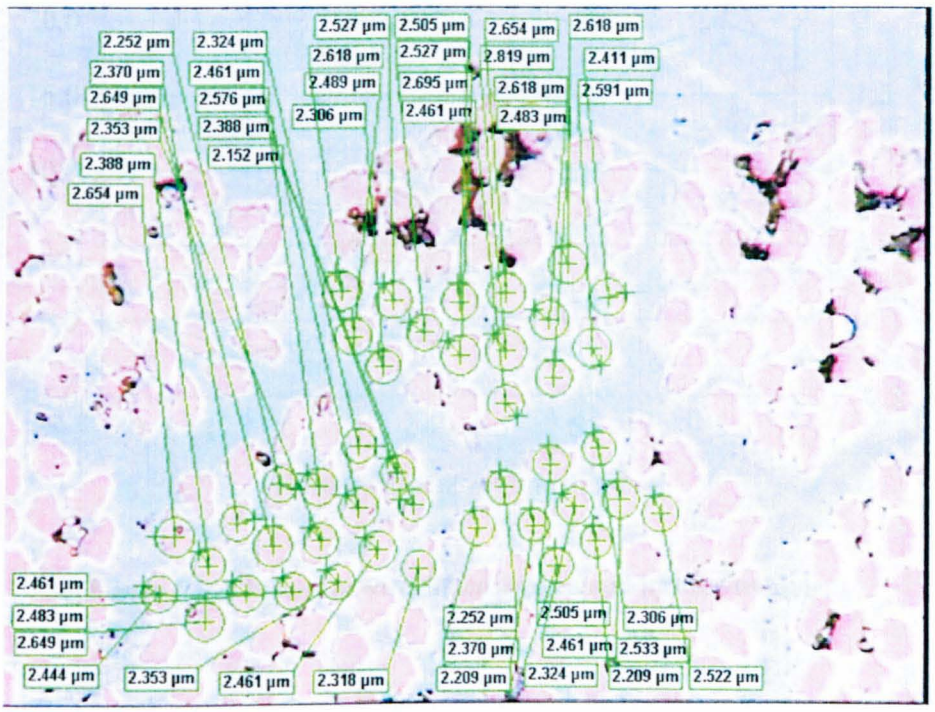

Figure 4.5 Measurement of filament size

4.5 Results

The results of the change in dimensions caused by the various heat-treatment regimes are shown in Figure 4.6. The y-axis scale on the right is for the change in wire length, volume and diameter. The scale for the much larger change in effective filament diameter is on the left. The details of the heat-treatments for the different regimes can be found in Chapter 3. Regime number 0 (meaning no heat-treatment) is included to give a reference point. The regime numbers have been ordered such that the heat-treatment duration increases with increasing regime number.

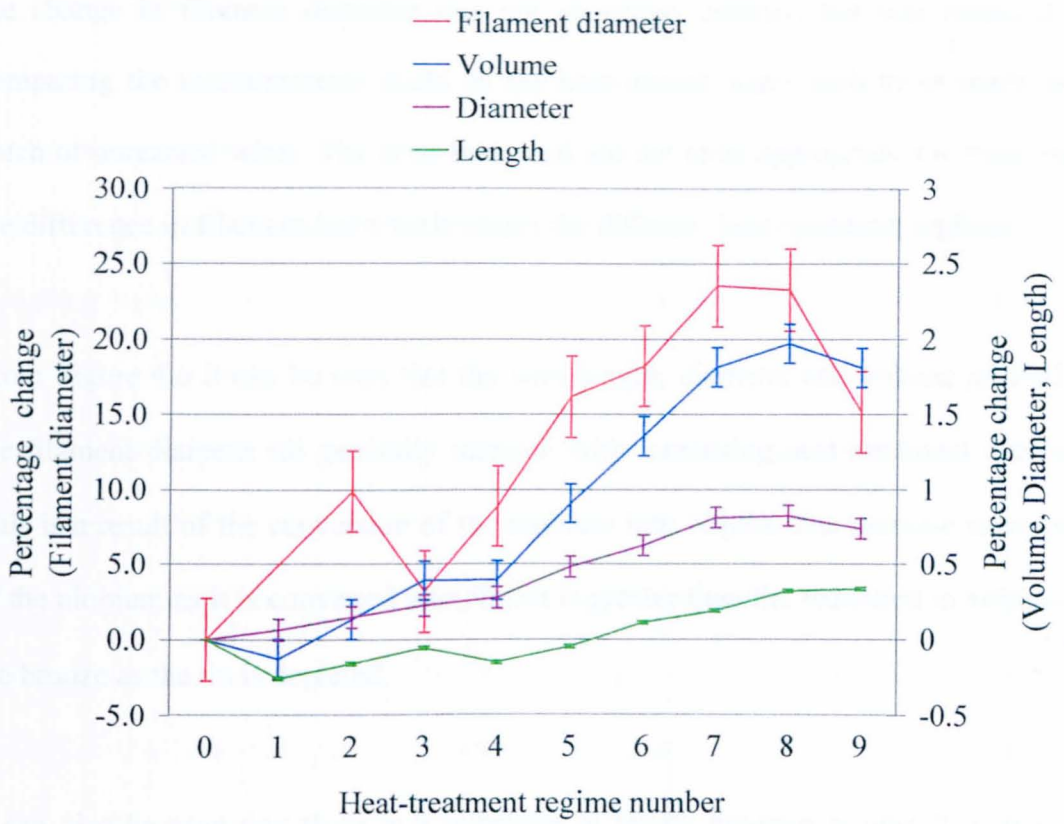

Figure 4.6 Changes in wire dimensions caused by heat-treatment

The error bars represent the confidence in the accuracy of the measurements, i.e. there is approximately 95% confidence that the true value lies somewhere within the range of the error bar (the error bars do not therefore represent the scatter in the measurements; although this scatter is shown in Figure 4.7). If there is no overlap of error bars then there is statistical confidence that there really is a difference between the two points. The error bars for the filament diameter measurements have been calculated differently from those for the volume, diameter and length. They represent the 95% confidence of the average filament diameter rather than the change in filament diameter caused by the heat-treatment. The reason for this is that it was not possible to make filament diameter measurements on the same filaments before and after heat-treatment because of the destructive nature of the measurement. Therefore,

the change in filament diameter was not measured directly, but was obtained by comparing the measurements made on the heat-treated wires with those made on a batch of unreacted wires. The error bars used are the most appropriate for visualising the difference in filament diameter between the different heat-treatment regimes.

From Figure 4.6 it can be seen that the wire length, diameter and volume as well as the filament diameter all generally increase with increasing heat-treatment duration. This is a result of the conversion of the niobium into Nb_3Sn. The increase in volume of the niobium as it is converted into Nb_3Sn is greater than the reduction in volume of the bronze as the tin is depleted.

It can also be seen that there is a reduction in length between regime 0 (unreacted wires) and regime 1, and between regimes 3 and 4. There also appears to be a small reduction in volume between regime 0 and 1. A change in the residual stresses within the wires caused by the heat-treatment is probably the cause of these reductions. Firstly, as the wires are heated up, residual stresses are produced because the constituent materials have different coefficients of thermal expansion. They are higher for copper and bronze than for niobium, so the axial stresses produced are compressive for the former and tensile for the latter. The stresses in the bronze, however, are relieved by a creep mechanism at the high temperatures. This stress relief causes the length of the wire to decrease because the axial tensile force on the niobium is reduced. Thus, this would tend to make the wires decrease in length because the expansion during heating is less than the contraction during cooling.

Curiously, there also appears to be a decrease in the filament diameter between regimes 8 and 9, the two longest heat-treatment regimes. This is also mirrored by a small decrease in wire volume and diameter, although this decrease is less than the measurement error. Such a decrease in filament diameter is hard to explain and may be experimental error. Further study would be required to confirm this observation.

For the measurement of wire length, each wire was measured separately. Therefore a measurement of the change in wire length was obtained for each of the 25 wires of each heat-treatment batch. The mean values and the scatter of the results within each batch are shown in Figure 4.7. The error bars represent 2 standard deviations above and below the mean (95% of the measurements made on the individual wire samples will lie within this range).

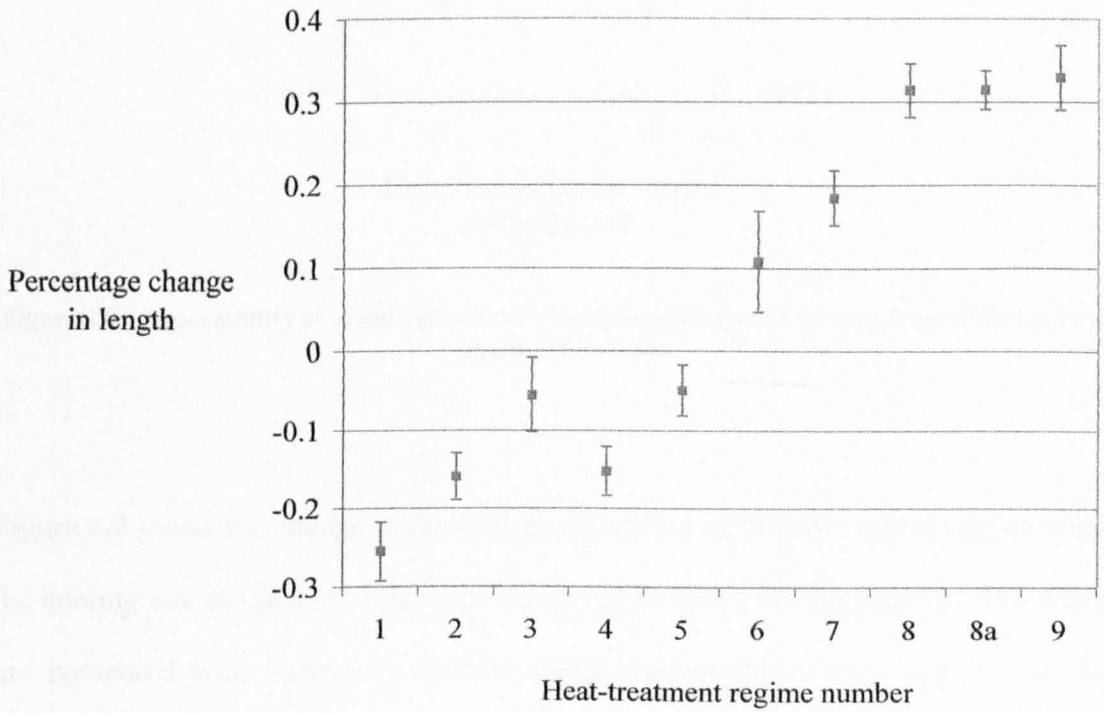

Figure 4.7 The scatter in the measurement of the change in wire length

Heat-treatment regime number 8 was carried out on two separate batches of wires in order to produce more samples required for the etching experiment described in Chapter 7. There was therefore an opportunity to compare the results from the two batches to see if any variation in results was being introduced by variations in how the heat-treatment was carried out. The results in Figure 4.8 show that there was no difference in the results from the two batches.

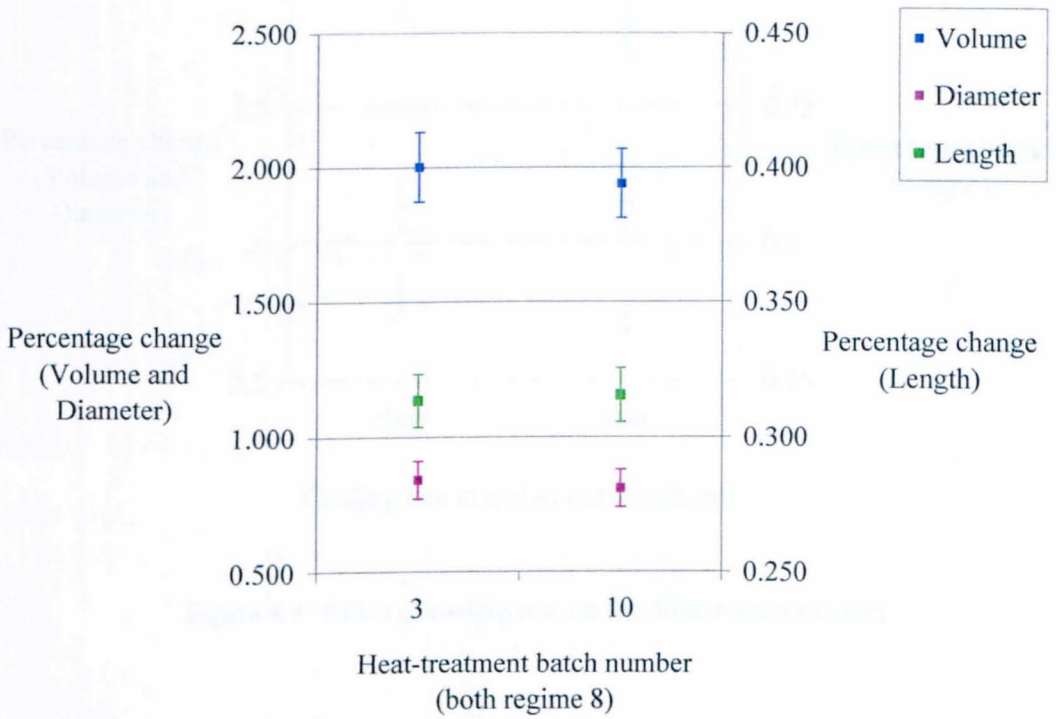

Figure 4.8 Repeatability of measurements of dimensional changes for wires from different heat-treatment batches

Figure 4.9 shows the change in dimensions caused by the heat-treatment regime where the cooling rate at the end of the heat-treatment was very fast (regime 8a). The results are compared with those of a heat-treatment regime with a slow cooling rate but identical in all other respects (regime 8). The regimes had long heat-treatment durations ensuring that a large proportion of the filaments would have been converted

to Nb_3Sn. Regime 8 is the heat-treatment recommended by the manufacturer to fully react the wire. It can be seen that the effect of the cooling rate on the changes to the wire dimensions was statistically insignificant, i.e. less than measurement error.

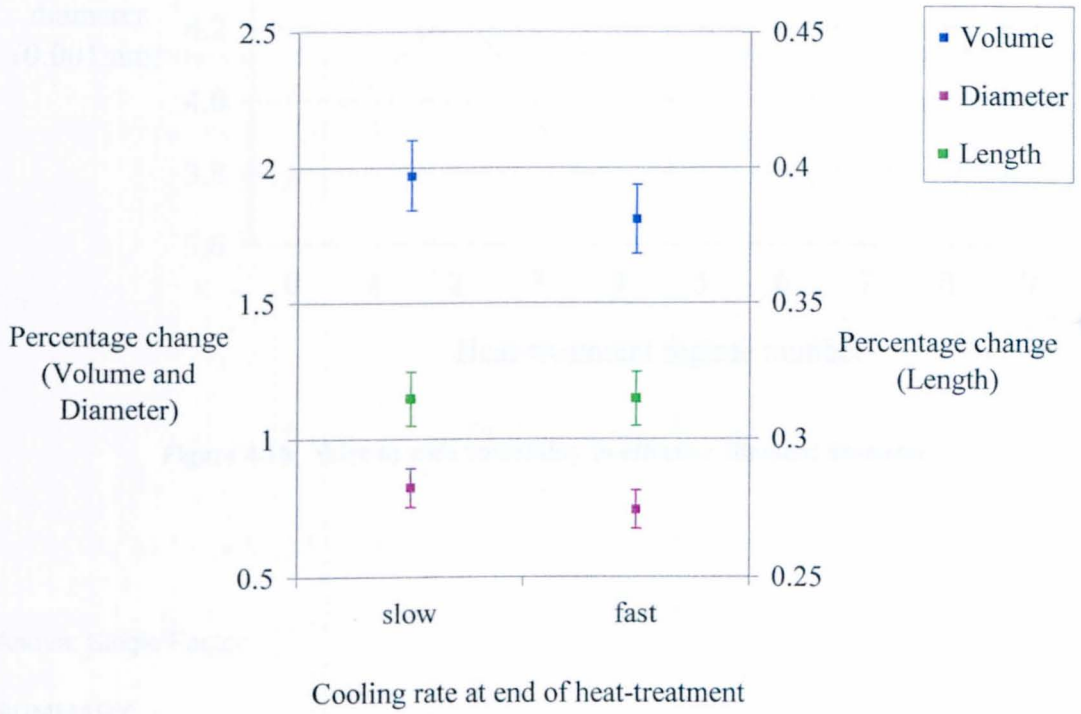

Figure 4.9 Effect of cooling rate on the dimensional changes

The measurement of effective filament diameter for each heat-treatment regime was obtained by taking the mean of the measurements from 3 wire samples from the batch. The spread of results between the 3 wire samples is shown in Figure 4.10. It can be seen that the wire to wire variation is quite large. The standard deviation between wires has been calculated by carrying out an Analysis of Variance, which is shown in Figure 4.11.

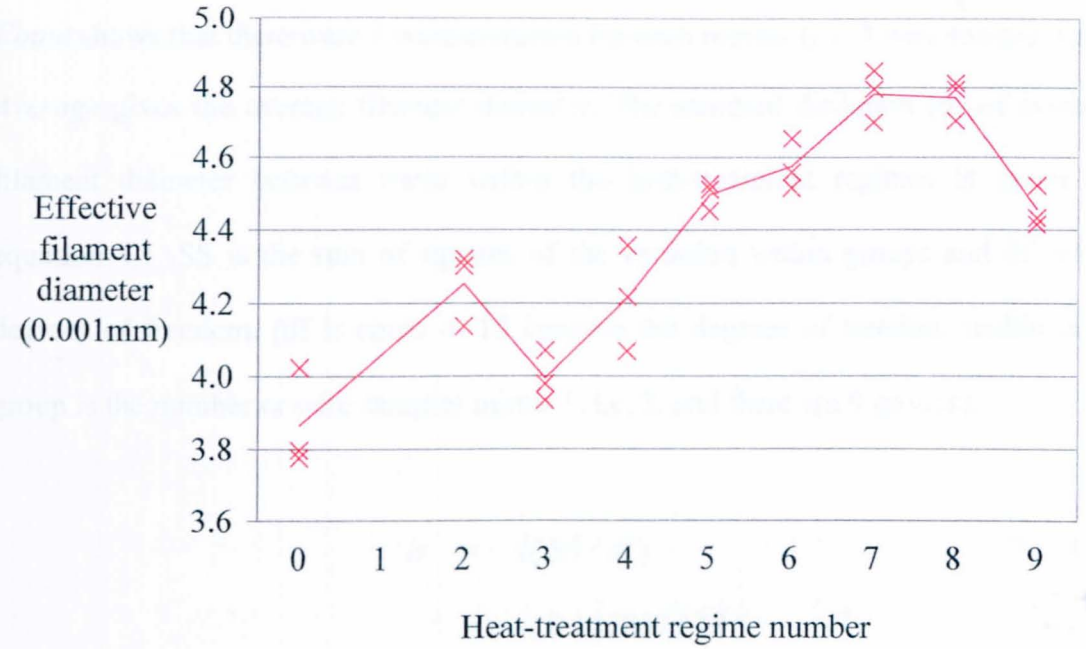

Figure 4.10 Wire to wire variability in effective filament diameter

Anova: Single Factor

SUMMARY

Groups	*Count*	*Sum*	*Average*	*Variance*
Row 1	3	11.58945	3.863151	0.018959
Row 2	3	12.75378	4.251259	0.010188
Row 3	3	11.97671	3.992237	0.004885
Row 4	3	12.63654	4.21218	0.020915
Row 5	3	13.48438	4.494795	0.001556
Row 6	3	13.7224	4.574134	0.004977
Row 7	3	14.33998	4.779993	0.005743
Row 8	3	14.30908	4.769694	0.00338
Row 9	3	13.36712	4.455706	0.003251

ANOVA

Source of Variation	*SS*	*df*	*MS*	*F*	*P-value*	*F crit*
Between Groups	2.49181	8	0.311476	37.95734	1.01E-09	2.510158
Within Groups	0.147707	18	0.008206			
Total	2.639518	26				

Figure 4.11 Analysis of Variance calculation

In Figure 4.11, *Row 1* to *Row 9* represent the 9 different heat-treatment regimes, *Count* shows that there were 3 measurements for each regime (i.e. 3 wire samples) and *Average* gives the average filament diameter. The standard deviation (σ) of average filament diameter between wires within the heat-treatment regimes is given by equation 4.1. SS is the sum of squares of the variation within groups and df is the degrees of freedom. (df is equal to 18 because the degrees of freedom within each group is the number or wire samples minus 1, i.e. 2, and there are 9 groups).

$$\sigma = \sqrt{(SS/df)} \quad (4.1)$$

$$= \sqrt{(0.147707/18)} \quad (4.2)$$

$$= 0.091 \text{ microns} \quad (4.3)$$

According to standard statistics theory, the 95% confidence interval of the mean is equal to ± 2 standard errors of the mean. The standard error of the mean (sem) is given by,

$$sem = \sigma/\sqrt{n} \quad (4.4)$$

where n is the number of wire samples measured for each heat-treatment regime.

Thus,

$$sem = 0.091/\sqrt{3} \quad (4.5)$$

$$= 0.052 \text{ microns} \quad (4.6)$$

Figure 4.6 shows the percentage change in filament diameter from the value for the unreacted wires (3.86 microns) rather than the actual filament diameter, so the 95%

confidence intervals (ci) shown by the relevant error bars have been calculated as follows:

$$ci = \pm\left(\frac{2\,x\,sem}{3.86}\right) x\,100 \tag{4.7}$$

$$= \pm 2.7\,\% \tag{4.8}$$

The effective filament diameter in the 3 regions (outer, middle and inner as shown in Figure 4.4) are shown in Figure 4.12. There is little difference in the filament size across the 3 regions for all the heat-treatment regimes. This indicates that tin starvation does not reduce the growth of Nb_3Sn in any particular region and that Nb_3Sn growth is uniform throughout the wire cross-section.

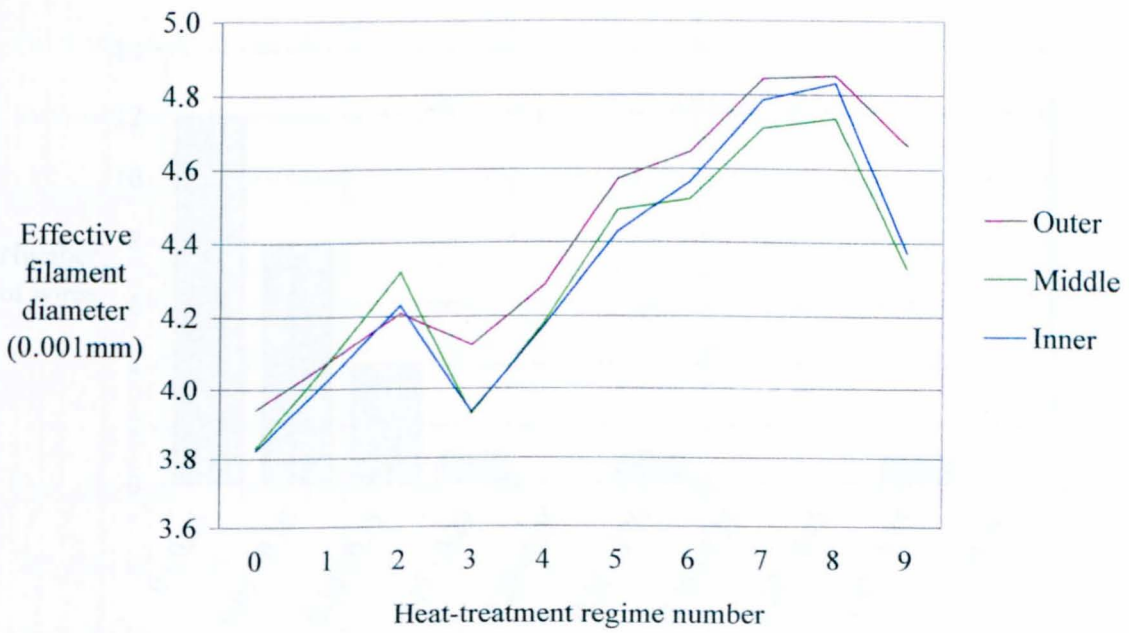

Figure 4.12 Effective filament diameter in different regions of the cross-section

The symmetry of the wires was also investigated by comparing the measurements of filament diameter in the outer, middle and inner regions on one side of each wire sample with the opposite side. Figure 4.13 is a histogram showing the asymmetry of all 27 wire samples that were analysed. There was no systematic variation in the asymmetry with increasing heat-treatment duration, so the results from all 27 wire samples have been analysed together. The figure shows that for the majority of the wires the symmetry was reasonably good. Approximately 90% have a difference in filament diameter on opposite sides of less than 0.2 micron or 5% of the average filament diameter. The largest asymmetry measured was 0.41 micron or 10% of the average filament diameter. It should be remembered that the diametric line on which the 6 regions were located was selected at random. Therefore, only asymmetry in one direction has been measured. The true asymmetry will therefore be somewhat worse than the measurements show.

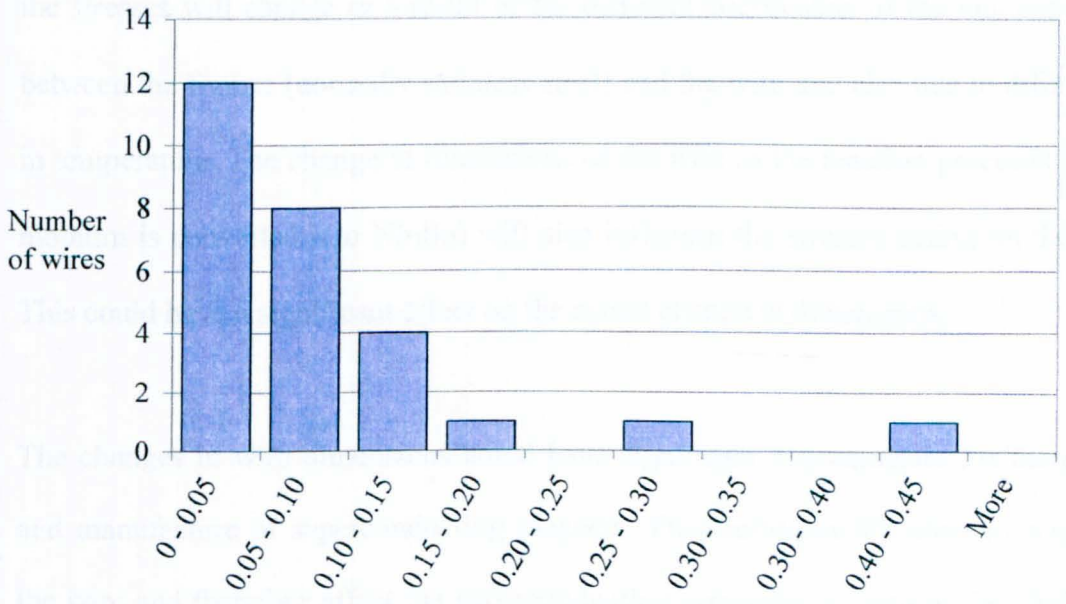

Figure 4.13 Asymmetry in effective filament diameter across the wires

The variation in effective filament diameter within each of the separate regions was similar for all regions and heat-treatment regime. The average standard deviation of all 162 regions was 0.16 micron.

4.6 Conclusions

Wire length, diameter and volume generally all increased as a result of the heat-treatment process. When given the heat-treatment recommended by the wire supplier (regime 8), the increase in length, diameter and volume was 0.3, 0.8 and 2.0% respectively. However, the wires were not subjected to any applied loads or restraints during the heat-treatments given as part of this research. This will not normally be the case in practice. For the common "wind and react" manufacturing process, the wire will be subjected to the axial tension and transverse compression from the winding process. Then, as the temperature ramps up at the start of the heat-treatment process the stresses will change as a result of the different coefficients of thermal expansion between the former (normally stainless steel) and the wire and also due to differences in temperature. The change in dimensions of the wire as the reaction proceeds (as the niobium is converted into Nb_3Sn) will also influence the stresses acting on the wire. This could have a significant effect on the actual change in dimensions.

The changes in wire dimensions could have significant consequences for the design and manufacture of superconducting magnets. They influence the stresses acting on the wire and therefore affect the superconducting properties as well as the likelihood of quenches occurring during magnet operation. The increase in length will tend to make the wire become loose on the former and between layers within the coil. The

increase in diameter will tend to have the opposite effect, increasing transverse compressive stresses between layers and also increasing axial tension. Other factors also have an influence on the tightness of the wire in the coil after the heat-treatment process. These include the material and design of the former onto which the coil is wound, the winding configuration, how much space there is between adjacent turns and the material and thickness of any winding mat or paper that is sometimes used between layers.

CHAPTER 5

Measurement of mechanical properties

5.1 Introduction

To understand how superconducting wires perform under the loading they experience, it is desirable to know the mechanical properties at 4 K, the operating temperature of most low temperature superconducting magnets. Facilities for testing at 4 K were not available and were beyond the budget of the project. In any case, testing at 4 K is very difficult and results therefore generally suffer from significant measurement error. It was therefore concluded that the best approach would be to obtain good data of the properties at room temperature and 77 K and to use extrapolation to obtain the properties at 4 K. The data at room temperature and 77 K would also be useful in their own right for verifying the F. E. models presented in Chapter 6. The mechanical properties were obtained by tensile testing; the apparatus, experimental method and results are presented in this chapter. Some of the content of this chapter has been published previously in Harvey, Fellows, Durodola, Vázquez-Navarro and Twin (2005), Harvey, Fellows, Durodola and Twin (2005) and Harvey et al. (2006).

5.2 Experimental challenges

Obtaining accurate measurements of the mechanical properties of superconducting wires (primarily elastic modulus, yield strength and stress-strain curve) presents a considerable experimental challenge. One problem is the small diameter of the wires, typically in the range of 0.4mm to 1.5mm. The wires have to be handled very carefully to avoid stressing them beyond the yield stress prior to testing them as this would affect the results. The yield stress is generally very low exacerbating the problem. Measuring the strain on such small diameter wires is also problematic. The weight of even the smallest extensometers can cause the wires to bend. If there is any

bend in the wire specimen, the measurement of strain will generally be erroneous. The specimen will appear to be less stiff than in reality because the strain measurement will include the strain associated with the sample straightening out. The act of straightening out a wire specimen prior to a tensile test will stress parts of the wire beyond the yield stress, thus affecting the results. Straightening out a wire specimen during the test will result in uneven stresses across the cross-section. One side of the wire will experience higher tensile stress than the average. Local yielding could therefore occur at stresses much lower than the yield stress. It is therefore desirable to have straight wire specimens for testing. In practice, however, superconducting wire comes wound on a spool and therefore has a residual curvature.

Fitting extensometers onto the wires also presents serious difficulties. It tends to be a very delicate operation where the wires can easily be bent or stressed beyond the yield point in the process. Another problem is that heat-treated Nb_3Sn superconducting wires are very brittle, making handling even more difficult. Wire samples can easily be broken by the application of a small bending moment. Even if complete fracture does not occur, some filaments may fracture within the wire sample thus affecting the results of the test.

The tensile testing apparatus and method were chosen and developed to meet these experimental challenges as best as possible.

5.3 Tensile testing apparatus and method

A Mayes 100 servo-hydraulic machine fitted with a 5kN loadcell was used for the tensile testing. This is shown in Figure 5.1. The loadcell was placed between a universal joint and the test specimen. This ensured that only axial loads were transmitted through the loadcell and was necessary because of the small cross-section of the test specimens. If the loadcell was not fitted in the way described, any slight misalignment of the test specimen from the axis of the machine would have resulted in a bending moment being transferred to the loadcell, and a significant error in the load reading could have been produced.

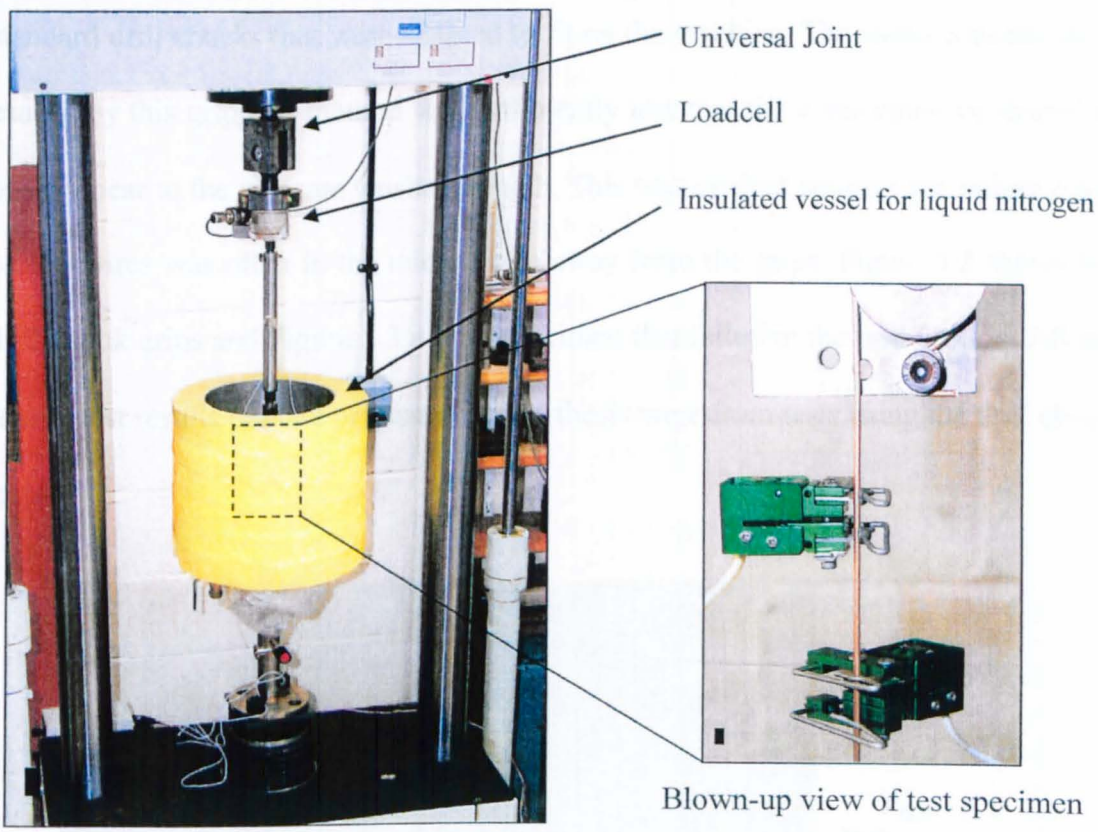

Figure 5.1 Tensile testing apparatus

An extension rod was fitted directly under the loadcell to keep it away from the liquid nitrogen, as a change in the loadcell temperature could have affected the readings. For

the room temperature tests, the vessel for the liquid nitrogen was removed to allow easier access to the test specimens. When the testing method was first being developed, the pulley grips as shown in Figure 5.1 were used. The test specimens used at this time were NbTi superconducting wire and stainless steel wire (the results of these tests are not presented here) and were sufficiently ductile that they could be wrapped around the pulleys. An advantage of using pulley grips is that they don't introduce significant stress concentration points and therefore enable the ultimate tensile strength to be measured. To test brittle Nb_3Sn superconducting wires, however, pulley grips are not suitable because it is not possible to wrap the wire around the pulleys. An alternative gripping method was developed for testing brittle wires using standard drill chucks that were adapted to fit on the machine. The stress concentration caused by this gripping method was sufficiently low that the wires could be loaded to or very near to the ultimate tensile strength. This was evident because the failure point on the wires was often in the mid-section away from the grips. Figure 5.2 shows the drill chuck grips and Figure 5.3 a wire specimen that failed in the mid-section. All the tensile test results that are presented in this thesis were from tests using the drill chuck grips.

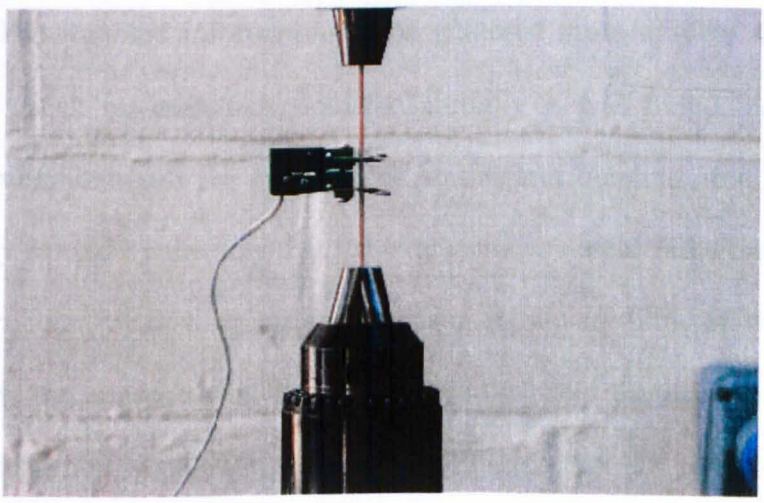

Figure 5.2
Drill chuck grips

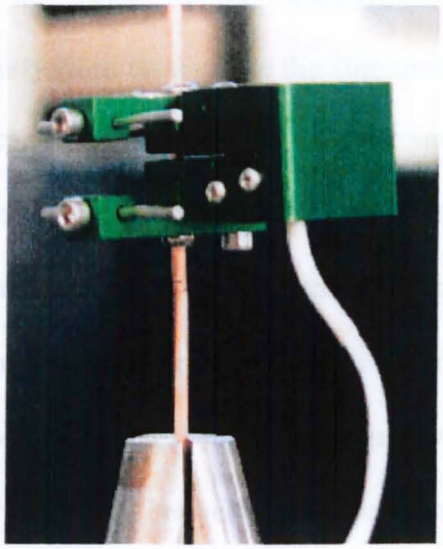

Figure 5.3
Photograph showing the location of a failure point

For measuring the strain, miniature extensometers weighing only 8 g were attached to the test specimens, as shown in Figure 5.1. The extensometers were produced by Epsilon Technology Corporation from Jackson, Wyoming, USA. It was desirable to use small and lightweight extensometers because the larger the size and weight, the more the measurement is distorted by causing the wire specimens to bend. This is particularly the case at the start of the tensile test when the axial load is low. Whenever possible two extensometers were used, although as they were being shared with Oxford Instruments, for some of the testing only one was available. The advantage of having two was that two sets of strain data could be obtained from each test. This enabled information to be gathered more quickly as well as providing a cross check on each extensometer. Initially it was found that there was a lot of variability between the two sets of strain data obtained, but this was found to be largely caused by the way that the extensometers were fitted onto the wire specimens. In particular, by how square the extensometers were fitted on the wire specimens and also by the alignment of the spring clips that held the extensometers on the wire. It was important to position the spring clips such that the point of contact between the spring clip and the wire was adjacent to the knife edges. If the contact points were not

aligned, the slope of the stress-strain curve obtained from the test differed significantly from tests where the alignment was good, particularly at the beginning of the curves. However, because of their small size, it was not an easy task to fit the extensometers as described. After considerable practice, however, it was found that the difference in the results obtained from the two extensometers on a single wire specimen was considerably less than the difference between separate wire specimens. It therefore became less important to use two extensometers and also indicated that the variability obtained between wire specimens was not a result of variations in the way the extensometers were attached. The delicacy of the extensometers meant that just by normal handling it was possible to distort them slightly such that the gauge length would change. Because of this, the gauge lengths were measured and the extensometers were re-calibrated at quite regular intervals, approximately once per week. Calibration was done at room temperature using a specialised tool for calibrating extensometers made by Instron. According to the extensometer manufacturer, the calibration at liquid nitrogen temperature would be within 2% of the room temperature calibration, and so the room temperature calibration was used for the liquid nitrogen tests as well.

A strain rate of approximately 400 microstrain/second was used for all the tensile tests apart from those that were carried out to investigate the effect of the strain rate. To investigate the mechanical properties for wires that experience some cyclic loading, as could be the case in practice, the stress and strain were measured over several load cycles with the load being increased on each cycle. The first load cycle was taken to a load just above the yield stress. This produced several hysteresis loops. Another advantage of doing the tests this way was that the elastic modulus could be measured

accurately. This was because the linear slope associated with elastic deformation could be measured at the start of each of the loading and unloading sequences.

When clamping the wire specimens in the drill chuck grips, care had to be taken not to transmit any significant load to the specimens. The wires being investigated had very low yield points meaning that plastic deformation would occur at loads as low as about 40N. For the same reason, any bending also had to be avoided. To keep the load as close to zero as possible the testing machine was put into 'standby load' just before the second drill chuck clamp was tightened up. In practice, the standby load had to be set to a low value of tensile force to prevent the control going unstable. A value of around 10N was used, which was maintained by the machine's digital controller as the drill chuck was tightened up.

The measurements of load, stress, machine displacement, and strain were captured using Spider-8 data-logging equipment and software supplied by HBM GmbH, Darmstadt, Germany. The data was exported to Excel (spreadsheet software by Microsoft Corporation, USA) for analysis.

5.4 Specimen preparation

A requirement of the wire specimen preparation was to make them as straight as possible. There were two reasons for this. Firstly, the brittle reacted wires would fracture if they experienced even a slight bending load. If the wires were bent at the start of the tensile test they would experience bending loads as well an axial load. This would cause them to fracture at relatively low loads. Secondly, for the accurate

measurement of strain, the extensometers needed to be attached to straight portions of wire. The wire used for this project was supplied in the form of a continuous length wrapped onto a spool and because of this had a residual curvature when unwrapped. The radius of this residual curvature was approximately 50cm. The wire specimens that were to be heat-treated were straightened by hand. This was done carefully so as not to overstrain the wire at any particular point. Interestingly, it was found that after the wires had been straightened out, a significant proportion of the original curvature would recover if the wires were left for a few minutes or more. This indicated that a degree of creep deformation was taking place at room temperature. It was found that the wires had to be straightened approximately 3 times before they would remain sufficiently straight (sufficiently straight was considered to be when the deviation was no more than approximately ±1mm along the 175mm length). The act of straightening the wires would have changed the mechanical properties to a certain extent by introducing some work hardening and changing the residual stresses. This probably would not have affected the mechanical properties, however, because of annealing during the heat-treatment. Only the wire specimens that were not heat-treated were not straightened prior to tensile testing. However, the act of clamping the specimens in the drill chuck clamps had the effect of straightening them. There was therefore no concern that the extensometers would give unreliable results as a result of the wires being bent. The bending moment acting on the wires to hold them straight would have produced an axial stress gradient across the wire cross-section, compressive on one side and tensile on the other. It was considered that this would be better than straighteneing the wires by hand prior to testing as this would introduce work hardening and change the residual stresses.

The wire specimens were cut from the spool and randomised before being divided up into the different batches for heat-treatment. To prepare the specimens for tensile testing, about 10mm were cut off the ends in case there were any end effects on the mechanical properties. The remaining length was then cut in half. One half was used for the tensile test and the other half was kept for future reference.

5.5 Data processing techniques

The elastic modulus of each of the wire specimens was obtained by measuring the linear slope of the stress-strain curve over the regions where the deformation was purely elastic. These elastic regions were at the start of each of the loading sequences as well as the start of each of the unloading sequences (it was found, in some cases at least, that the slope at the start of the first loading sequence was a little less than for the subsequent loading and unloading sequences and so was disregarded). The elastic regions, however, were very short and so to aid the measurement the slope of the stress-strain curve was plotted against strain. The slope at each point was calculated using the average stress and strain values over a fixed number of measurement points before and after the point in question. It was then relatively easy to read off the value of the modulus over each of the appropriate regions. Figure 5.4 illustrates this technique.

There are a number of discontinuities in the slope of the stress-strain curve, which occur at the points where the loading changes direction. The elastic modulus can be seen to be fairly consistent at the start of all of the loading and unloading sequences and is approximately 115GPa in this particular specimen.

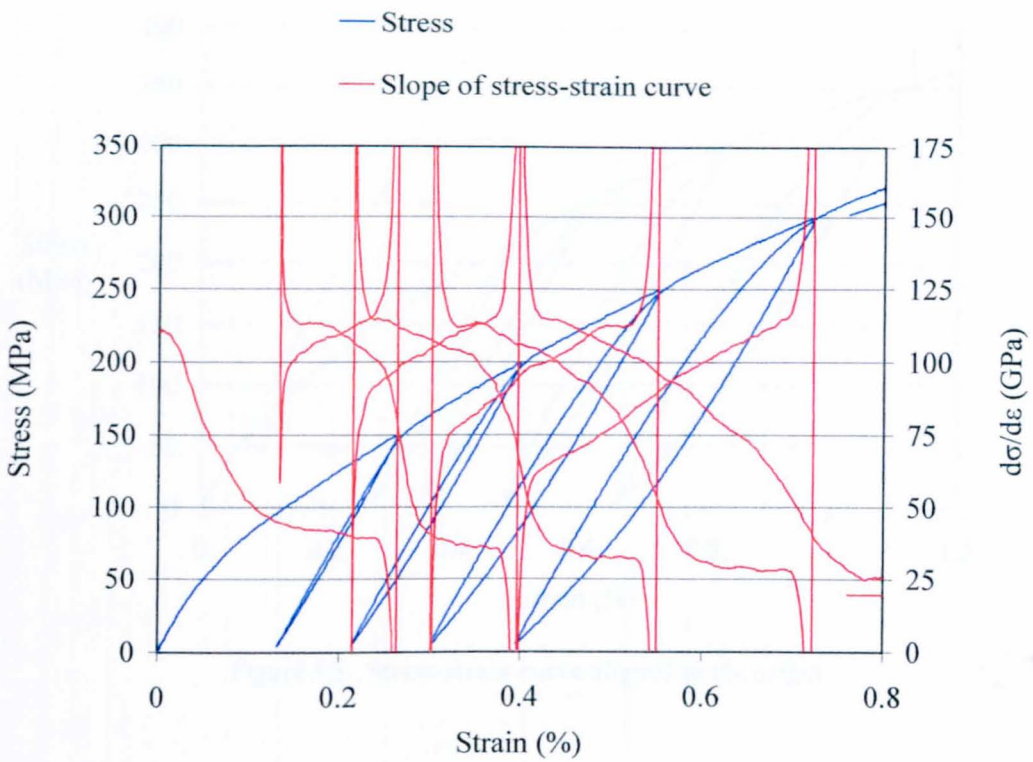

Figure 5.4 Example of graph used for the measurement of the elastic modulus

The elastic modulus obtained by the method described in the preceding section was used in a second data processing technique; to align the stress-strain curve to the origin. This was necessary because the start point for the test was not actually zero stress due to the small amount of tension required to maintain load control and to prevent the load going negative which would cause the wire to buckle. Also, the strain measurement was more susceptible to error at the start of the test when the load is low. This is because the wire specimen is not pulled straight and is also quite flexible when subjected to bending loads. At higher loads the tensile force pulls the wire specimen straight and prevents it bending under the weight of the extensometers or because of any slight misalignment in the way the extensometers were attached. The method used to align the curves to the origin is illustrated in Figure 5.5.

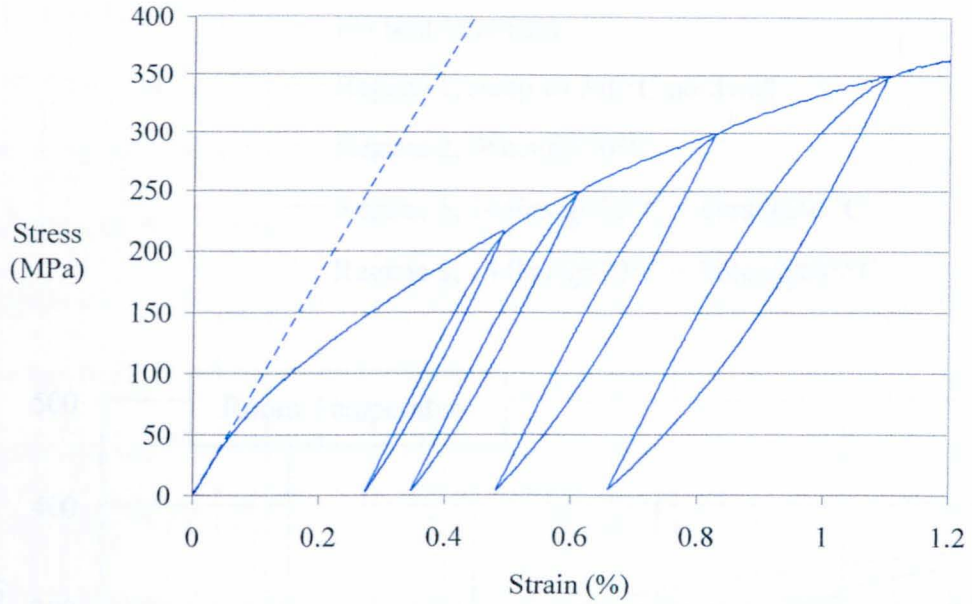

Figure 5.5 Stress-strain curve aligned to the origin

It was assumed that the slope at the start of the stress-strain curve should be equal to the elastic modulus obtained by the method described in the preceding section. A straight line from the origin and with the slope of the elastic modulus was added to the stress-strain graph. If this line did not appear to be tangential to the stress-strain curve, the curve was shifted to the left or right on the graph to the position of best fit with the Elastic Modulus line. This was done by simply adding or subtracting the appropriate value to or from all the strain readings.

5.6 Results

5.6.1 Stress-strain curves

Figure 5.6 shows the influence of the heat-treatment process on the mechanical properties at room temperature (approximately 300K) and at liquid nitrogen temperature (77K).

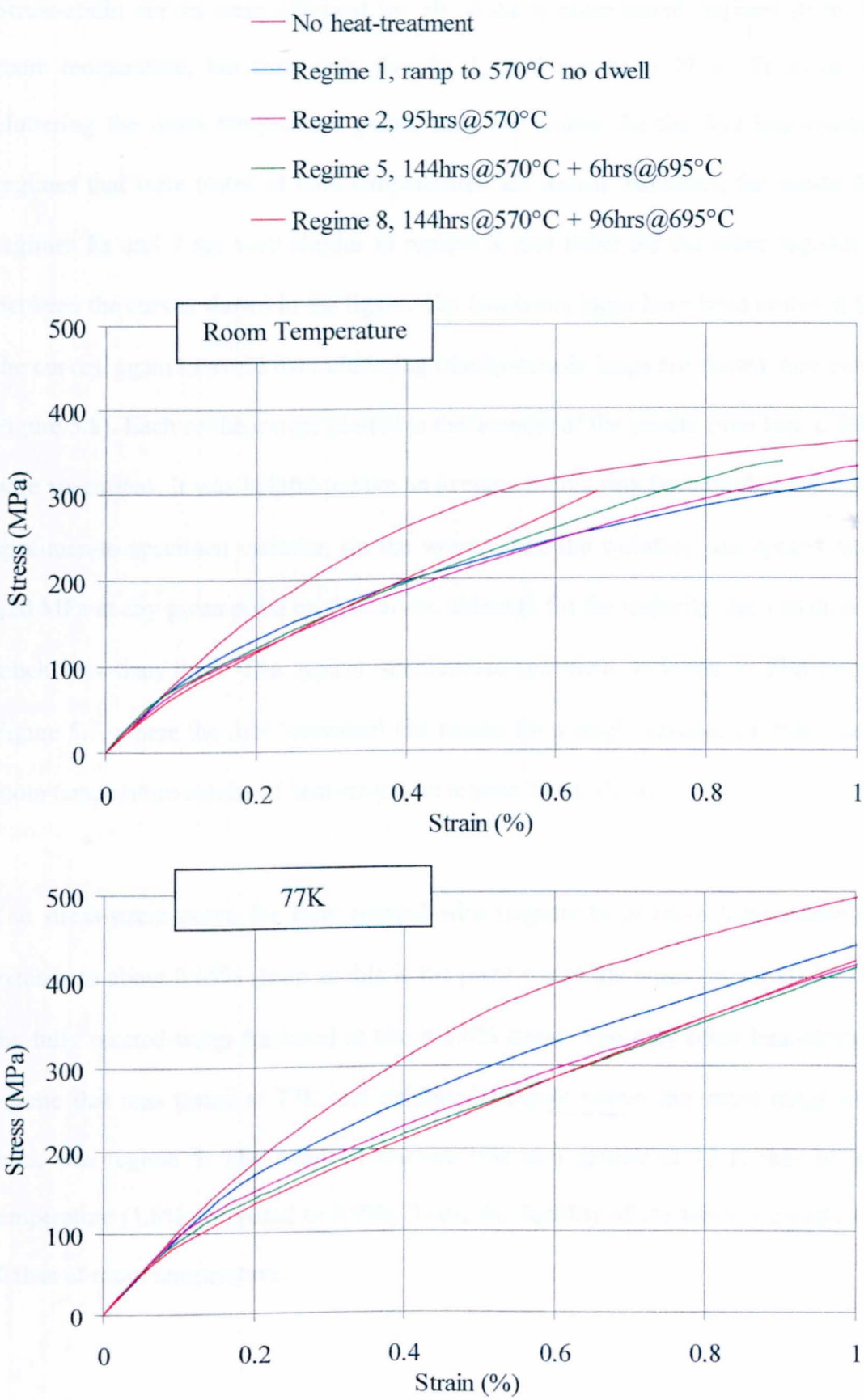

Figure 5.6 Effect of the heat-treatment process on the mechanical properties

Stress-strain curves were obtained for all of the heat-treatment regimes (0 to 9) at room temperature, but from only five (0, 1, 2, 5 and 8) at 77 K. To avoid over cluttering the room temperature graph, only the results for the five heat-treatment regimes that were tested at both temperatures are shown. However, the results from regimes 8a and 9 are very similar to regime 8, and those for the other regimes fall between the curves shown in the figure. The hysteresis loops have been removed from the curves, again to avoid over cluttering (the hysteresis loops are shown, however, in Figure 5.8). Each of the curves plotted is the average of the results from four different wire specimens. It was helpful to take an average in this way because there was some specimen-to-specimen variation (in the worst cases, the variation was approximately ±20 MPa at any given point on the curves, although for the majority, the variation was much less than this). The typical specimen-to-specimen variation is illustrated in Figure 5.7, where the four individual test results for a single variable (in this case the room temperature results of heat-treatment regime 2) are shown.

The stress-strain curve for fully reacted wire (regime 8) at room temperature only extends to about 0.65% strain as this is the point where the wires fractured. At 77 K, the fully reacted wires fractured at about 1.0% strain. The only other heat-treatment regime that was tested at 77K and exhibited fracture within the strain range of the tests, was regime 5. The strain at fracture was also greater at 77 K than at room temperature (1.6% compared to 0.9%). Thus, the ductility of the wires is greater at 77 K than at room temperature.

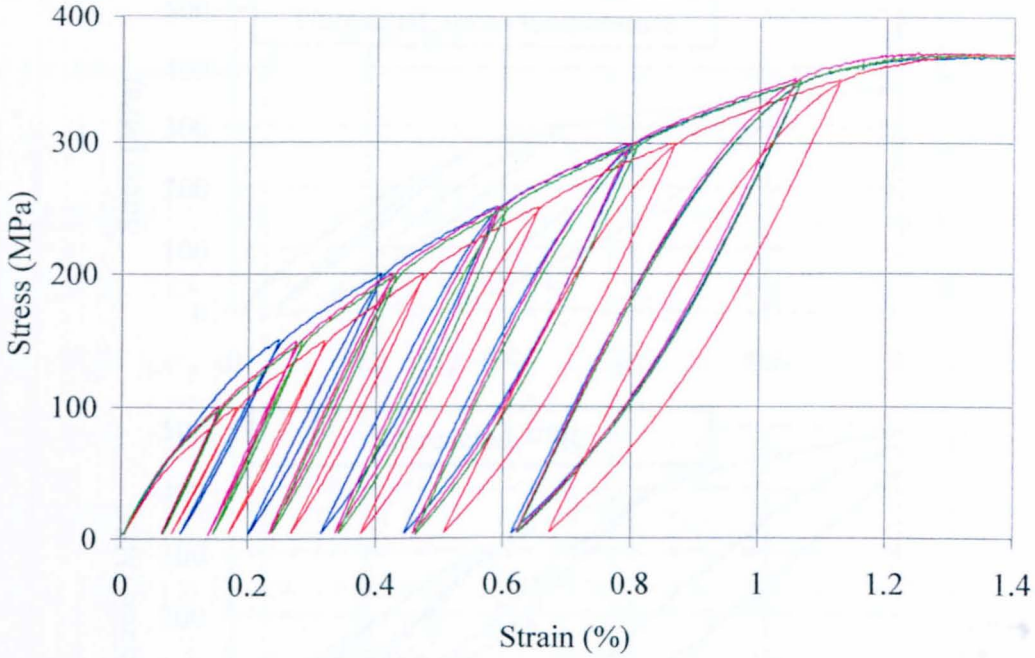

Figure 5.7 Graph showing the specimen-to–specimen variation in results

Stress-strain curves obtained from some of the individual tensile tests are shown in Figure 5.8. These curves show the hysteresis loops produced by the loading and unloading cycles carried out during the tests. The general pattern of these hysteresis loops is similar for all the heat-treatment regimes.

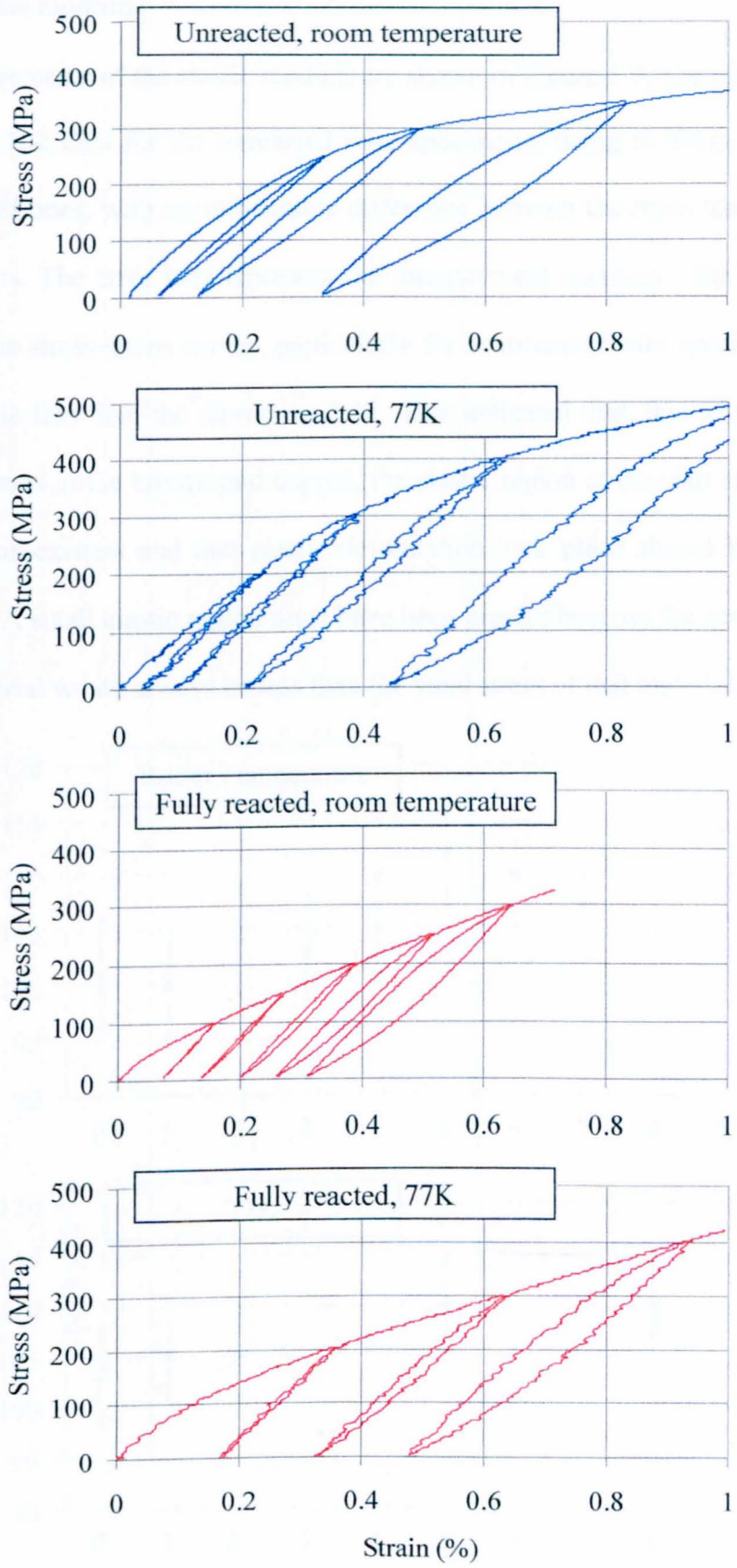

Figure 5.8 Stress-strain curves showing loading and unloading cycles

5.6.2 Elastic modulus

The measurements of the elastic modulii are shown in Figure 5.9. The elastic modulus was about 102 GPa for the unreacted wire specimens, rising to about 110 GPa for fully reacted ones, with no measurable difference between the room temperature and 77 K results. The error bars represent the measurement accuracy. The slopes at the origin of the stress-strain curves, particularly for heat-treated wire specimens, tended to be a little less than the elastic modulii. This indicated that, due to residual axial tensile stresses in the bronze and copper, the elastic region at the start of the test was virtually non-existent and that plastic deformation took place almost from the very beginning. A small elastic region must have been present because the residual stresses in any material would always be less than the yield stress of that material due to creep.

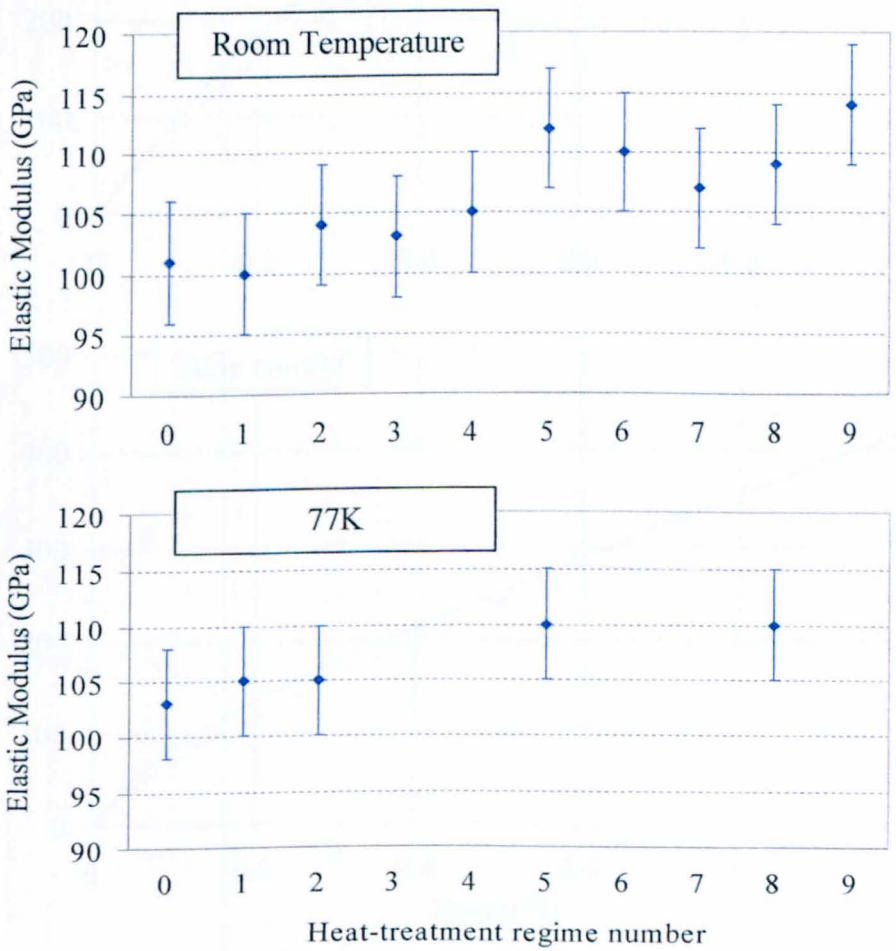

Figure 5.9 Effect of the heat-treatment process on the elastic modulus

5.6.3 Effect of temperature

The effect that the temperature had on the results is shown in Figure 5.10, where the stress-strain curves obtained at both room temperature and at 77 K are plotted on the same graphs. Each curve represents an average of the results from tests on four wire specimens.

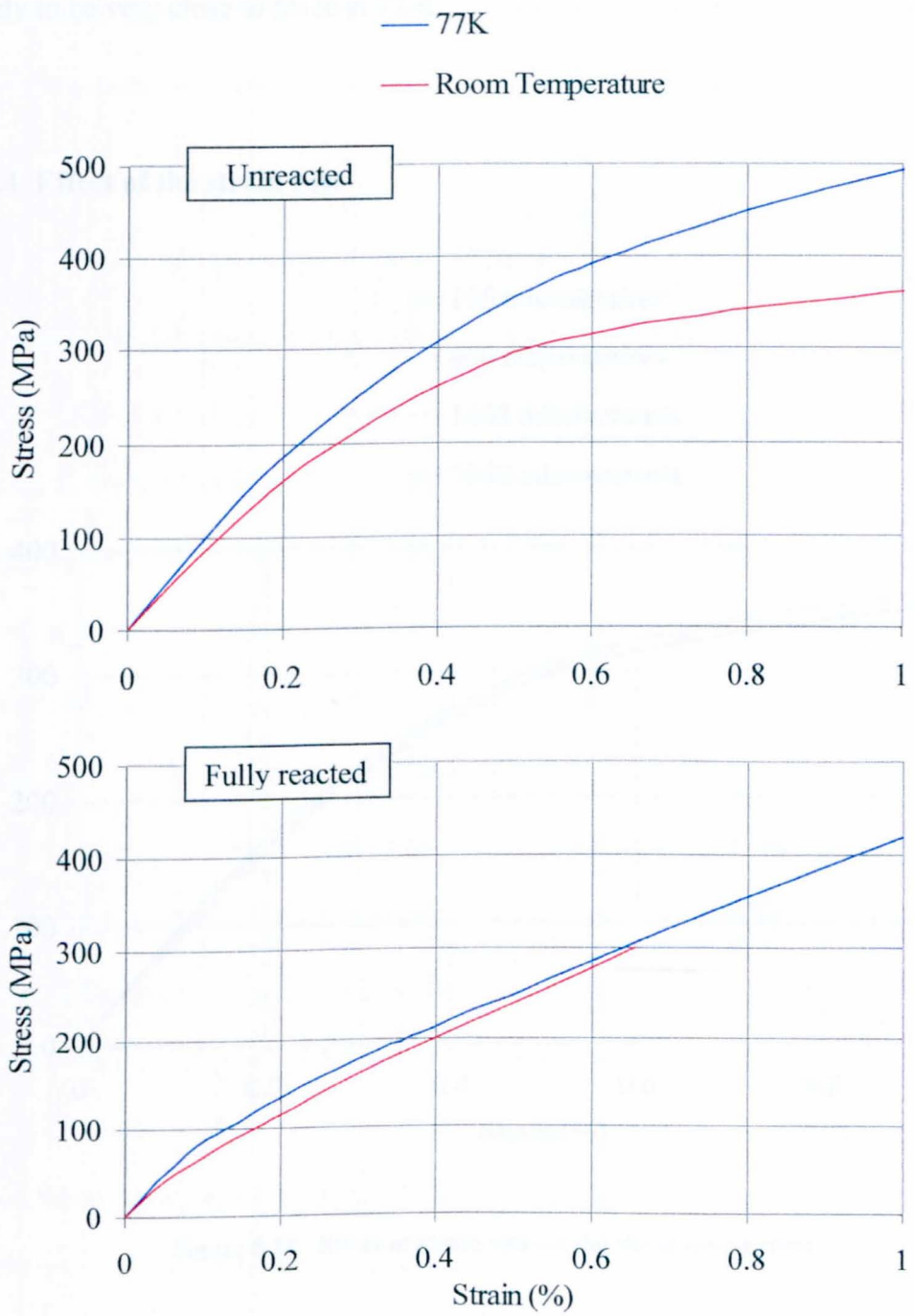

Figure 5.10 Effect of temperature on the mechanical properties

Interestingly, Figure 5.10 shows that for fully reacted wire specimens, there is not a lot of difference between the mechanical properties at room temperature and 77 K. This suggests that the mechanical properties at 4 K, the operating temperature of Nb_3Sn superconducting magnets, could be estimated with quite a high degree of confidence by extrapolation from the results at 77 K. In fact, the properties at 4 K are likely to be very close to those at 77 K.

5.6.4 Effect of the strain rate

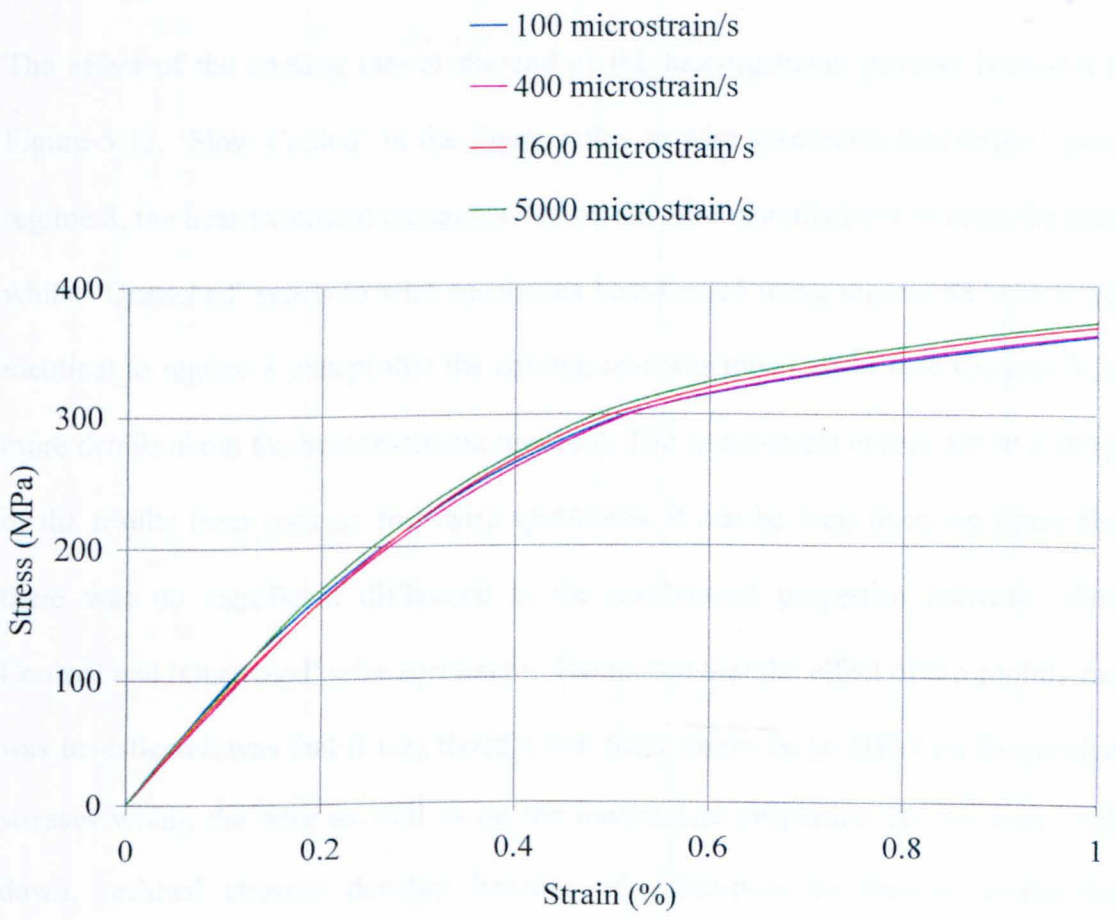

Figure 5.11 Effect of strain rate on the stress-strain curve

The effect that the strain rate used in the tensile tests had on the results is shown in Figure 5.11. Tensile tests were made on three wire specimens at each of the four different strain rates ranging from 100 to 5000 microstrain per second. Once again the wire specimens and the order of the tests were randomised. The curves plotted in the figure are an average of the six stress-strain curves obtained at each strain rate (3 tests multiplied by 2 extensometers). It can be seen that the strain rate does have an effect, but only a relatively small one over the range of strain rate investigated.

5.6.5 Effect of the heat-treatment cooling rate

The effect of the cooling rate at the end of the heat-treatment process is shown in Figure 5.12. 'Slow Cooled' in the figure refers to wire specimens heat-treated using regime 8, the heat-treatment recommended by the wire manufacturer to react the wire, whilst 'Quenched' refers to wire specimens heat-treated using regime 8a, which was identical to regime 8 except that the cooling rate was much faster (see Chapter 3 for more details about the heat-treatment regimes). The stress-strain curves are an average of the results from tests on four wire specimens. It can be seen from the figure that there was no significant difference in the mechanical properties between 'Slow Cooled' and 'Quenched' wire specimens. The reason that the effect of the cooling rate was investigated was that it was thought that there might be an effect on the residual stresses within the wire as well as on the mechanical properties. As the wire cools down, residual stresses develop because of differences in thermal contraction coefficients between the constituent materials of the wire. Time dependent creep will relieve these residual stresses during the cool-down, particularly at the start of the cool-down when temperatures are high. Although no noticeable effect was observed in the stress-strain curve, it is probable that the residual stresses were affected by the

cooling rate, but by not enough to significantly alter the stress-strain curve. It has already been shown (Figure 5.10) that for fully reacted wire specimens there is only a small difference in the mechanical properties at room temperature and 77 K. The residual stresses are, however, known to be significantly different at the two temperatures. Knowledge of the residual stresses is of particular interest because the superconducting properties depend strongly on the stress within the Nb_3Sn filaments.

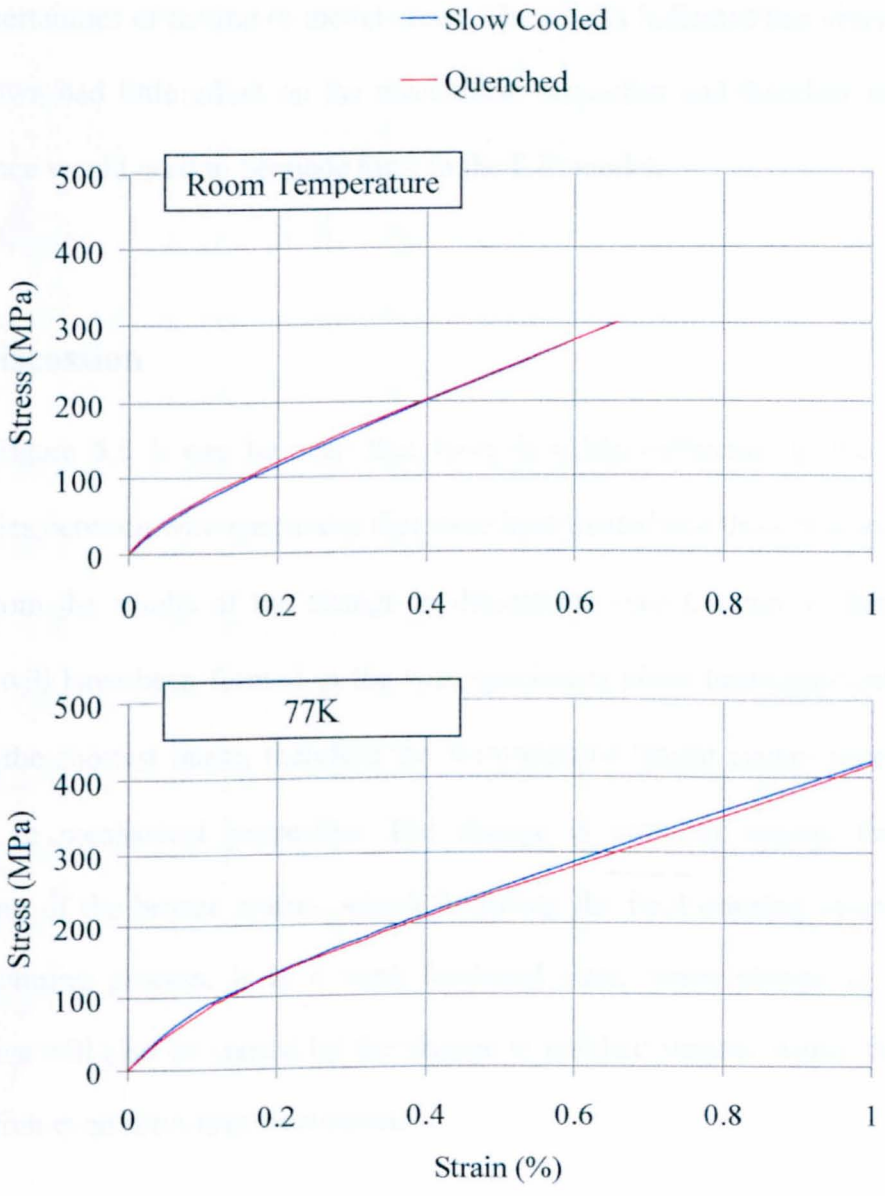

Figure 5.12 The effect of the cooling rate on the mechanical properties

Another reason for investigating whether the cooling rate had any effect on the mechanical properties was to provide data for the development of the finite element models (see Chapter 6). Any attempt to try to model creep deformation within the wire as it cools down at the end of the heat-treatment would be prone to uncertainty. By cooling wire specimens as quickly as possible the effect of creep would be minimised, because of its time dependent nature. The residual stresses would effectively be locked-in. This data could then be used to verify the F.E. model without the uncertainties of having to model creep. The results indicated that creep during the cool-down had little effect on the mechanical properties and therefore only a small allowance would need to be made for it in the F.E. model.

5.7 Discussion

From Figure 5.6 it can be seen that there is a big difference in the mechanical properties between wire specimens that were heat-treated and those that were not. It is clear from the results of the change in dimensions (see Chapter 4) that very little Nb_3Sn will have been formed in the wire specimens given heat-treatment regimes 1 and 2 (the shortest ones), therefore the formation of Nb_3Sn cannot account for the change in mechanical properties. The change is probably mainly the result of annealing of the bronze matrix, which following the final drawing operation of the manufacturing process, is in a work hardened state. Some change in mechanical properties will also be caused by the change in residual stresses within the wire that result from even short heat-treatments.

For strains from zero to about 0.5% there is very little difference in the room temperature mechanical properties of the wire specimens given any of the heat-treatment regimes (except regime 0). And, excepting the unreacted wires and the shortest heat-treatment (regimes 0 and 1), the mechanical properties at 77 K are very similar for all the heat-treatment regimes up to about 1% strain. Thus, the mechanical properties remain reasonably constant despite the dramatic changes in the composition - the niobium filaments are completely converted into Nb_3Sn and the tin level within the bronze matrix is depleted from the initial 13 wt.% to approximately 5 wt.% after full reaction.

From Figure 5.8 it can be seen that the size of the hysteresis loops increases dramatically with increasing strain. This is evidence of increasing plastic deformation occurring during unloading. Some of the constituent materials of the composite wire have shorter elastic ranges than others, for example the copper has a shorter elastic range than the Nb_3Sn. During unloading the axial stress in all the materials reduces. For the materials with the shortest elastic ranges, the axial stress may fall below zero and become compressive. If this compressive stress exceeds the yield strength in compression, the resulting plastic deformation will cause the slope of the unloading curve to become less steep, leading to the formation of a hysteresis loop. The greater the amount of plastic deformation during unloading, the greater the size of the hysteresis loop.

5.8 Conclusions

1. The elastic modulus ranges from about 102 GPa for wires that were not heat-treated to about 110 GPa for fully reacted wires and is the same at room temperature and 77 K.

2. There is a significant difference in the mechanical properties of wires that were not heat-treated compared to those that had only short heat-treatments, which were insufficient to convert much of the niobium into Nb_3Sn. Annealing of the bronze matrix, which is in a work-hardened state prior to heat-treatment, is the major cause of the change in mechanical properties.

3. Apart from becoming more brittle, the mechanical properties do not change much for different durations of heat-treatment. There is very little difference in the stress-strain curves of wire specimens from all of the heat-treated batches (except the shortest heat-treatment at 77 K) up to about 0.5% strain at room temperature and 1% at 77 K. This is despite the fact that the composition changes dramatically from the shortest to the longest heat-treatment regime. Therefore, for this wire at least, the effect on the mechanical properties does not need to be considered when optimising the heat-treatment regime.

4. The mechanical properties of the fully reacted wire specimens were similar at room temperature and 77 K, suggesting that the properties at 4 K, the operating temperature of Nb_3Sn superconducting magnets, would be very close to those at 77 K.

5. The strain rate during the tensile tests, when in the range from 100 to 5000 microstrain per second, had only a small effect on the results.

6. The mechanical properties of wire specimens that were cooled rapidly at the end of the heat-treatment process were not measurably different from those that were cooled slowly.

CHAPTER 6

Finite element modelling

6.1 Introduction

Magnet designers are increasingly using modelling to help optimise the design of superconducting magnets. The models need to predict stresses and strains throughout the magnet when cooled down to its operating temperature of 4 K and subjected to the large forces that are produced when the magnet is energised. Models in the past have suffered from a lack of knowledge about the mechanical properties of the superconducting wire. Experimental testing of superconducting wire, such as that presented in Chapter 5, will help to increase this knowledge. It would also be useful, however, to be able to predict the mechanical properties by modelling the wire itself. Moreover, if the stresses and strains in the Nb_3Sn filaments could be modelled, the superconducting properties of the wire could then also be predicted. The benefit would be that the design of superconducting wire (constituent materials, volume fractions, positioning of the different constituent materials, etc) could be optimised quicker and at considerably less cost.

This chapter describes how the superconducting wire was modelled using the finite element method. A major factor influencing the validity of any model is how accurately the material properties are represented. An important part of the chapter is devoted to describing the material properties that were used, and where they came from. Finally, the results of the modelling work are compared with the experimental measurements, and the sensitivity to uncertainties in the model is assessed.

6.2 Description of the F.E. models and boundary conditions

The finite element package used for the modelling work was Ansys, which was available under a student license. Some earlier versions were used initially, but the majority of the work was with version 10. The reason that Ansys was used as opposed to an alternative package was that this was the application used by Oxford Instruments, the company sponsoring the project. Any models produced could then easily be transferred.

The finite element method is a numerical method that approximates a solution by dividing the medium of interest, in this case the superconducting wire, into discrete sub-divisions called elements. The solution should converge on the actual behaviour as the size of the elements is reduced. The solution within each element is assumed to be represented by an approximate continuous function. The complete solution is obtained by combining the individual solutions whilst allowing for continuity between elements, applying boundary conditions and solving for the unknowns. As is common when using the finite element method for structural analysis problems, Ansys uses a Lagrangian finite element formulation. This means that the elements move and change shape with the material is it deforms.

For the wire specimens used in the experiments, the length of the wire was much greater than the diameter. Therefore, any strain in the length direction would be planar, i.e. uniform across the cross-section. This would also be the case for superconducting wire used in practice. As there would be no variation in stress and strain in the length direction the models only needed to be one element thick. It was

necessary to have a 3D model, as opposed to a 2D one, because the stresses and strains needed to be modelled in all 3 directions.

The real wire had a manufactured twist in it such that the filaments spiral around the central core, one revolution every 3 cm. As the pitch of the twist was relatively long compared to the diameter of the wire, it was assumed that the mechanical properties would not be significantly different from a wire with no twist. Because of this and also because a model incorporating the twist would be considerably more complex, it was decided to model the wire with no twist.

The sole element type chosen to be used in the models was the quadratic 3D solid element denoted SOLID95. This is a 20 node element that can tolerate irregular shapes without much loss of accuracy. It is also well suited to model curved boundaries and can be tetrahedral as well as hexahedral.

The superconducting wire to be modelled was the same one used for the experimental investigations. This wire has 22866 Nb_3Sn filaments and so it was not practical to model a true representation of the cross-section. The models that have been produced are of simplified cross-sections. Other than the number of filaments, however, the models do represent the cross-section accurately in all other respects. In particular, the volume fractions of all the constituent materials are accurately reproduced. Due to the symmetrical nature of the wire it was possible to model only a 30^{o} wedge of the cross-section. The model that was closest to the true cross-section had the Nb_3Sn distributed in 618 filaments throughout the cross-section. These filaments obviously had to be much larger than the real filaments in order that the correct volume fraction was

maintained. The true cross-section has 618 bundles of filaments, with each bundle containing 37 filaments. Each of the 618 filaments in the model were located at the same positions as the bundles in the real wire. Due to the limit of nodes that a model could have with the Ansys student license, 618 was about the maximum number of filaments that could be modelled with a reasonable mesh density. Two other models were produced that had the Nb_3Sn distributed in 30 and 6 filaments. The effect of the number of filaments used in the model could be assessed by comparing the results from the three models. A judgement could then be made as to whether the results would be significantly different if a true representation of the wire cross-section with 22866 filaments could have been modelled. The three models are shown in Figure 6.1. The only major difference between the 3 models is the way that the Nb_3Sn is distributed within the bronze matrix.

The models were based on the volume fractions of the fully reacted wire. Thus, the area of the filaments was based on the total area of the Nb_3Sn filaments and not the area of the niobium filaments of unreacted wire. Some of the analyses that were carried out, however, involved modelling the heating up stage of the heat-treatment process, i.e. prior to the filaments being converted from niobium to Nb_3Sn. The area of the filaments was therefore about 37 % (Cave and Weir 1983) too large for these analyses, but as will be shown in the results section, the heating up stage has very little effect on the final mechanical properties. It was therefore not considered necessary to allow for the change in filament area in the models.

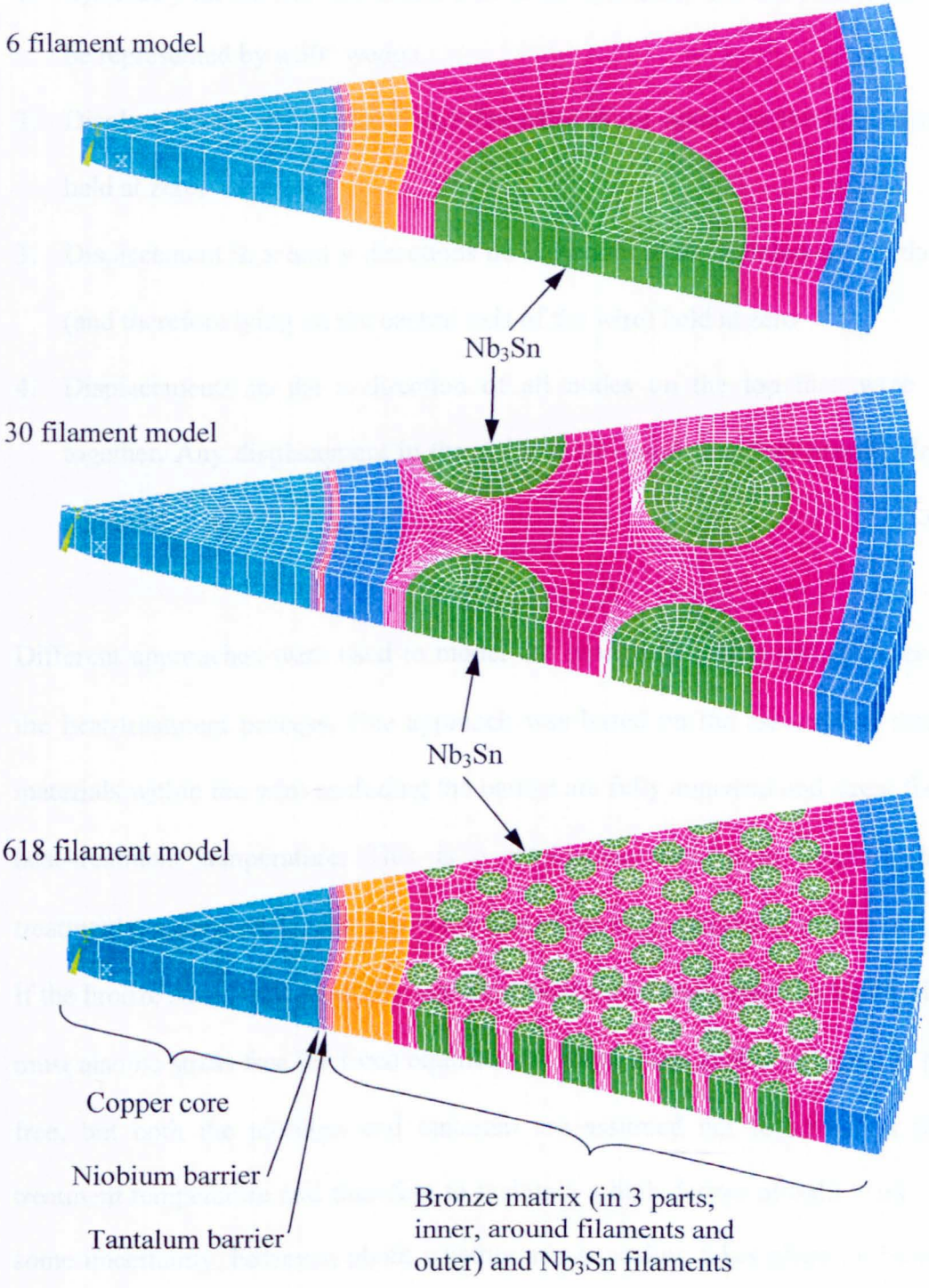

Figure 6.1 Finite element meshes used to model the superconducting wire

The boundary conditions applied to the models were as follows:

1. Symmetry on the two side faces. Due to the symmetry the full cross-section could be represented by a 30° wedge.
2. Displacement in the z direction (wire axis) of all nodes on the bottom face was held at zero.
3. Displacement in x and y directions on the nodes at the pointed end of the wedge (and therefore lying on the central axis of the wire) held at zero
4. Displacements in the z direction of all nodes on the top face were coupled together. Any displacement in the z direction would therefore remain planar and parallel.

Different approaches were used to model the changes in stress and strain caused by the heat-treatment process. One approach was based on the assumption that all the materials within the wire excluding the barrier are fully annealed and stress free at the heat-treatment temperature. This is a reasonable assumption because the heat-treatment temperature is well above the annealing temperatures of bronze and copper. If the bronze stress relieves at the heat-treatment temperature then the Nb_3Sn filaments must also be stress free for force equilibrium. The barrier is also assumed to be stress free, but both the niobium and tantalum are assumed not to anneal at the heat-treatment temperature and therefore to maintain a high degree of cold work. There is some uncertainty, however, about whether any annealing takes place in the niobium. Another approach takes into consideration that the stresses may not be completely relieved. This is because the heat-treatment temperature is not high enough to stress relieve the tantalum in the barrier and the stresses in the copper core may not stress relieve because they are largely hydrostatic in nature. There is an uncertainty with this

approach, however, because the residual stress of the pre-reacted wire is unknown. For simplicity, the wire is assumed to be stress free before heating the wire up to the heat-treatment temperature. At the heat-treatment temperature, or a little lower to allow for some creep (see below), the bronze and Nb_3Sn filaments are annealed and stress relieved. This is done by applying "Birth and Death" to the appropriate elements of the model.

The types of load steps used to model the heat-treatment process were as follows:

1. Temperature change. Either heating up or cooling down during the heat-treatment. Creep was allowed for by selecting a lower temperature. For example, to allow for creep during the cool-down at the end of the heat-treatment, the wire was assumed to be stress free until the temperature dropped below a certain value. The temperature change modelled would therefore be from the temperature below which creep was assumed not to take place, to room temperature.
2. Annealing and/or stress-relieving. This was done by applying 'Birth and Death' to the appropriate elements. The elements were killed prior to the annealing or stress-relieving taking place and afterwards the elements were born again. To anneal the elements, the material properties were changed at the time of their re-birth.

To obtain stress-strain curves from the models, a pressure was applied to the top surface of the model and the resultant strain was recorded. A negative pressure was applied to produce an axial tensile stress.

6.3 Analytical validation of model

A basic form of the finite element models was validated using an analytical solution. However, it was only possible to produce an analytical solution for a very simplified case. The simple case considered was a mono-filamentary wire, where the filament is located in the centre. Therefore, there were only two materials to consider and both were assumed to deform only elastically, i.e. no plastic deformation. Although, this was very different from the real multi-filamentary composite wire, it was possible to validate some of the key features of the model. The features that could be validated were as follows:

1. The use of symmetry in which the wire is modelled as a 30° wedge.
2. The boundary conditions where the bottom face is restrained in the z direction and the displacements in the z direction of the nodes on the top face were coupled together.
3. The method of applying a temperature change
4. The method for obtaining the stress-strain curve, i.e. applying a pressure to the top surface.

The analytical solution was based on the Lamé equation (Ross 1987). The full description of the analytical solution is given in Choy et al. (1995). The solution gives the 3 dimensional stresses and strains throughout the mono-filament wire produced by a temperature change and an applied axial load or strain. Using the material properties of copper and Nb_3Sn for the two materials, the finite element model was found to be in agreement with the analytical solution with less than 1 % error.

6.4 Material properties

There were 7 different materials used in the models as listed in Table 6.1:

Material	Location
Copper	Core
Niobium	Barrier (also filaments prior to reaction)
Tantalum	Barrier
Bronze	Matrix inner
Bronze	Matrix central
Bronze	Matrix outer
Nb_3Sn	filaments

Table 6.1 Materials used in finite element models

Three different bronze materials were used because the properties of the bronze vary depending on the location. The bronze that surrounds the filaments has a small grain size that is essentially dependent on the filament spacing. The bronze on the outside of the wire has a large grain size and probably a higher tin content than the bronze surrounding the filaments. The bronze close to the barrier layer has a large grain size and a tin content that is probably close to that of the bronze surrounding the filaments. Information about the grain size and tin content in the bronze after heat-treatment comes from Tang et al. (1981), McDonald et al. (1983), Markiewicz and Goddard (2002) and Tan et al. (2004).

The material properties used in the models are based on Mitchell (2005 *Cryogenics*). Mitchell's objective was to provide a complete and internally consistent set of data. He has produced an excellent resource, using a wide range of reference data.

However, as Mitchell himself recognised, appropriate measurements on copper and bronze are particularly sparse and also he did not take the effect of grain size into consideration. It was found that some of the values for yield stress and UTS given by Mitchell's equations do not agree very well with published data. Using the same reference that Mitchell used (Simon et al. 1992), more appropriate values of yield stress and UTS at room temperature and below have been used for this research.

6.4.1 Coefficient of thermal expansion

In Mitchell (2005 *Cryogenics*) thermal expansion is given by equations for the thermal strain relative to the length at a reference temperature. For example, for Nb_3Sn the thermal strain is given by

$$\Delta L/L = -0.187 + \left(5.490\times10^{-6}\,T\right) + \left(3.296\times10^{-9}\,T^2\right) - \left(8.261\times10^{-13}\,T^3\right) \qquad (6.1)$$

where ΔL is the change in length relative to the length at 293 K and T is the temperature in Kelvin.

Using these equations, the change in length relative to 968 K (the heat-treatment temperature) has been calculated for all the constituent materials and is shown in Figure 6.2.

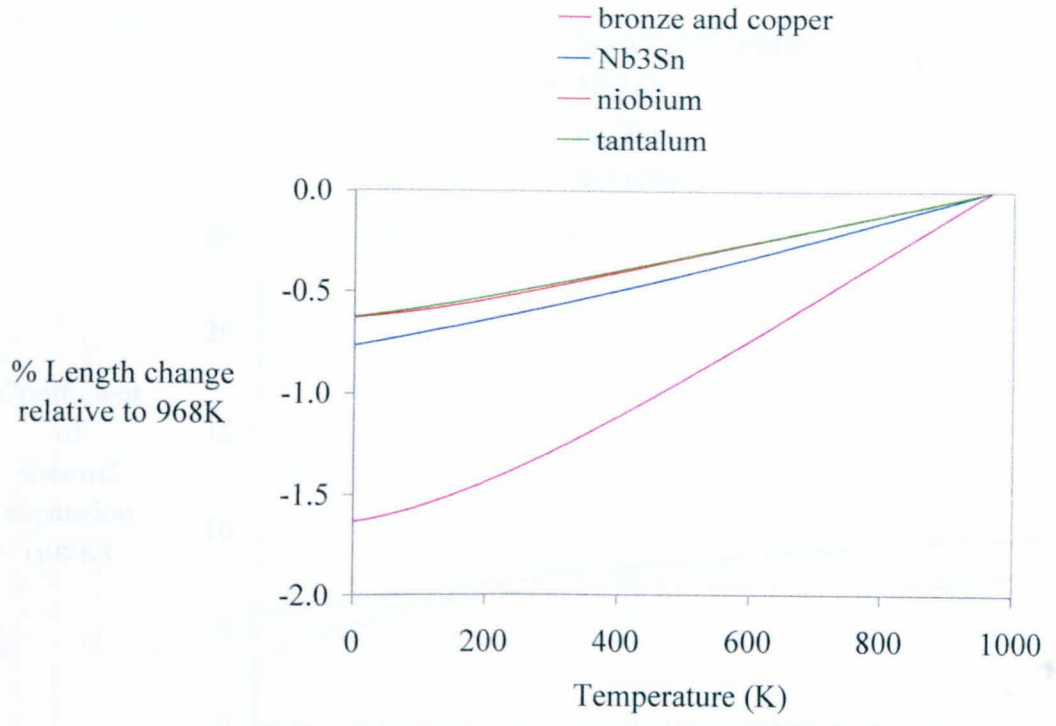

Figure 6.2 Thermal contraction of constituent materials

To obtain the coefficients of thermal expansion, α, the equations for thermal strain were differentiated with respect to the temperature T. Thus, for the Nb_3Sn example

$$\alpha = 5.490\times10^{-6} + \left(2\times 3.296\times10^{-9}\, T\right) - \left(3\times 8.261\times10^{-13}\, T^2\right) \qquad (6.2)$$

Figure 6.3 shows the coefficients of thermal expansion for all the constituent materials.

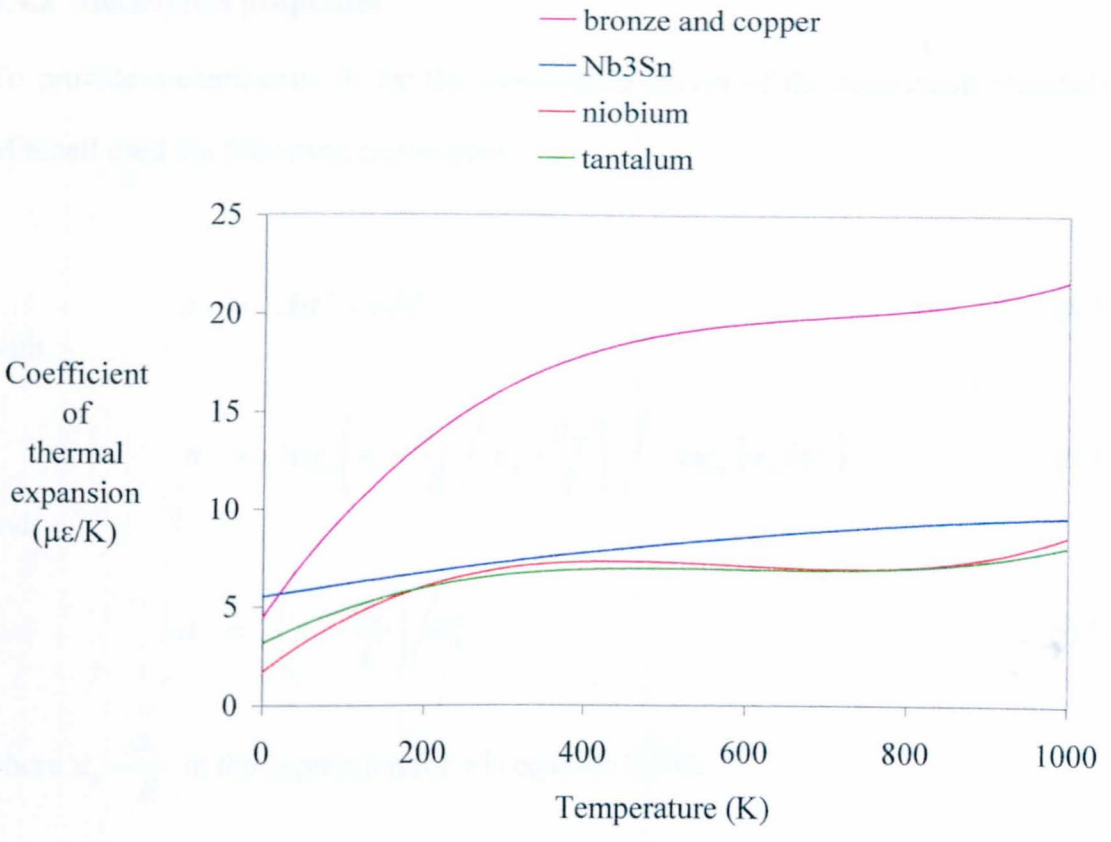

Figure 6.3 Coefficients of thermal expansion

The graphs in Figures 6.2 and 6.3 show the continuous variation with temperature, however, to describe the variation in properties with temperature within the F. E. software, the material properties were entered at only six discreet temperatures; 4, 77, 293, 500, 700 and 968 K.

6.4.2 Mechanical properties

To provide a continuous fit for the stress-strain curves of the constituent materials, Mitchell used the following expressions.

$$\varepsilon = A\sigma^n + \sigma/E \tag{6.3}$$

with

$$n = \log_e\left(\varepsilon_u - \frac{\sigma_u}{E} \Big/ \varepsilon_y - \frac{\sigma_y}{E}\right) \Big/ \log_e\left(\sigma_u/\sigma_y\right) \tag{6.4}$$

and

$$A = \left(\varepsilon_u - \frac{\sigma_u}{E}\right) \Big/ \sigma_u^n \tag{6.5}$$

where $\varepsilon_y - \frac{\sigma_y}{E}$ in the expression for n is equal to 0.002.

σ_y is therefore equivalent to the 0.2% proof stress of the generated curve.

Mitchell's explanation for using this fit was that it is more suitable for finite element analysis than the more conventional $\sigma = A\varepsilon^m$, which has infinite modulus at the start of the curve.

The curves used by Mitchell can be conveniently modified to include the effect of cold work. This is illustrated in Figure 6.4. The curve given by the expressions is effectively shifted in the negative strain direction (to the left on a normal stress-strain graph) by the amount of permanent cold work strain. The initial part of the stress-strain curve, up to the point where it intersects the shifted curve, is then simply a straight line with the slope of the Young's modulus.

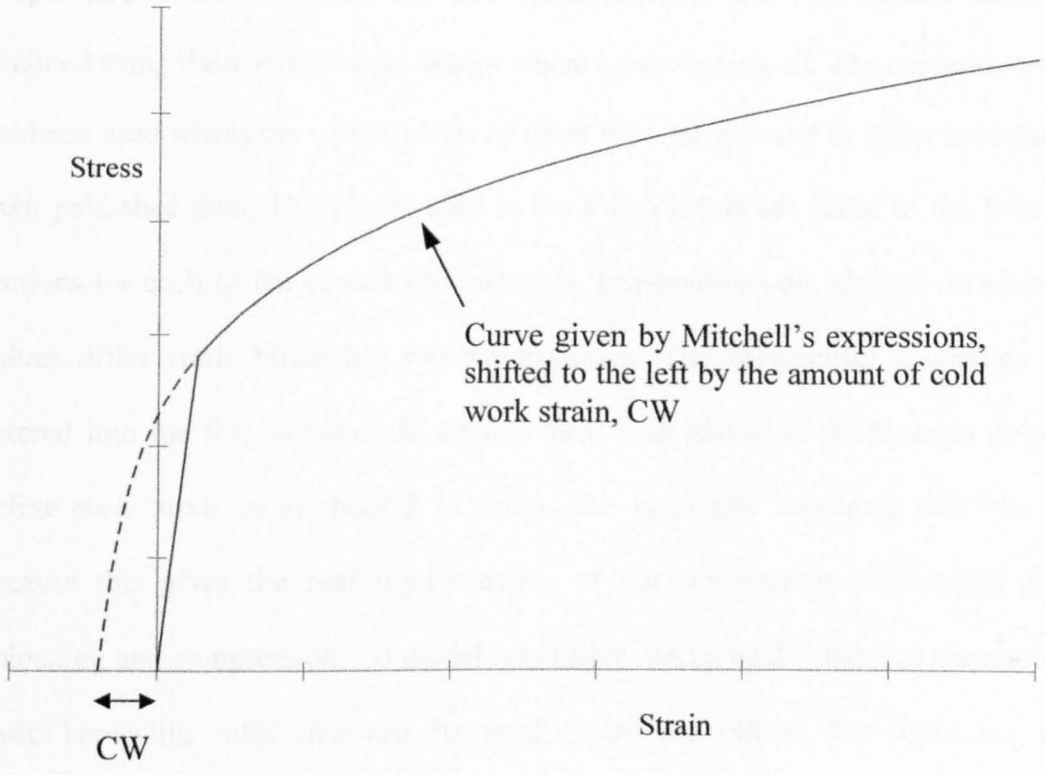

Figure 6.4 Effect of cold work on stress-strain curve

With no cold work applied, the curves generated by Mitchell's expressions have no elastic range. The slope at the origin is equal to the Young's modulus, but plastic deformation (a reduction in slope) begins from the start. By applying cold work to the curves, an elastic range is produced. It was necessary to have an elastic range in order to input the mechanical properties into the F.E. software, therefore a small amount of cold work was applied to the curves for the annealed materials (copper and bronze). In fact, this produced more realistic stress-strain curves than those with no cold work, but didn't have a significant affect on the stress and strain values as a whole.

For each of the different constituent materials, Mitchell also produced expressions for the UTS, yield stress, Young's modulus and elongation (σ_u , σ_y , E *and* ε_u), in which

temperature is the only variable. The values used in the F.E. models have been obtained using these expressions except where otherwise stated. The expressions have not been used where the values given by them have been found to differ substantially from published data. The values used in the F.E. models are given in the following sections for each of the constituent materials. Explanations are also given where the values differ from Mitchell's recommendations. The mechanical properties were entered into the F.E. software in tabular form with about 10 stress-strain points to define each curve up to about 2 % strain. The kinematic hardening rule was used because this gives the best representation of the stress-strain relationship during unloading and compression. To model non-linear mechanical behaviour there are two basic hardening rules that can be used (there are others, but these are more complicated and require a lot more data on the material behaviour). The two basic hardening rules are isotropic hardening and kinematic hardening. Generally, kinematic hardening is used when it is necessary to allow for the Bauschinger effect. Therefore, kinematic hardening was used for this research (when the isotropic hardening rule was used instead of kinematic, the hysteresis loops virtually disappeared). A detailed explanation of the different hardening rules can be found in Ansys (1998), Section 8.3.1.1 Plasticity.

6.4.2.1 Copper

The material properties for copper used in the models are given in Table 6.2.

Temperature (K)	E (GPa)	σ_y (MPa)	σ_u (MPa)	ε_u (%)
4	137	33	436	43
77	136	30	358	40
293	128	27	216	32
500	115	23	107	26
700	102	18	65	20
968	91	13	45	14

Table 6.2 Mechanical properties of copper

Poisson's ratio was assumed to be 0.34 (Simon et al. 1992).

The values for E and ε_u were obtained from Mitchell's equations. For σ_y and σ_u the high temperature values were also obtained from Mitchell's equations, but the low temperature values were found to differ from values obtained from Mitchell's main reference, Simon et al. (1992). Figure 6.5 compares the values of ultimate tensile strength, σ_u, obtained from Mitchell's equations with those obtained from Simon et al. (1992) assuming a grain size of 50 μm, the same as assumed by Mitchell. The grain size of the copper in the wire specimens was approximately of this order as could be observed on some of the micrographs of wire cross-sections

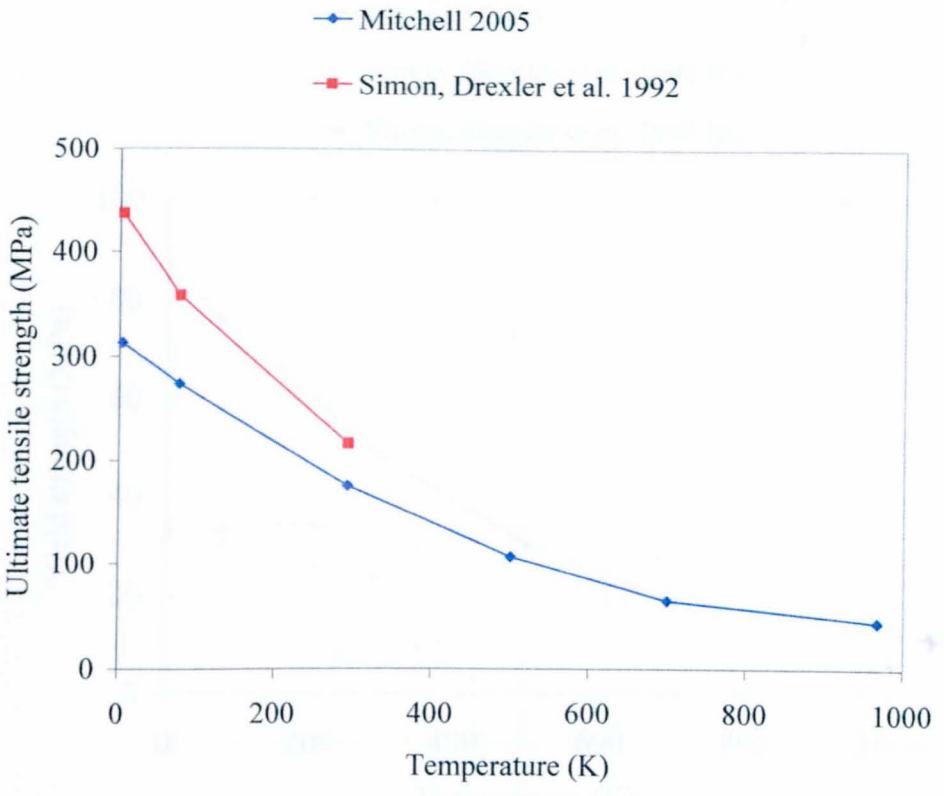

Figure 6.5 Comparison of σ_u values obtained from different sources

It was decided to adopt the values obtained from Simon et al. (1992), as Mitchell's equations do not provide a good enough fit to this reference data. However, Mitchell's equations were used for the high temperature values because Simon et al. (1992) only looked at the properties up to room temperature.

Figure 6.6 compares the values of yield stress, σ_y, obtained from Mitchell's equations with those obtained from two different sources within Simon et al. (1992). The first one comes from the Chapter 2, Oxygen free copper: tensile properties, and the second from Chapter 20, Phosphor bronze: tensile properties. The grain size is again assumed to be 50 μm. To obtain properties for copper from the data for phosphor bronze, the term for phosphor content used in the equation of best fit to the data is set to zero.

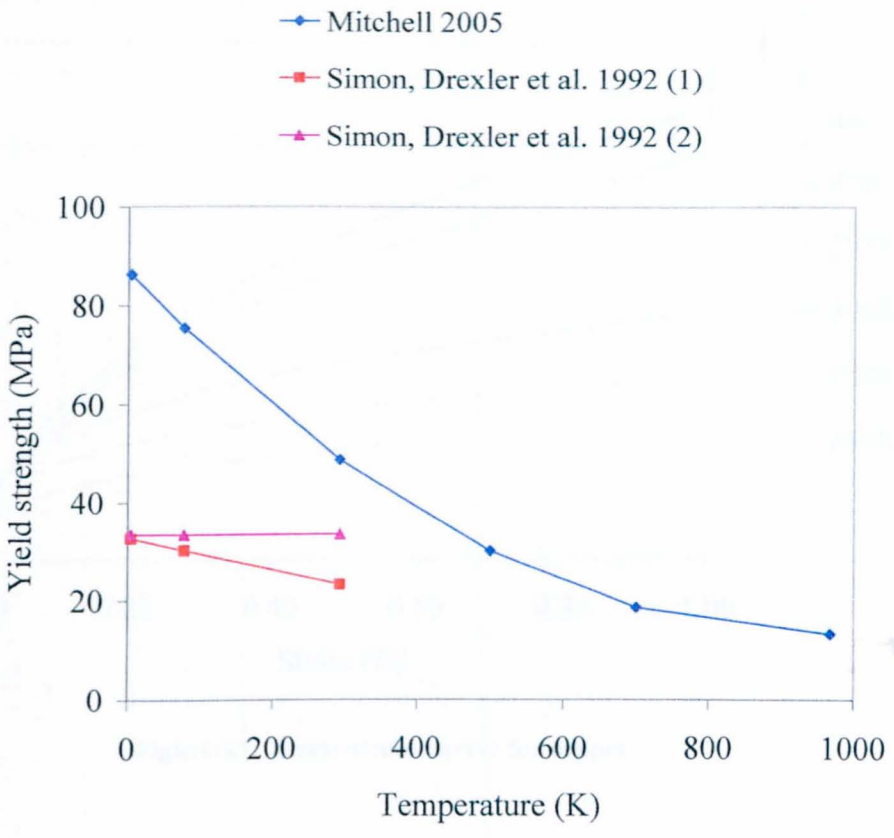

Figure 6.6 Comparison of σ_y values obtained from different sources

It can be seen from Figure 6.6 that the values for yield stress at 4 K given by both the sources within Simon et al. (1992) are in agreement. The agreement is also reasonable at 77 and 293 K. It was decided, therefore, to adopt the values given by the oxygen free copper data within Simon et al. (1992) for the properties at low temperature (4 and 77 K) and to use Mitchell (2005 *Cryogenics*) for the properties at high temperature (700 and 968 K). The properties at the intermediate temperatures (293 and 500 K) were interpolated from the high and low temperature properties.

Figure 6.7 shows the stress-strain curves that are produced using Mitchell's expressions with the properties given in Table 6.2 and a small amount of cold work (0.005 %).

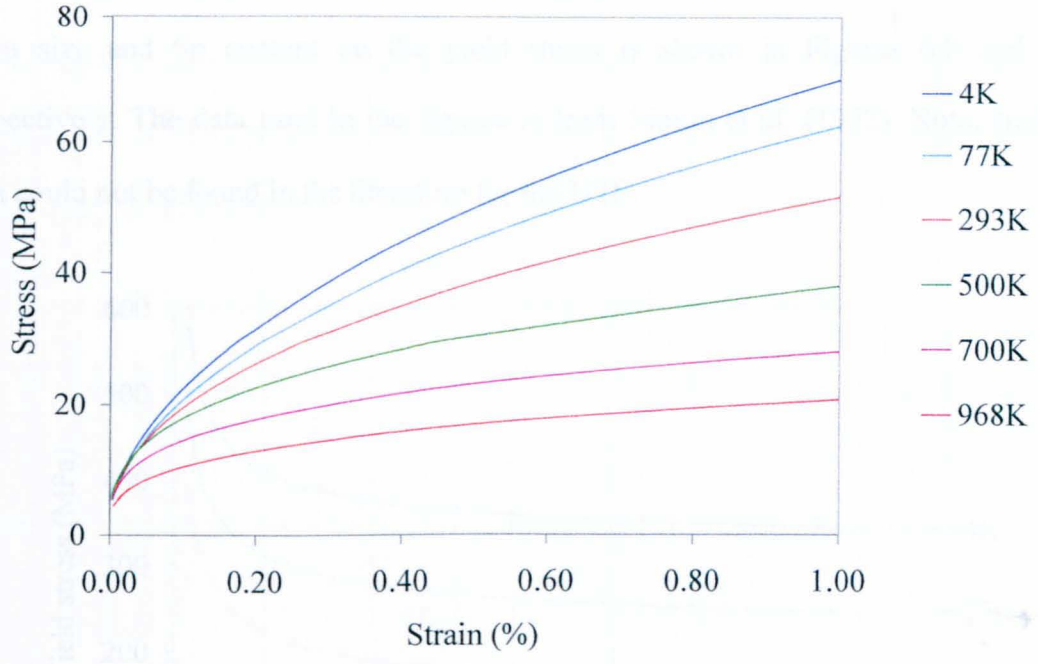

Figure 6.7 Stress-strain curves for copper

6.4.2.2 Bronze

Different mechanical properties were used for the bronze before and after heat-treatment and in different locations within the superconducting wire. This was because the tin within the bronze is depleted during the heat-treatment and the tin content and the grain size vary substantially throughout the cross-section. The tin content before the heat-treatment is 13 wt.% and is depleted to somewhere around 3 and 8 wt.% after the niobium has been converted to Nb_3Sn. The tin content after reaction is also probably lower in the bronze matrix surrounding the filaments than in the bronze close to the outside of the wire or close to the barrier (McDonald 1983 and Tan 2004). The grain size in the bronze matrix surrounding the filaments is largely dependent on the filament spacing (Markiewicz and Goddard 2002) and so, for the wire used in this research, this suggests it would be around 3 μm. The grain size of the bronze in the regions where there were no filaments could be observed on the microscope images of

wire cross-sections and was substantially larger at around 50 μm. The effect of the grain size and tin content on the yield stress is shown in Figures 6.8 and 6.9 respectively. The data used in the figures is from Simon et al. (1992). Note, similar data could not be found in the literature for the UTS.

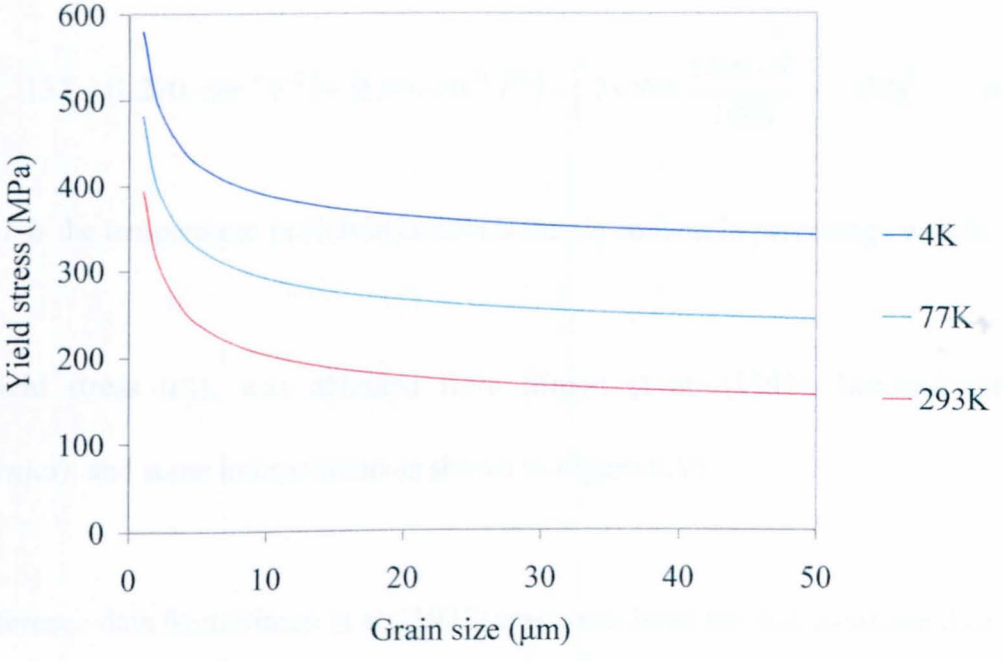

Figure 6.8 Effect of grain size on yield stress of bronze (8wt.%Sn)

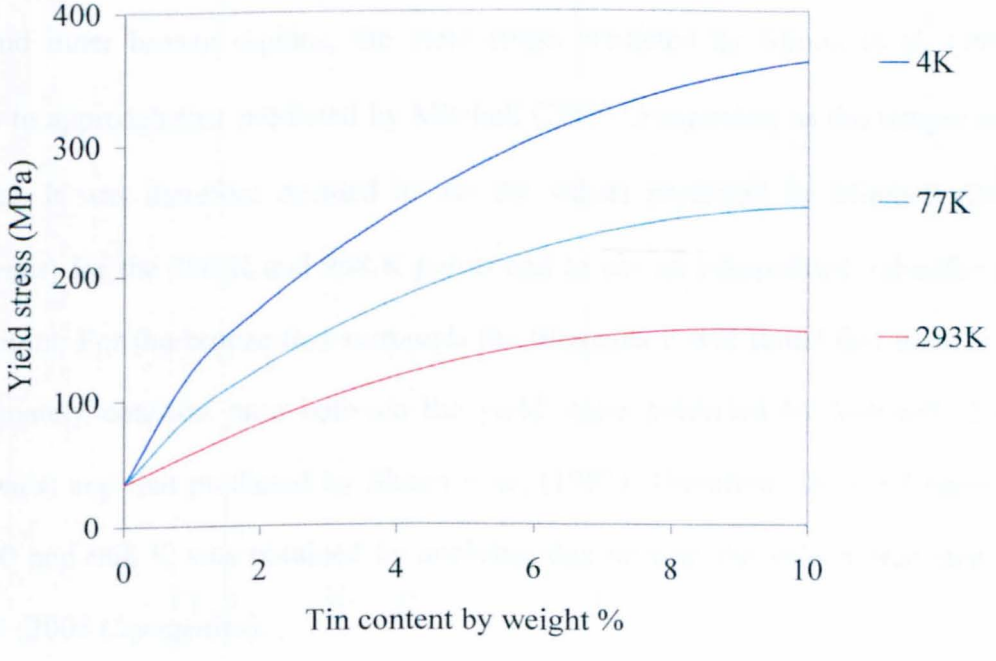

Figure 6.9 Effect of the tin content within the bronze on the yield stress

The Young's modulii (E), and elongation (ε_u) for the different bronzes used in the modelling was taken from Mitchell's equations. However, an error was discovered in the equation for E. Mitchell provided the correct equation in a private communication. That equation is as follows:

$$E = 137 - \left(1.270\times10^{-4}\,T^{2}\right) + \left(8.00\times10^{-8}\,T^{3}\right) - \left(2\times Sn\times\frac{1000-T}{1000}\right) \quad \text{GPa} \qquad (6.6)$$

where T is the temperature in Kelvin and Sn is the tin content in percentage weight.

The yield stress (σ_y), was obtained from Simon et al. (1992), Mitchell (2005 *Cryogenics*) and some interpolation as shown in Figure 6.10.

The reference data from Simon et al. (1992) was considered the best available data for the temperature range that they covered (up to room temperature) and so this source was used for the bronze in all three regions. For the top two graphs in Figure 6.10, the outer and inner bronze regions, the yield stress predicted by Simon et al. (1992) appears to approach that predicted by Mitchell (2005 *Cryogenics*) as the temperature increases. It was therefore decided to use the values predicted by Mitchell (2005 *Cryogenics*) for the 700 K and 968 K points and to use an interpolated value for the 500 K point. For the bronze that surrounds the filaments it was found that there is an approximately constant ratio between the yield stress predicted by Mitchell (2005 *Cryogenics*) and that predicted by Simon et al. (1992). Therefore, the yield stress at 500, 700 and 968 K was obtained by applying this ratio to the values predicted by Mitchell (2005 *Cryogenics*).

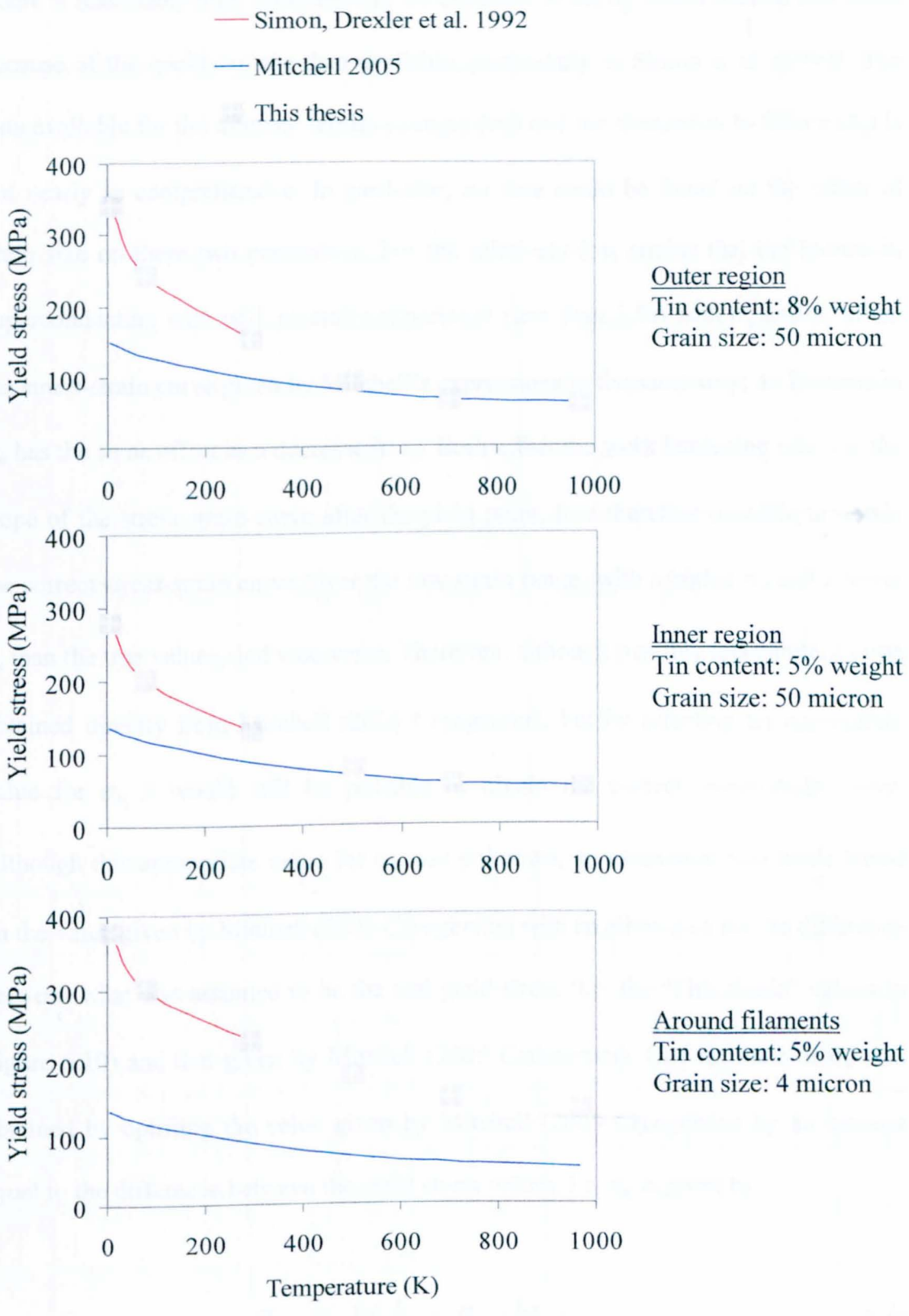

Figure 6.10 Yield stress of bronze in reacted wire

There is reasonably high confidence in the accuracy of the σ_y values used in this thesis because of the quality of the data available, particularly in Simon et al. (1992). The data available for the ultimate tensile strength (σ_u) and the elongation to failure (ε_u) is not nearly as comprehensive. In particular, no data could be found on the effect of grain size on these two parameters. For the relatively low strains that the bronze in superconducting wire will generally experience (less than 2 %) both σ_u and ε_u affect the stress-strain curve given by Mitchell's expressions in the same way; an increase to σ_u has the same effect as a decrease in ε_u. Both affect the work hardening rate, i.e. the slope of the stress-strain curve after the yield point. It is therefore possible to obtain the correct stress-strain curve (over the low strain range) with a higher σ_u and a lower ε_u than the true values, and vice-versa. Therefore, although possibly inaccurate, ε_u was obtained directly from Mitchell (2005 *Cryogenics*), but by selecting an appropriate value for σ_u it would still be possible to obtain the correct stress-strain curve. Although this appropriate value for σ_u was unknown, an estimation was made based on the value given by Mitchell (2005 *Cryogenics*) with an allowance for the difference between what was assumed to be the real yield stress (i.e. the "This thesis" values in Figure 6.10) and that given by Mitchell (2005 *Cryogenics*). One estimate of σ_u was obtained by uplifting the value given by Mitchell (2005 *Cryogenics*) by an amount equal to the difference between the yield stress values, i.e. σ_u is given by:

$$\sigma_u = (\sigma_u)_M + \sigma_y - (\sigma_y)_M \tag{6.7}$$

where $(\sigma_u)_M$ and $(\sigma_y)_M$ are the ultimate tensile strength and yield strength given by Mitchell (2005 *Cryogenics*) and σ_y is the yield stress used for the modelling presented in this thesis.

When the bronze stress-strain curves were computed using this estimation of σ_u, however, the F.E. model did not produce a very good match with the experimentally measured stress-strain curve of the superconducting wire. Another estimate was obtained by assuming that the ratio of the real σ_u value to the value given by Mitchell (2005 *Cryogenics*) is the same as the ratio for the real σ_y value to the value given by Mitchell (2005 *Cryogenics*). Thus, this estimate of σ_u is given by:

$$\sigma_u = (\sigma_u)_M \times \left(\frac{\sigma_y}{(\sigma_y)_M} \right) \tag{6.8}$$

These estimates of σ_u along with the values given by Mitchell (2005 *Cryogenics*) are shown in Figure 6.11. Using stress-strain curves for bronze computed using values of σ_u estimated by the second method, the F.E. model produced a very good match with the experimental measurement at room temperature of the superconducting wire stress-strain curve (see Figure 6.16). The match wasn't so good at liquid nitrogen temperature (77 K), however. To achieve a better match at 77 K without changing the room temperature result, the 77 K σ_u values were reduced to a level between the estimate 1 and estimate 2 values, as shown in Figure 6.11.

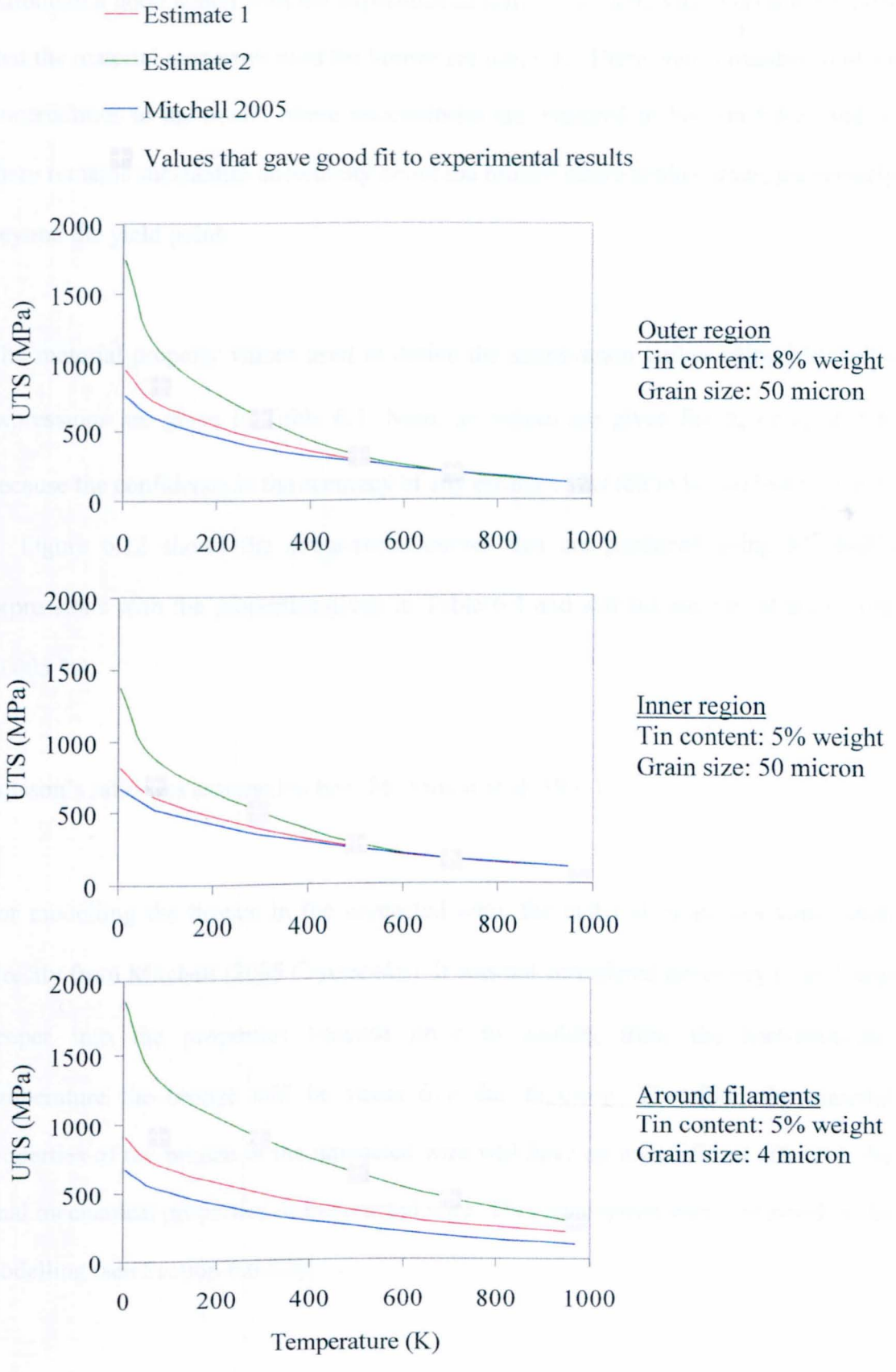

Figure 6.11 Ultimate tensile strength of bronze in reacted wire

Although a good match with the experimental results was achieved, it does not follow that the material properties used for bronze are accurate. There were a number of other uncertainties in the model (these uncertainties are explored in Section 6.6.2) and so there remains substantial uncertainty about the bronze stress-strain curves, particularly beyond the yield point.

The material property values used to define the stress-strain curves using Mitchell's expressions are given in Table 6.3. Note, no values are given for σ_u or ε_u at 4 K because the confidence in the accuracy of any estimate was felt to be too low to justify it. Figure 6.12 shows the stress-strain curves that are produced using Mitchell's expressions with the properties given in Table 6.3 and a small amount of cold work (0.005 %).

Poisson's ratio was assumed to be 0.36 (Simon et al. 1992).

For modelling the bronze in the unreacted wire, the material properties were taken directly from Mitchell (2005 *Cryogenics*). It was not considered necessary to look any deeper into the properties because prior to cooling from the heat-treatment temperature the bronze will be stress free due to creep. Therefore, the material properties of the bronze in the unreacted wire will have an insignificant effect on the final mechanical properties of the reacted wire. This assumption was confirmed in the modelling (see Section 6.6.2.2).

Temperature (K)	E (GPa)	σ_y (MPa)	σ_u (MPa)	ε_u (%)
4	121	340		
77	121	242	833	44
293	117	154	600	35
500	107	93	317	28
700	97	67	190	21
968	90	62	117	14

Outer region
Tin content: 8% weight
Grain size: 50 micron

Temperature (K)	E (GPa)	σ_y (MPa)	σ_u (MPa)	ε_u (%)
4	127	279		
77	127	201	700	43
293	121	132	509	34
500	110	82	280	27
700	99	57	166	21
968	90	52	103	14

Inner region
Tin content: 5% weight
Grain size: 50 micron

Temperature (K)	E (GPa)	σ_y (MPa)	σ_u (MPa)	ε_u (%)
4	127	378		
77	127	301	918	43
293	121	231	894	34
500	110	180	620	27
700	99	150	433	21
968	90	136	268	14

Around filaments
Tin content: 5% weight
Grain size: 4 micron

Table 6.3 Mechanical properties of bronze in reacted wire

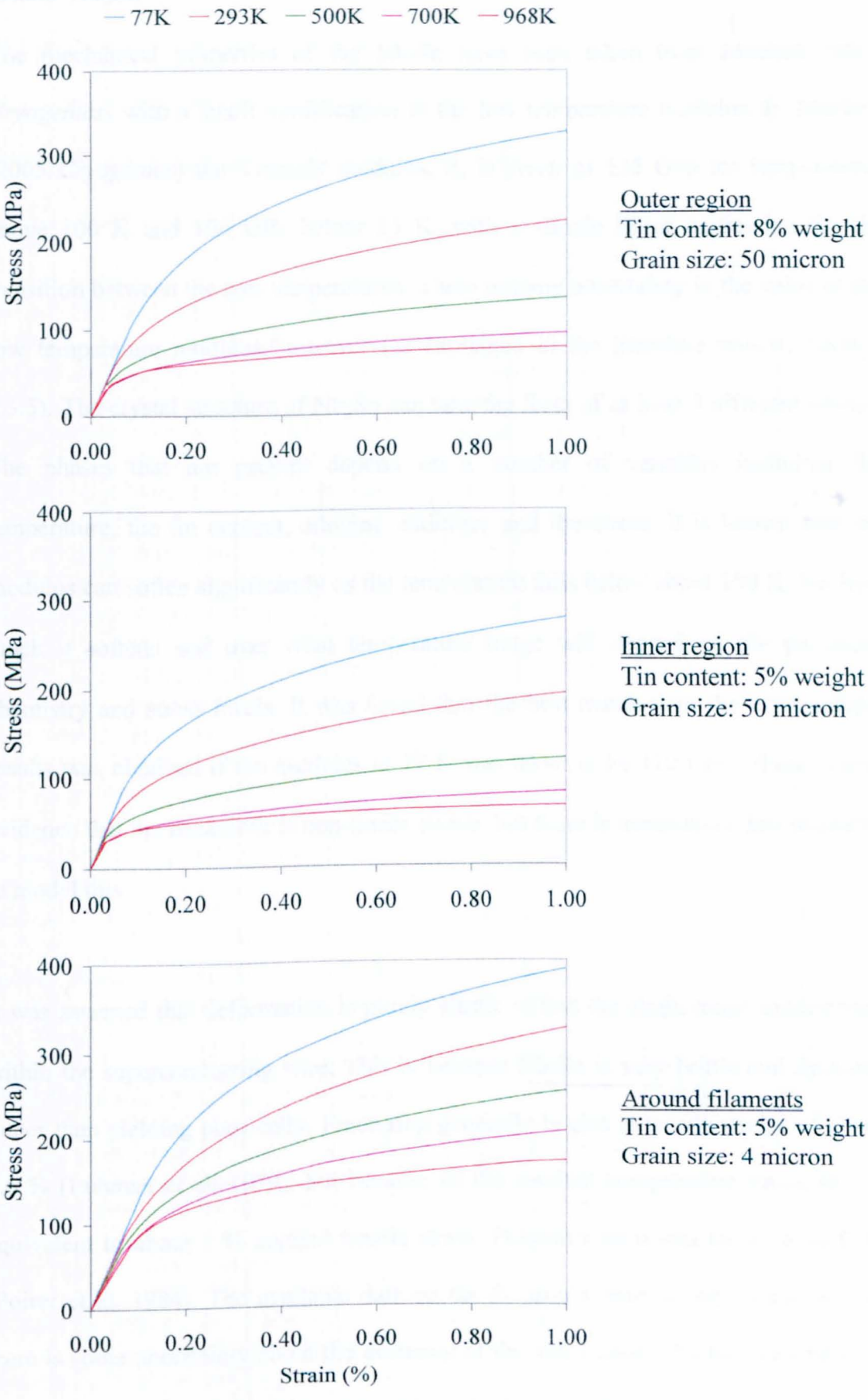

Figure 6.12 Stress-strain curves for bronze in reacted wire

6.4.2.3 Nb_3Sn

The mechanical properties of the Nb_3Sn have been taken from Mitchell (2005 *Cryogenics*) with a small modification to the low temperature modulus. In Mitchell (2005 *Cryogenics*) the Young's modulus, E, is given as 135 GPa for temperatures above 100 K and 100 GPa below 35 K, with a simple linear expression for the transition between the two temperatures. There is some uncertainty in the value of the low temperature modulus, however (as explained in the literature review, Section 2.3.5). The crystal structure of Nb_3Sn can take the form of at least 3 different phases. The phases that are present depend on a number of variables including the temperature, the tin content, alloying additions and the stress. It is known that the modulus can soften significantly as the temperature falls below about 100 K, but how much it softens and over what temperature range will depend on the particular chemistry and stress levels. It was found that the best match with the experimental results was obtained if the modulus at 77 K was taken to be 110 GPa. There is also evidence that the behaviour is non-linear elastic, but there is insufficient data available to model this.

It was assumed that deformation is purely elastic within the strain range experienced within the superconducting wire. This is because Nb_3Sn is very brittle and fractures rather than yielding plastically. Fracturing generally begins at tensile strains of about 0.6 % (Luhman et al. 1979), but because of the residual compressive stress, this is equivalent to about 1 % applied tensile strain. Poisson's ratio was taken to be 0.35 (Poirer et al. 1984). The available data on the Poisson's ratio is very scarce and so there is some uncertainty about the accuracy of the value used. Mitchell assumed the Poisson's ratio to be 0.3 but has not explained where the figure came from. Poirer et

al. (1984) showed that the Poisson's ratio has a significant temperature dependence. The room temperature value was reported as 0.22, rising to 0.46 below about 30 K. The value of the Poisson's ratio has been assumed to be constant with temperature in this thesis, however, because of the scarcity of data.

6.4.2.4 Niobium and Tantalum

It has been assumed that neither niobium nor tantalum stress relieve or anneal at the heat-treatment temperature (695 °C). The melting points of niobium and tantalum are 2750 K and 3290 K respectively, and the ratios of the heat-treatment temperature to the melting points are 0.35 and 0.21 respectively. As a general rule, creep and therefore stress relief does not occur below about 0.3 to 0.4 of the melting point (Ashby and Jones 1980). Annealing generally will require a higher temperature than stress-relief. Therefore, annealing or stress relief clearly does not take place in the tantalum. However, it is uncertain whether the niobium will stress relieve, although it is unlikely that it will anneal. The niobium only makes up a small fraction of the reacted wire and so the uncertainty about whether it stress relieves or anneals at the heat-treatment temperature will only have a very minor effect on the results.

With no annealing or stress relief taking place, the niobium and tantalum will be in a heavily cold worked condition following the extensive drawing down of the manufacturing process. Because of this, the material properties have been assumed to be elastic / perfectly plastic. The Young's modulii have been taken from Mitchell (2005 *Cryogenics*). The room temperature UTS values given by Mitchell did not agree with the values for cold worked niobium and tantalum quoted at www.rembar.com (Rembar Company is a well established and respected supplier of refractory metals).

Mitchell's values of 282 and 401 MPa for niobium and tantalum respectively compare to 588 and 650 MPa from the Rembar source. The Rembar values were considered to be more reliable as they were obtained from cold worked material. Mitchell's equations are based on the properties of annealed material. Thus, for the room temperature yield stress, the Rembar UTS values were used, although they were adjusted down by a small amount because the cold worked yield stress would be less than the UTS. The yield stress was assumed to be 50 MPa less than the UTS, although this was purely an estimate. The high temperature values for yield stress were based on Mitchell's UTS values, rounded to the nearest 100 MPa because of uncertainty about the accuracy. The yield stresses at the intermediate points, i.e. 500 and 700 K, were interpolated from the room temperature and 968 K values (again rounding to the nearest 100). The values at 77 K were obtained by assuming the ratio of the true value to that given by Mitchell was the same at 77 K and room temperature. There is clearly considerable uncertainty about the validity of the values used, but as the barrier only accounts for around 1% of the wire, inaccuracies in the values used would not have a significant effect in the overall mechanical properties of the wire predicted by the model.

Poisson's ratios are assumed to be 0.38 for niobium and 0.34 for tantalum (Mitchell 2005 *Cryogenics*). The values for Young's modulus and yield stress used in the modelling are given in Tables 6.4 and 6.5. The stress-strain curves are shown in Figures 6.13 and 6.14.

Temperature (K)	E (GPa)	σ_y (MPa)
77	108	800
293	105	538
500	102	300
700	99	200
968	94	100

Table 6.4 Mechanical properties of niobium

Temperature (K)	E (GPa)	σ_y (MPa)
77	186	900
293	180	600
500	174	400
700	169	300
968	162	200

Table 6.5 Mechanical properties of tantalum

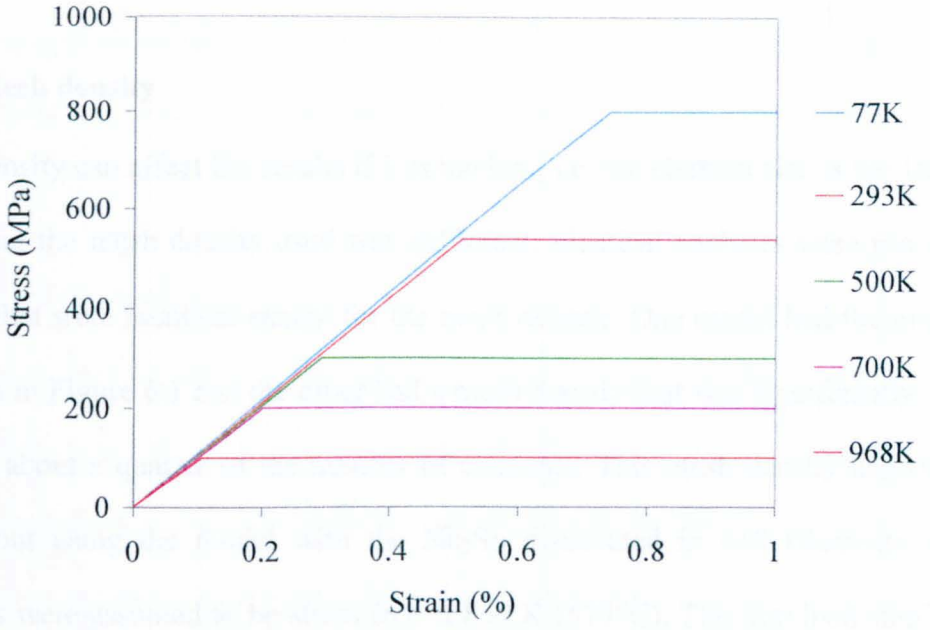

Figure 6.13 Stress-strain curves for niobium

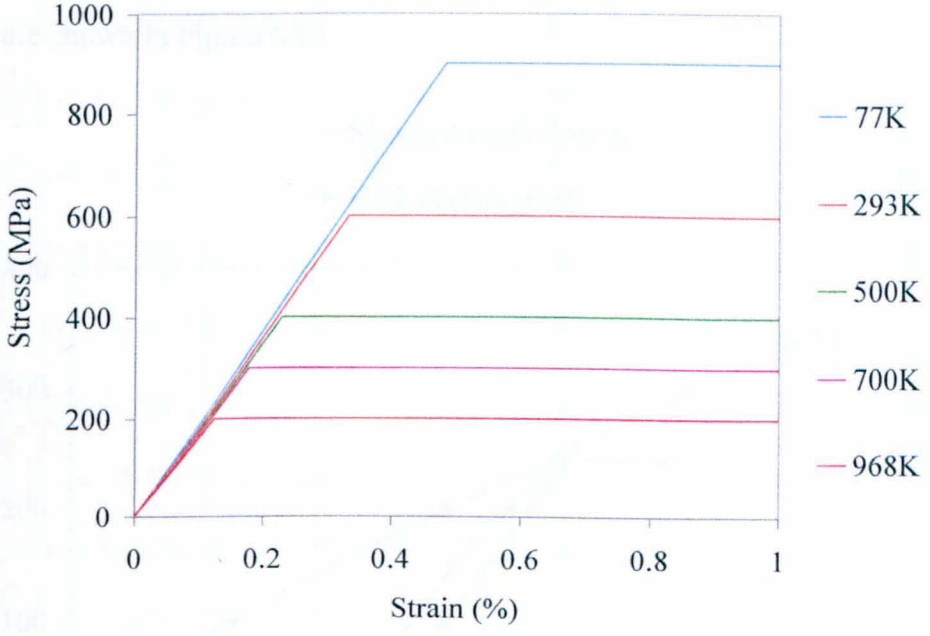

Figure 6.14 Stress-strain curves for niobium

6.5 Model checking

6.5.1 Mesh density

Mesh density can affect the results if it is too low, i.e. the element size is too large. To check that the mesh density used was sufficient, identical analyses were run on two models that were identical except for the mesh density. One model had the mesh that is shown in Figure 6.1 and the other had a mesh density that was significantly coarser and had about a quarter of the number of elements. This mesh density analysis was carried out using the model with the Nb_3Sn distributed in 618 filaments and all materials were assumed to be stress free at 850 K (577°C). The first load step was to cool the wire to room temperature simulating the cool-down at the end of the heat-treatment process. In subsequent load steps a negative pressure was applied to the top surface to produce the tensile stress. The stress-strain curves obtained from the two analyses are shown in Figure 6.15.

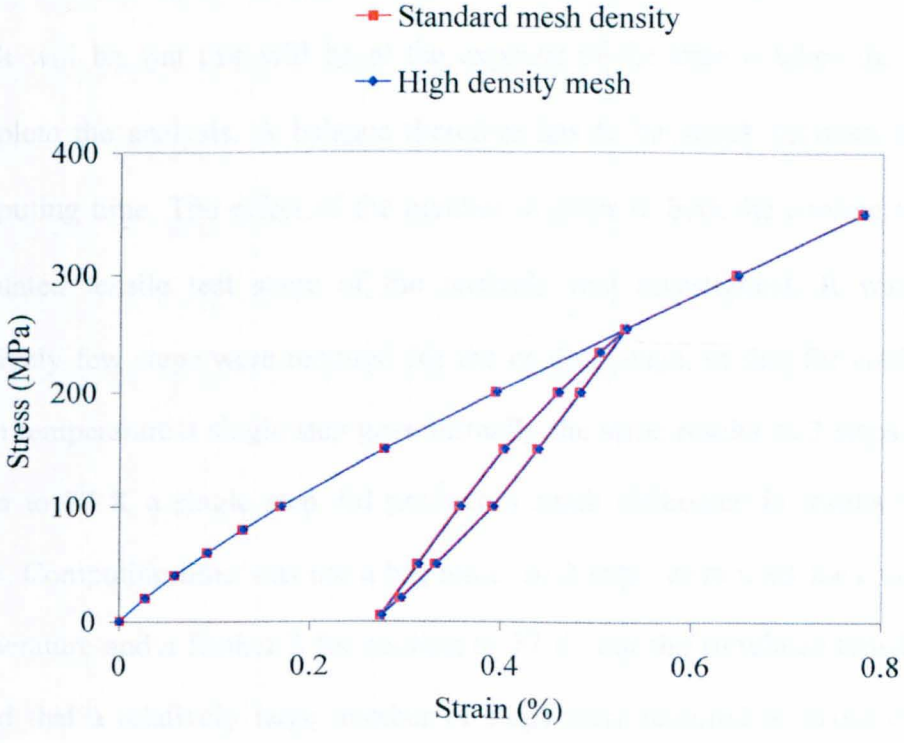

Figure 6.15 Mesh density validation

It can be seen from Figure 6.15 that there was no significant difference in the results using the two different mesh densities. It can therefore be concluded that the mesh density used was more than adequate for modelling the stress-strain curves.

6.5.2 Load stepping

The size of the load steps (or sub-steps, if these are used) can have an affect on the results if the material properties are non-linear. The finite element software computes a solution at each of the load steps (or sub-steps) and so effectively jumps from one step to the next. For a temperature change load step, for example, the software works by applying an instantaneous change in temperature and computes the stresses and strains that result. In the real world, however, the temperature will change in a continuous nature. The finite element solution does not take into account what happens between the two temperature set-points and can therefore produce an error if the size of the step is too large. The smaller the size of the steps the more accurate the result will be, but this will be at the expense of the time it takes the computer to complete the analysis. A balance therefore has to be struck between accuracy and computing time. The effect of the number of steps in both the cooling stage and the simulated tensile test stage of the analysis was investigated. It was found that relatively few steps were required for the cooling stage, in fact for cooling down to room temperature a single step gave virtually the same results as 3 steps. For cooling down to 77 K a single step did produce a small difference in results that multiple steps. Computing time was not a big issue, so 3 steps were used for cooling to room temperature and a further 3 for cooling to 77 K. For the simulated tensile test it was found that a relatively large number of steps were required to avoid errors. It was necessary to have a large number of steps in any case in order to extract the results at

multiple points on the stress-strain curve. Typically about 50 steps were used for a simulated tensile test with 3 hysteresis cycles and a maximum strain of 2%. The computing time for each analysis was approximately 20 to 30 minutes using a 1.4 GHz Pentium II processor with 512 MB of ram.

6.6 Results

There were a number of uncertainties with the F.E. model, particularly with some of the material properties. The effects of the various uncertainties on the stress-strain curves obtained by the analyses were investigated. By comparing the results with the experimentally determined stress-strain curve, it was possible to find 'best fit' values for the uncertainties that had significant effects on the stress-strain curve. For some of the uncertainties, this could be done more-or-less independently because the uncertainty affected the stress-strain curve in a unique way. For some of the other uncertainties no single 'best-fit' value exists. For these a match with the experimental results could be achieved by estimating the value of one property and then optimising another. The estimated value of the first property could then be modified if necessary. In all cases, the property values were only optimised within a range that could be considered reasonable from the available data in the literature. The F.E. results using these optimised values are compared with the experimental results in Section 6.6.1.

6.6.1 Finite element modelling results compared with experiment

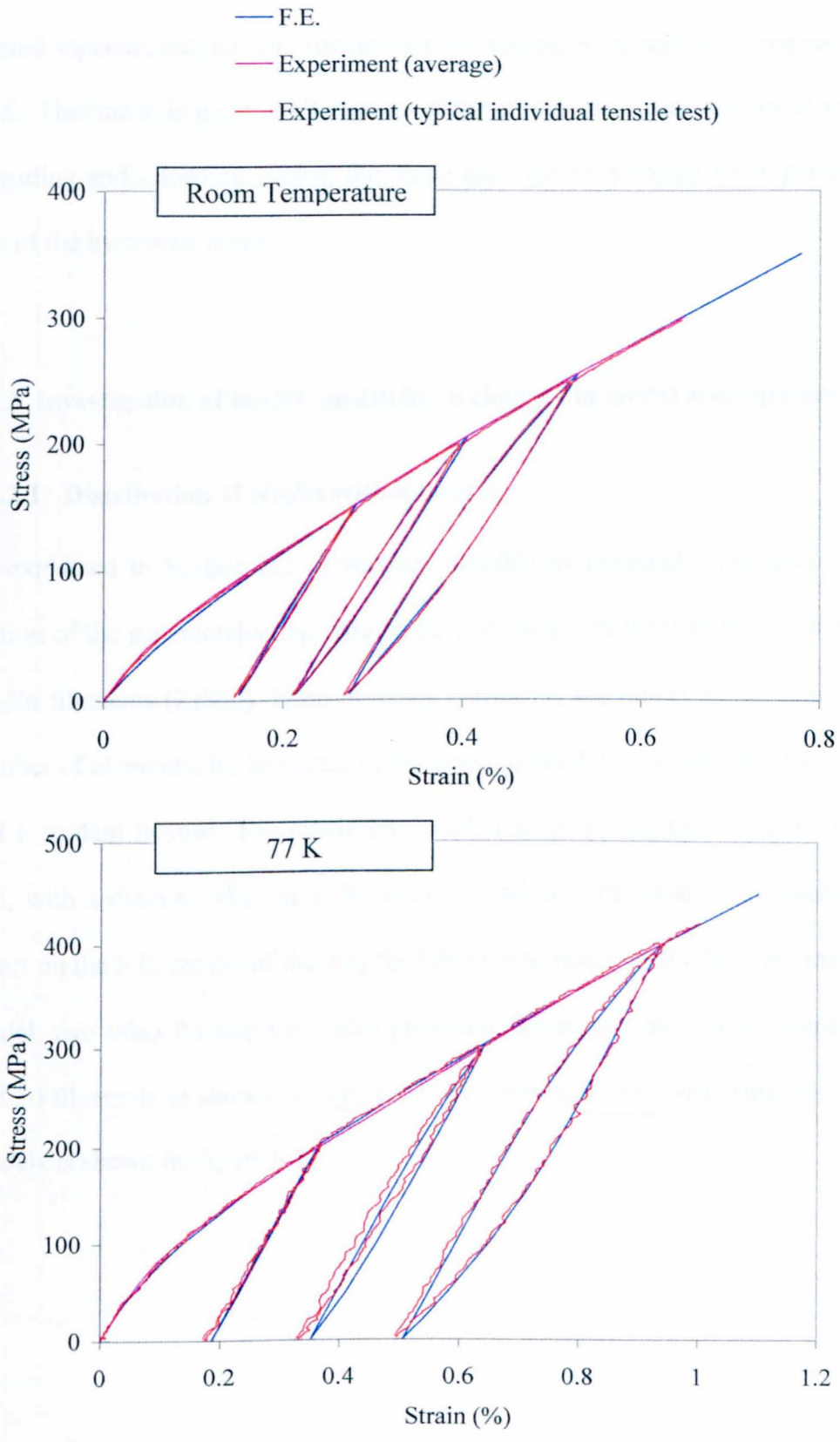

Figure 6.16 Comparison of finite element and experimental results

Figure 6.16 shows that a very good match was obtained between the finite element modelling results and the experimentally measured stress-strain curve of the fully reacted superconducting wire (heat-treatment regime 8) at both room temperature and 77 K. The match is good in all regions of the curves, the linear regions at start of the unloading and reloading cycles, the slope after plastic yielding takes place, and the size of the hysteresis loops.

6.6.2 Investigation of model sensitivity to changes in model assumptions

6.6.2.1 Distribution of Nb_3Sn within matrix

As explained in Section 6.2, it was not possible to accurately reproduce the cross-section of the superconducting wire in the F.E. model because of the large number of Nb_3Sn filaments (22866). Even utilising symmetry, the model would require a huge number of elements, far in excess of the maximum allowable with the Ansys package and a student license. The maximum number of filaments that were modelled was 618, with a diameter that gave the same overall volume fraction. To investigate the effect on the F.E. results of the way the Nb_3Sn was distributed within the matrix of the model, two other models were also produced. These had the Nb_3Sn distributed in 6 and 30 filaments as shown in Figure 6.1. The results of analyses using the 3 different models is shown in Figure 6.17.

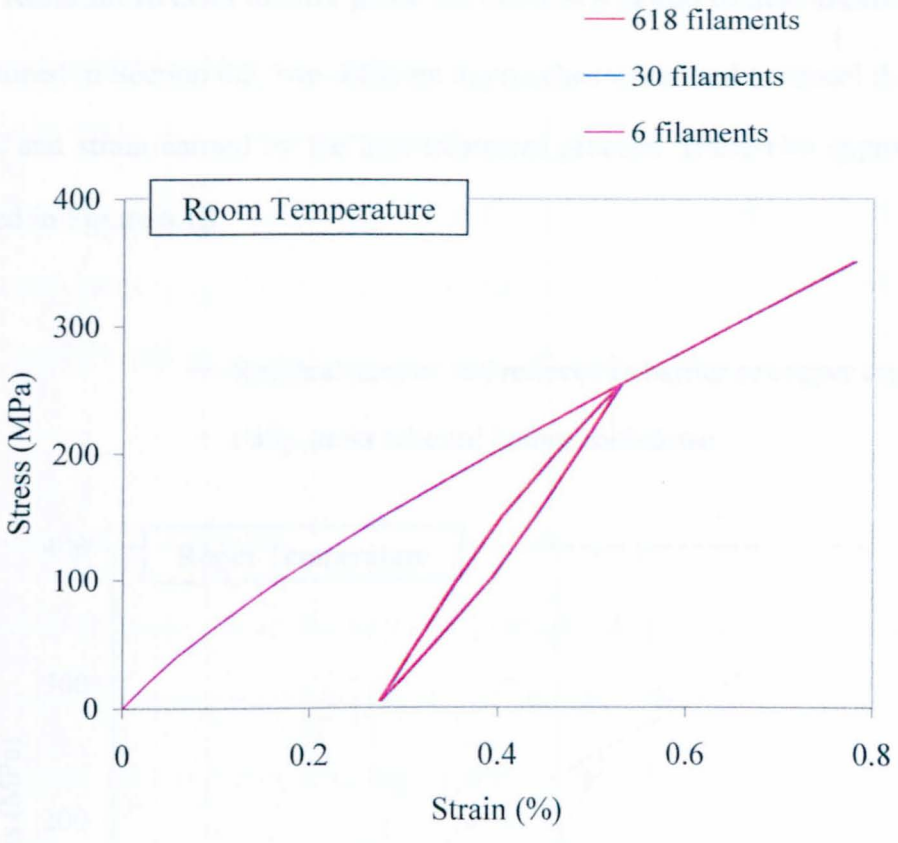

Figure 6.17 Model sensitivity to number of filaments

It can be seen from Figure 6.17 that it made virtually no difference to the results whether the Nb_3Sn was modelled as 618, 30 or 6 filaments within the wire cross-section. By extrapolation, it is reasonable therefore to conclude that if the true number of filaments were modelled then the result would also not be significantly different. (Note, however, that this does not mean that real wires with such filament numbers would not have different properties. The mechanical properties of the bronze matrix is strongly influenced by the grain size and this is governed by the filament spacing. Therefore, the greater the number of filaments the stronger the bronze. For all 3 of the models, however, the mechanical properties of the bronze were the same and equal to that of the bronze matrix of the real wire with 22866 filaments).

6.6.2.2 Residual stresses in wire prior to cool-down at end of heat-treatment

As explained in Section 6.2, two different approaches were used to model the changes in stress and strain caused by the heat-treatment process. These two approaches are compared in Figure 6.18.

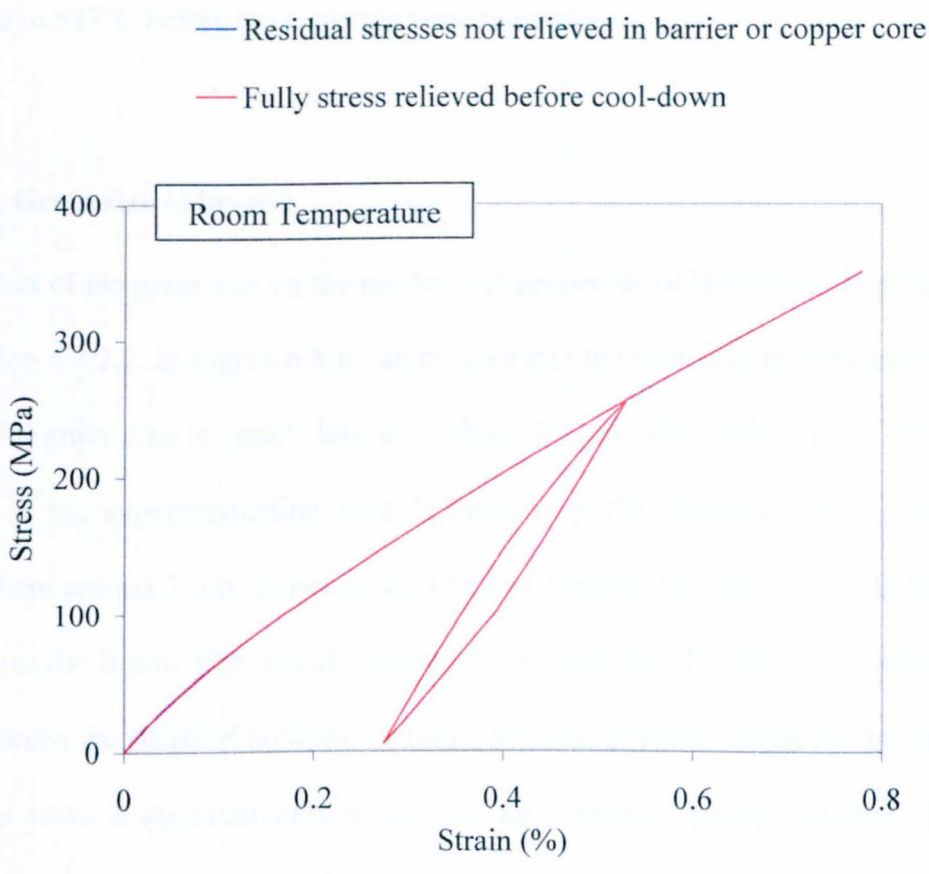

Figure 6.18 Model sensitivity to assumed residual stresses prior to cool-down

It can be seen that both approaches produced the same results for the stress-strain curve of the wire after cool-down. The explanation for this is that the residual stresses that are generated as the wire is cooled from the heat-treatment temperature are much larger than the uncertainty about what, if any, residual stresses exist just prior to the cool-down. The "birth and death" technique to relieve the stresses and anneal the materials was applied in different ways, but the results were the same in all cases. For

example, in one analysis the bronze and Nb_3Sn elements were "killed" after the temperature was raised from room temperature to 695°C, the temperature was then lowered to 577°C (to allow for stress relief during the cool-down) before the elements were reinstated. In other analyses the bronze and Nb_3Sn elements were "killed" at a lower temperature (e.g. 577°C), the temperature was then raised to 695°C, then lowered to 577°C before the elements were reinstated.

6.6.2.3 Grain size of bronze

The effect of the grain size on the mechanical properties of bronze has been described in Section 6.4.2.2. In Figure 6.8 it can be seen that the influence is particularly strong when the grain size is small, less than about 10 μm. The grain size of the bronze matrix in the superconducting wire is limited by the filament spacing and so is somewhere around 3 μm. Between the filament bundles the grain size will be a little larger, maybe 8 μm. The model assumes the bronze has the same properties within and between the filament bundles, therefore the best estimate to use for the grain size in these areas is approximately 4 μm (i.e. the filament spacing between filaments adjusted slightly to allow for the larger grain size between filament bundles). The grains will also not be regular and there will be some variation in size. Therefore, there is some uncertainty about what value to use for the grain size to compute the mechanical properties. The sensitivity of the model to the grain size is shown in Figure 6.19.

Grain size was one of three uncertainties that had similar effects on the results, the other two being the tin content within the bronze and the amount of stress relief that occurred during the cool-down at the end of the heat-treatment. It was therefore not

possible to find a single 'best match' value for the grain size, independent of the values used for the other two uncertainties.

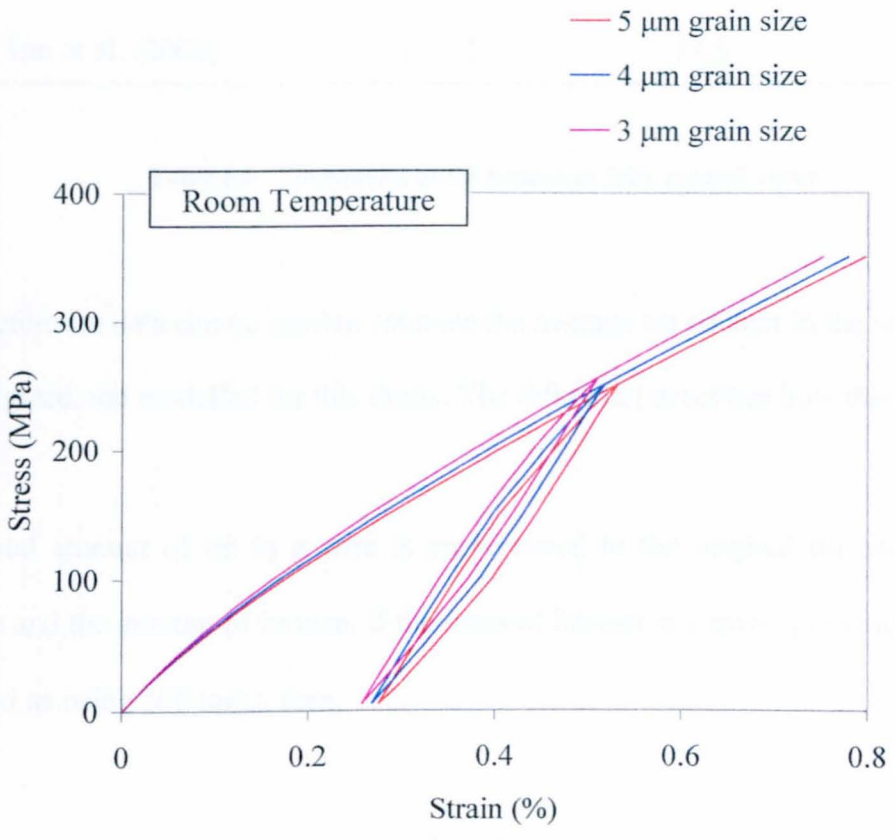

Figure 6.19 Model sensitivity to grain size of bronze matrix

6.6.2.4 Tin content within bronze

During the heat-treatment, tin diffuses out of the bronze and into the niobium filaments to form Nb_3Sn. The amount of tin left in the bronze depends on the duration of the heat-treatment, the niobium/bronze volume fraction ratio and the location of the bronze, as discussed in Section 6.4.2.2. The tin content was not known exactly, although a good estimate could be made using data published by other researchers. The average tin content in fully reacted wires as measured by McDonald et al. (1983) and Tan et al. (2004) is shown in Table 6.6.

Source	Bronze : Nb ratio	Tin content Pre-reaction (wt.%)	Tin content Post-reaction (wt.%)
McDonald et al. (1983)	2.96 : 1	13.5	3.7
Tan et al. (2004)	3.6 : 1	13.5	4.4

Table 6.6 Tin content of the bronze in fully reacted wires

This reference data can be used to estimate the average tin content in the wire that was investigated and modelled for this thesis. The following describes how this was done:

The total amount of tin in a wire is proportional to the original tin content in the bronze and the amount of bronze. If the mass of bronze in a given pre-reaction wire is denoted as being 100 units, then,

$$100 = (M_{Sn})_{BR1} + M_{Cu} \tag{6.9}$$

where $(M_{Sn})_{BR1}$ is the mass of tin in the bronze of the pre-reacted wire and M_{Cu} is the mass of copper.

As the mass of bronze was taken to be 100 units,

$$(M_{Sn})_{BR1} = (C_{sn})_{BR1} \tag{6.10}$$

and

$$M_{Cu} = 100 - (C_{sn})_{BR1} \tag{6.11}$$

where $(C_{sn})_{BR1}$ is the tin content in the bronze of the pre-reacted wire (wt.%Sn).

Some of the tin diffuses out of the bronze during the reaction to form Nb_3Sn. The mass of tin that is left in the bronze can be calculated using the measured tin content of the bronze in the reacted wire, $(C_{Sn})_{BR2}$.

$$(C_{Sn})_{BR2} = \frac{(M_{Sn})_{BR2}}{M_{Cu} + (M_{Sn})_{BR2}} \times 100 \qquad (6.12)$$

where $(M_{Sn})_{BR2}$ is the mass of tin in the bronze of the reacted wire and M_{Cu} is the mass of copper in the bronze, which is unaffected by the reaction.

Thus,

$$(M_{Sn})_{BR2} = \frac{(C_{Sn})_{BR2} \times M_{Cu}}{[100 - (C_{Sn})_{BR2}]} \qquad (6.13)$$

Now,

$$(M_{Sn})_{BR1} = (M_{Sn})_{BR2} + (M_{Sn})_{Nb3Sn} \qquad (6.14)$$

where $(M_{Sn})_{Nb3Sn}$ is the mass of tin in the Nb_3Sn filaments of the reacted wire.

Using equations 6.9 to 6.15 and the reference data from Table 6.6, $(M_{Sn})_{Nb3Sn}$ can be calculated. If it is assumed that the tin content of the Nb_3Sn filaments in the fully reacted wires investigated for this thesis is the same as for the wires used for the reference data, then the tin content in the bronze of the fully reacted wires investigated for this thesis can be calculated. Consider a length of the wire investigated for this thesis that contains a mass of niobium filaments equal to that contained in the

reference wire denoted as having 100 units of mass of bronze from which equations 6.9 to 6.15 where derived. The mass of bronze in the pre-reacted wire, M_{BR}, can be calculated as follows,

$$M_{BR} = 100 \times \frac{R}{R_{ref}} \tag{6.15}$$

where R and R_{ref} are the bronze to niobium ratios for the wire investigated for this thesis and the reference wire.

The mass of tin and copper in the bronze are given by,

$$(M_{Sn})_{BR1} = \frac{(C_{Sn})_{BR1}}{100} \times M_{BR} \tag{6.16}$$

and

$$M_{Cu} = \left(1 - \frac{(C_{Sn})_{BR1}}{100}\right) \times M_{BR} \tag{6.17}$$

where $(C_{Sn})_{BR1}$ is the pre-reaction tin content of the bronze in the wire investigated for this thesis.

From equation 6.15, the mass of tin in the bronze after being fully reacted is given by,

$$(M_{Sn})_{BR2} = (M_{Sn})_{BR1} - (M_{Sn})_{Nb3Sn} \tag{6.18}$$

where $(M_{Sn})_{Nb3Sn}$ is equal to that for the reference wire.

The tin content of the bronze in the reacted wire can be calculated using equation 6.12 and substituting in terms from equations 6.15 to 6.18. The results are 7.2 and 6.3 wt.%Sn using the reference data from McDonald et al. (1983) and Tan et al. (2004), respectively. The lower figure is probably more realistic as the bronze to niobium ratio for the wire reported by Tan et al. was closer to that of the wire investigated for this thesis. The bronze to niobium ratio of the wire investigated by McDonald et al. was significantly lower than the wire investigated for this thesis and as a result it is possible that not all of the niobium was converted into Nb_3Sn during the reaction. This would lead to an overestimate of the tin content.

McDonald et al. (1983), Markiewicz and Goddard (2002) and Tan et al. (2004) all showed that there is a significant variation in bronze tin content across the cross-section. Generally, the tin content is lower in the areas close to the filaments and higher in areas away from the filaments. Assuming a spread in tin content similar to that reported in the 3 research papers and assuming an overall average of about 6wt.%, the best estimate for the tin content was 8 wt.% in the bronze around the outside of the wire and 5 wt.% elsewhere.

To investigate the model sensitivity to the tin content, the tin content was varied within a reasonable range for the bronze located around the filaments. Figure 6.20 shows the effect on the results of slightly higher and lower tin contents.

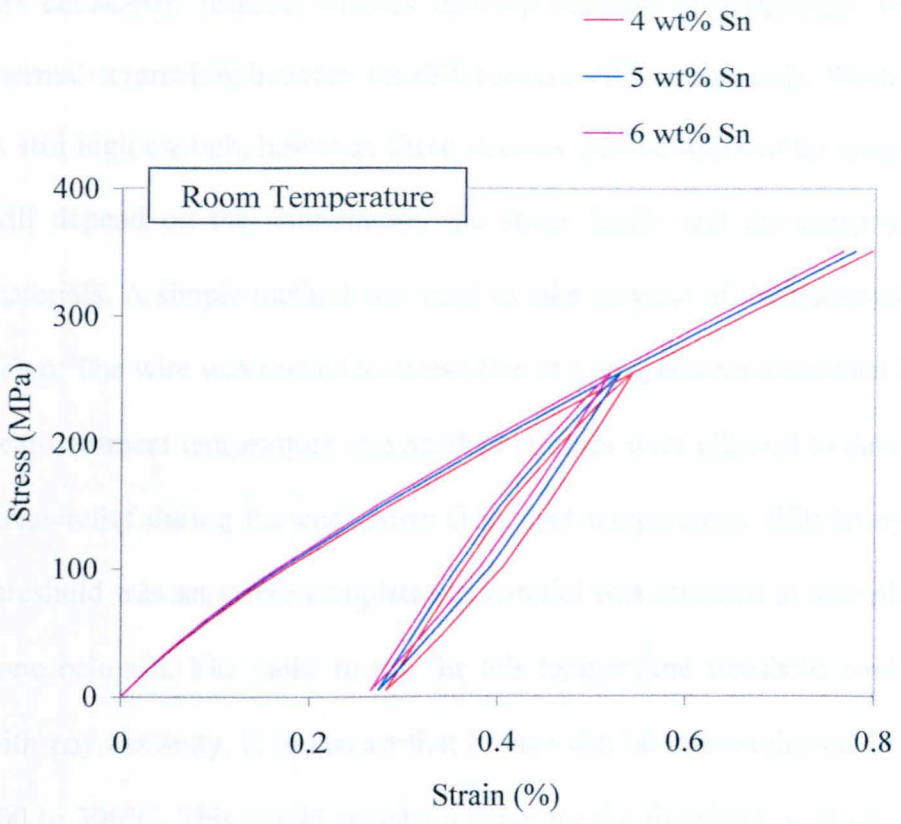

Figure 6.20 Model sensitivity to tin content in bronze

Tin content was one of three uncertainties that had similar effects on the results, the other two being the grain size of the bronze and the amount of stress relief that occurred during the cool-down at the end of the heat-treatment. It was therefore not possible to find a single 'best match' value for the tin content, independent of the values used for the other two uncertainties. Therefore, an estimate for the tin content of 5 wt.% was used.

6.6.2.5 Stress relief on cool-down at end of heat-treatment

As explained in Section 6.2, the wire has generally been assumed to be in a stress-free condition just prior to the cool-down at the end of the heat-treatment process. During

the cool-down residual stresses develop because of differences in coefficients of thermal contraction between the different constituent materials. While the temperature is still high enough, however, these stresses will be relieved by creep. The creep rate will depend on the temperature, the stress levels and the creep properties of the materials. A simple method was used to take account of the stress-relief during cool-down. The wire was treated as stress-free at a temperature somewhat below the actual heat-treatment temperature and residual stresses were allowed to develop without any stress-relief during the cool-down from that temperature. Effectively, a temperature threshold was set where complete stress-relief was assumed to take place above it, but none below it. The value to use for this temperature threshold could not be known with any certainty. It is known that bronze can be stress-relieved by heat-treating at 200 to 300°C. This would suggest a value for the threshold of around there would be appropriate. This is also supported by Ahoranta et al. (2008) who found that a threshold temperature of 177 to 227°C gave the best match between predicted and experimentally derived values for the axial residual strain in Nb_3Sn filaments. This cannot be considered accurate, however, because of uncertainties about the constituent material properties used in the modelling. Indeed, the experimental results obtained from the wires that were rapidly cooled at the end of the heat-treatment suggest that a much higher value should be used. Those results, given in Chapters 4 and 5, suggest that very little stress-relief occurs during the cool-down. Rapidly cooled wires would be expected to experience much less stress-relief than slow cooled wires and therefore exhibit measurably different change in length and stress-strain curves. The results showed that there were no differences. Also, work by Flükiger (1982) suggested that residual stresses begin to build up from at least 800 K. For this reason it was concluded that the threshold temperature should be relatively close to the heat-

treatment temperature. The effect on the results of using a range of values close to the heat-treatment temperature is shown in Figure 6.21.

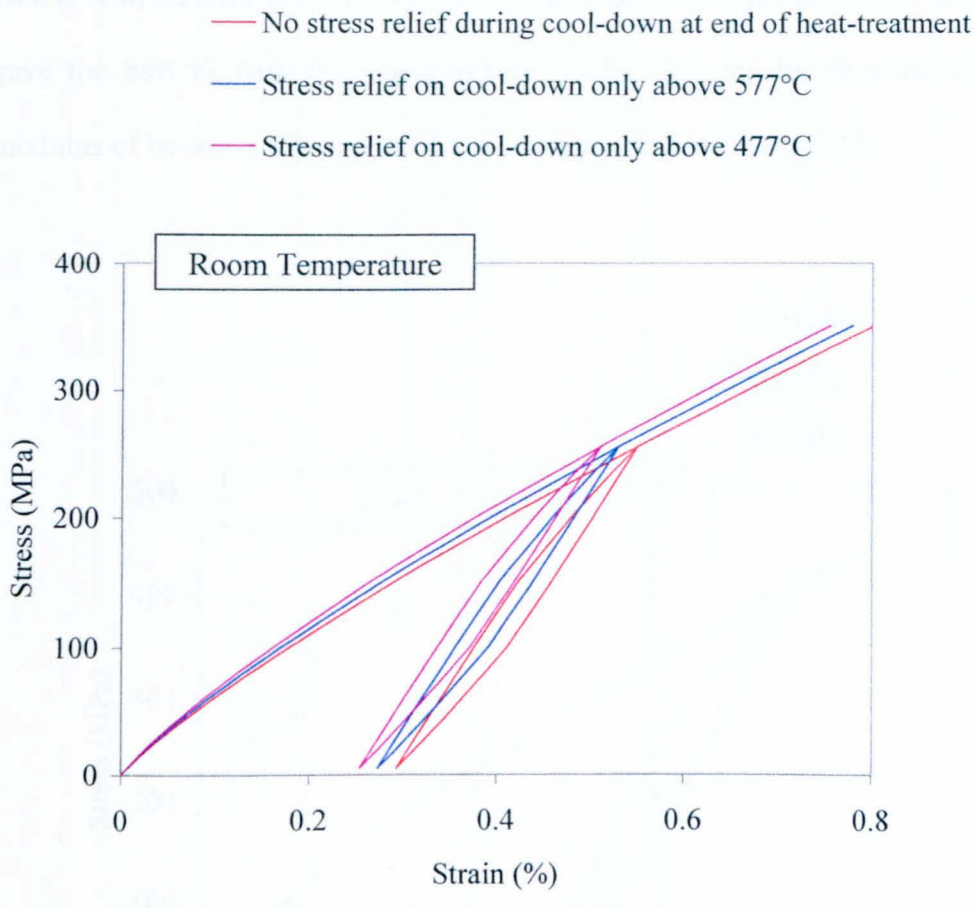

Figure 6.21 Model sensitivity to stress relief during cooling at the end of the heat-treatment

Stress relief on the cool-down was one of three uncertainties that had similar effects on the results, the other two being the grain size and tin content of the bronze. It was therefore not possible to find a single 'best match' value for the threshold temperature, independent of the values used for the other two uncertainties. However, with best estimate values used for the other two uncertainties, a threshold temperature of 577°C (850 K) produced the best match with experiment.

6.6.2.6 Young's modulus of Nb_3Sn

As described in Section 6.4.2.3, there is some degree of uncertainty about the modulus of Nb_3Sn at temperatures below about 100 K. The modulus was assumed to be 135 GPa at temperatures above 100 K and it was found that a modulus of 110 GPa at 77 K gave the best fit with the experimental results. The results obtained with a 77 K modulus of between 100 and 120 GPa are compared in Figure 6.22.

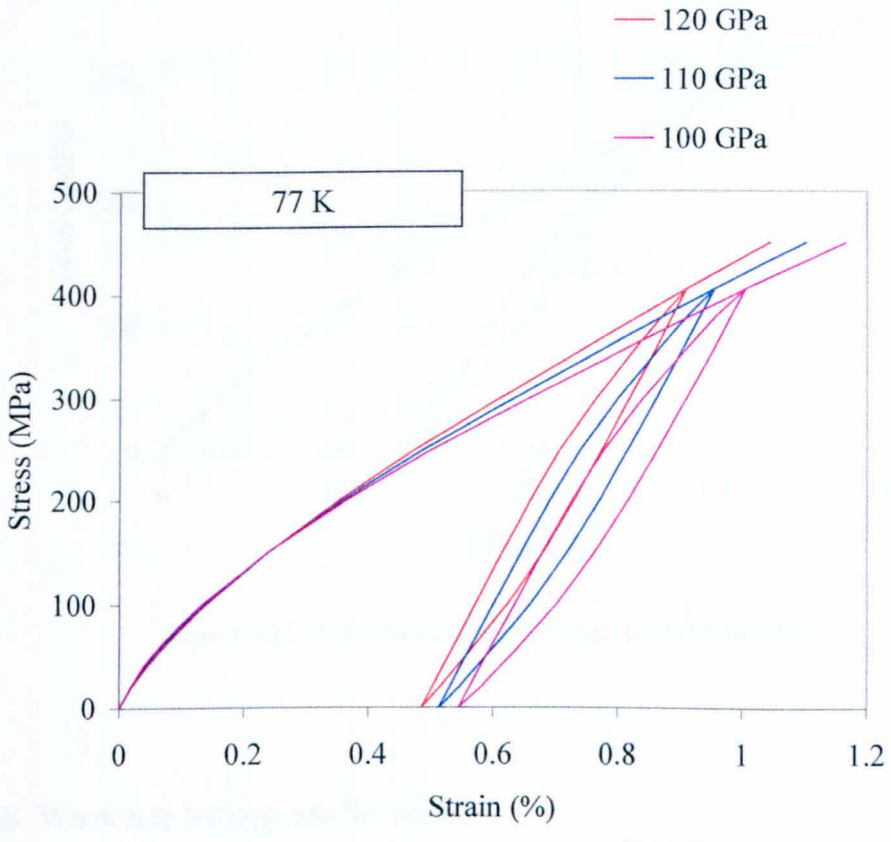

Figure 6.22 Model sensitivity to modulus of Nb_3Sn at 77 K

6.6.2.7 Poisson's ratio of Nb_3Sn

As explained in Section 6.4.2.3, the data available for the Poisson's ratio of Nb_3Sn is scarce. It can be seen from Figure 6.23 that the value used had virtually no effect on the stress-strain curve obtained by the F.E. analysis.

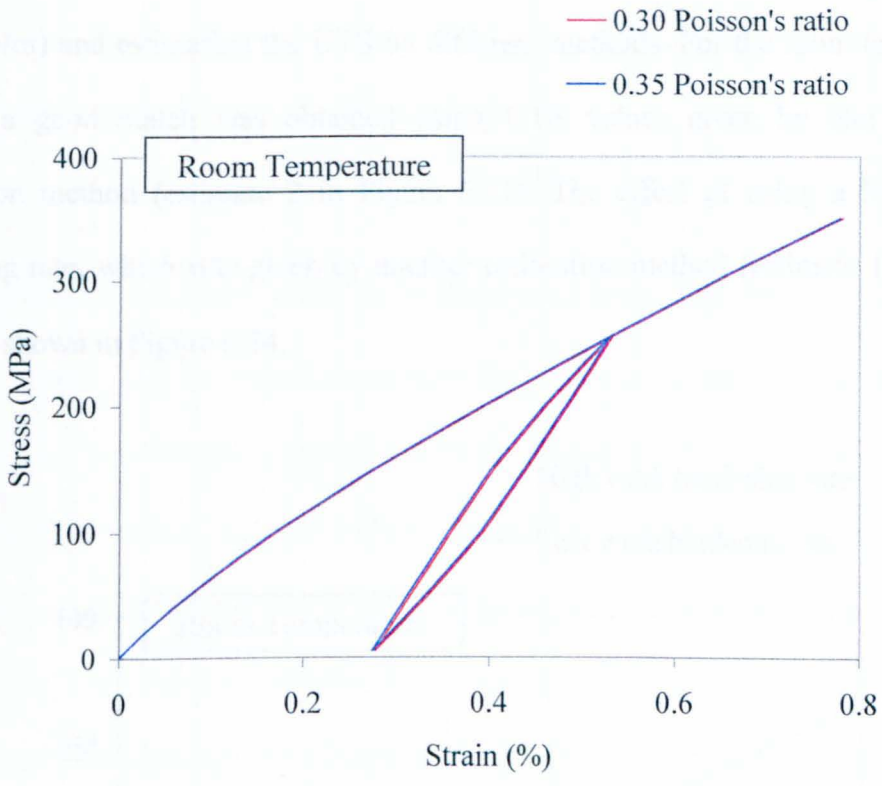

Figure 6.23 Model sensitivity to Poisson's ratio of Nb_3Sn

6.6.2.8 Work hardening rate for bronze

As explained in Section 6.4.2.2, there is a lot of uncertainty about the UTS and elongation for the bronze in the superconducting wire. There is therefore some uncertainty about stress-strain curves of the bronze, as the UTS and elongation are used in Mitchell's expressions (see Section 6.4.2) to compute the stress-strain curve. In contrast, the Young's modulus and yield stress, which are also used in Mitchell's expressions, are known with a good degree of confidence. Thus, uncertainty about the

UTS and elongation effectively means that there is only uncertainty about the work hardening rate, i.e. the slope of the stress-strain curve after the yield point. To obtain a match with the experimental results, different work hardening rates were used in the modelling as described in Section 6.4.2.2. The different work hardening rates were obtained by fixing the elongation to the value predicted by (Mitchell 2005 *Cryogenics*) and estimating the UTS by different methods. For the room temperature results, a good match was obtained using UTS values given by one particular estimation method (estimate 2 in Figure 6.11). The effect of using a lower work hardening rate, which was given by another estimation method (estimate 1 in Figure 6.11), is shown in Figure 6.24.

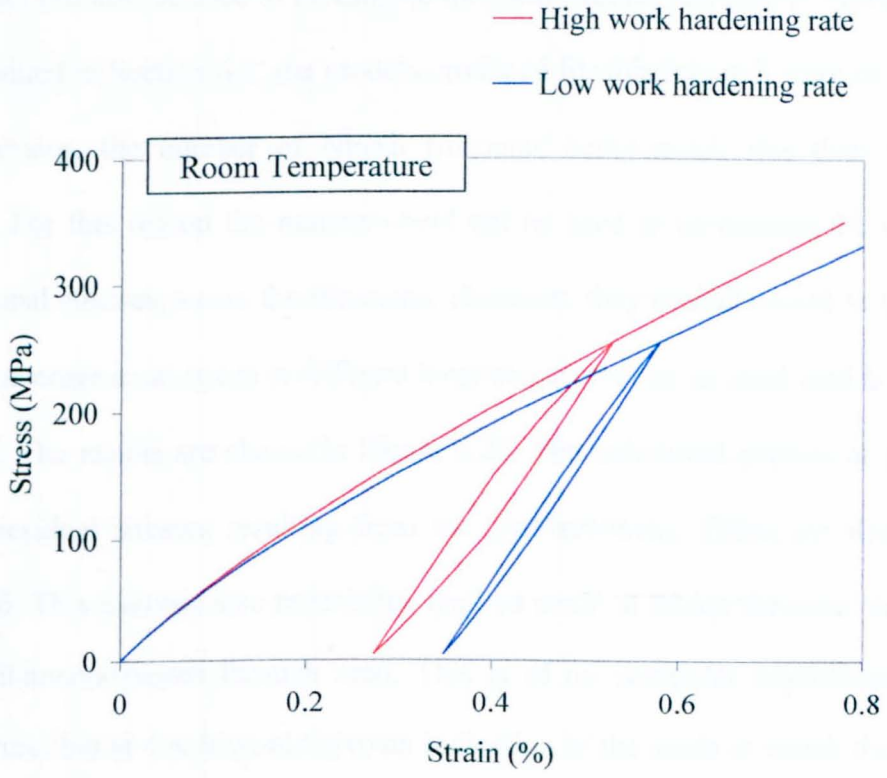

Figure 6.24 Model sensitivity to work hardening rate of bronze

Of all the uncertainties in the model whose effects were investigated, only the work hardening rate of bronze had any significant effect on the width of the hysteresis loop. Another uncertainty that would also influence this is the assumption that the materials behaviour is accurately modelled with the kinematic hardening rule. The work hardening rate of the bronze that gave the best match with the experimental results was not dependent on the assumptions made for the other uncertainties, because these had little effect on the width of the hysteresis loops.

6.6.3 Evolution of stresses within individual constituent materials

As well as modelling the overall stress-strain behaviour of a superconducting wire the F.E model can also be used to investigate the local stresses and strains within the wire. As explained in Section 6.2, the models produced for this research were of simplified cross-sections, the number of Nb_3Sn filaments being much less than the actual number. For this reason the models could not be used to investigate the complex 3 dimensional stresses across the filaments. However, they could be used to investigate how the average axial stress in different locations evolves as an axial load is applied to the wire. The results are shown in Figure 6.25. The individual stresses at zero strain are the residual stresses resulting from the heat-treatment. These are also given in Table 6.6. This analysis also reveals the applied strain at which the axial stress in the Nb_3Sn filaments passes through zero. This is of no particular importance at room temperature, but at 4 K it would give an indication of the strain at which the optimum superconducting properties would be achieved. An analysis at 4 K is not shown here because of uncertainty about the material properties at 4 K, particularly the strength of the bronze.

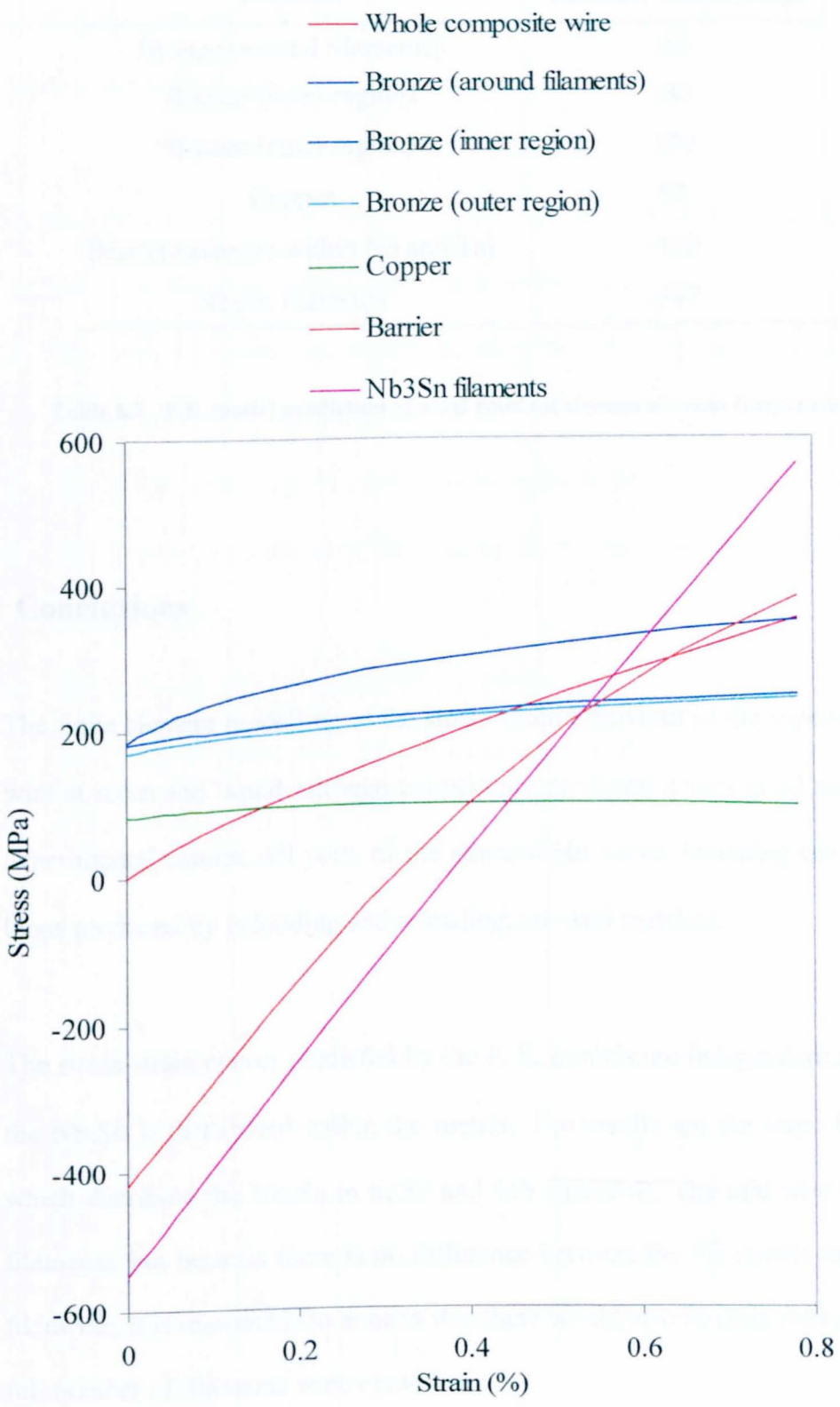

Figure 6.25 F.E. prediction of axial stresses within constituent materials at room temperature

Location	Residual Stress (MPa)
Bronze (around filaments)	185
Bronze (inner region)	183
Bronze (outer region)	170
Copper	82
Barrier (average within Nb and Ta)	-418
Nb_3Sn filaments	-547

Table 6.7 F.E. model prediction of axial residual stresses at room temperature

6.7 Conclusions

1. The finite element modelling of the stress-strain behaviour of the superconducting wire at room and liquid nitrogen temperature produced a very good match to the experimental results. All parts of the stress-strain curve, including the hysteresis loops produced by unloading and reloading, are well matched.

2. The stress-strain curves predicted by the F. E. models are independent of the way the Nb_3Sn is distributed within the matrix. The results are the same for models which distribute the Nb_3Sn in 6, 30 and 618 filaments. The real wire has 22866 filaments, but because there is no difference between the FE results for 6 to 618 filaments, it is reasonable to assume that there would also be little difference if the full number of filaments were modelled.

3. The axial residual stresses in the wire at room temperature predicted by the F. E. model are -550 MPa for the Nb_3Sn filaments, around 170-190 MPa for all the bronze and 82 MPa for the copper core.

4. There is some uncertainty with a number of the assumptions made. The main uncertainties that have a significant effect on the results are:
   i) The work hardening rate of bronze within the wire, i.e. the form of the stress-strain curve after the yield point.
   ii) The Young's modulus of Nb_3Sn at low temperatures
   iii) The amount of stress-relief that occurs during the cool-down at the end of the heat-treatment
   iv) The grain size and tin content of the bronze
   v) How well the kinematic hardening rule represents the stress-strain behaviour of the constituent materials

CHAPTER 7

Etching experiment: validation of the F. E. model and the measurement of residual stresses

7.1 Introduction

To model a superconducting wire it is necessary to know the material properties of the constituent materials. A major factor influencing the validity of any model is how accurately the material properties are represented. Normal material testing is problematic because superconducting wires are complex multi-filamentary composites and it is not possible to separate the constituent materials to such an extent that they can be tested in the normal way (i.e. a tensile test). The material properties are strongly influenced by the structure of the composite wire and its fabrication history, in particular the heat-treatment. It is therefore not possible to obtain material samples for testing that are in the same condition as those found in the wires. The experimental method described in this chapter provides data to validate the F. E. model presented in Chapter 6, and because the method provides data that is directly related to the properties of only selected parts of the wire cross-section, the data is particularly useful for validating the constituent material properties.

Differences in the coefficients of thermal contraction between the constituent materials cause residual stresses to be produced when the wires are cooled from the heat-treatment temperature. This is of particular interest because the superconducting properties of the wire are strongly dependent on the strain state of the Nb_3Sn. It is therefore desirable to measure these residual stresses, both to obtain accurate values for specific wires and for the validation of predictive models. Awaji et al. (2006) used neutron diffraction to measure the residual strain in Nb_3Sn filaments. Neutron diffraction is, however, an expensive and time consuming process. Also, results can only be obtained for grains that are orientated in particular directions. Overall values

are obtained by averaging the results. This could potentially lead to errors if insufficient numbers of grain orientations can be analysed. The experimental method described in this chapter provides an alternative method for the measurement of residual stresses in superconducting wires.

7.2 Description of method

The experimental method described in this chapter has similarities to methods described by Entwistle and Myerscough (1983) and Hojo et al. (2004). Entwistle and Myerscough investigated the axial internal stress in steel wire by measuring the change in length of the wire as its diameter was continuously reduced by dissolution in nitric acid. Hojo et al. investigated the mechanical properties and the thermal residual stress distribution of copper in Nb_3Sn superconducting wire. The stabiliser copper was removed in stages from the outside of the wire by immersion in nitric acid and the stress-strain curves were measured. The Young's modulus, axial residual stress and the plastic zone part of the stress-strain curve for the copper were obtained by comparing the stress-strain curves before and after etching away the copper. The analysis required the change in length caused by etching away the copper, but this was not measured directly. Instead, the yield strength of the copper was estimated and from this the change in length was calculated. The experimental method employed for this thesis is a combination of the methods used by Entwistle and Myerscough (1983) and Hojo et al. (2004). The bronze matrix material of the superconducting wire was etched away in stages. After each etching process the diameters and lengths of the wires were measured, and stress-strain curves were obtained by tensile testing some of the etched specimens.

The analysis of the results was based on a simple force balance equation. The wire cross-section is treated as being composed of two parts, a central core and an outer ring joined at radius r as shown in Figure 7.1.

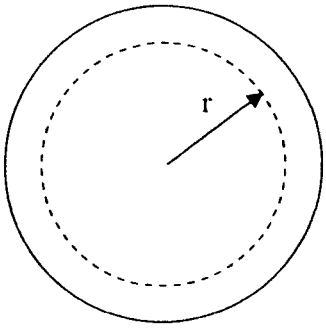

Figure 7.1 Analytical treatment of wire cross-section

The total axial force in the wire is the sum of the axial force in the two parts, as given by the following equation.

$$\sigma_T A_T = \sigma_1 A_1 + \sigma_2 A_2 \tag{7.1}$$

where σ is the stress, A is the cross-sectional area and the suffixes 1, 2 and T refer to the two parts of the wire and the whole wire respectively.

Now, if radius r is the radius to which the wire is etched down to, the stress in the material that has been etched away can be obtained from the following equation.

$$\sigma_2 = \frac{\sigma_T A_T - \sigma_1 A_1}{A_2} \tag{7.2}$$

where σ_T and σ_1 are obtained from the stress-strain curves of the wire before and after the etching operation. The strain associated with the change in length that results from

the etching operation is applied to the stress-strain curve of the etched wire to ensure that the strain values are relative to the same original length. This was done by simply shifting the curve along the strain axis by the strain associated with the change in length, dL, as illustrated in Figure 7.2.

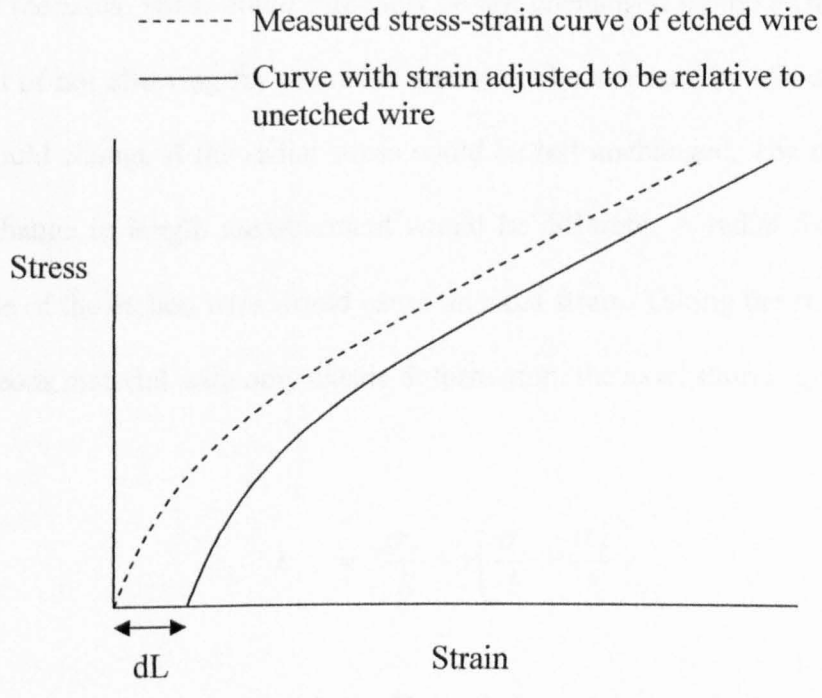

Figure 7.2 Illustration of the method used to make strain relative to original length

By applying this equation, stress-strain curves for the material that was etched away could be derived. However, the initial parts of the curves from zero strain up to the change in length strain could not be derived directly. This was because the measured stress-strain curve of the etched wire only starts from the change in length strain. By extrapolating the curves back, however, the derived stress-strain curve for the material that was etched away could be extended back to zero applied strain. The average axial residual stress in the two parts of the wire could then be obtained by simply reading off the stress at zero applied strain.

The method described above has a significant flaw, however. It makes no allowance for any lateral stresses. It only considers the axial stresses. When an outer layer is removed by etching to radius, r, the axial force in that layer is removed, but if there is any radial stress at radius r prior to etching, then the radial force acting on the etched wire is also removed. The method would accurately account for the 3 dimensional stresses if the radial stress could somehow be left unchanged by the etching operation. The effect of not allowing for the radial stress can be assessed by evaluating how the results would change if the radial stress could be left unchanged. The major effect is that the change in length measurement would be different. A radial force applied to the outside of the etched wire would cause an axial strain. Taking the simple case of a homogeneous material with only elastic deformation, the axial stain is given by

$$\varepsilon_z = \frac{\sigma_z}{E} - \nu\left(\frac{\sigma_x}{E} + \frac{\sigma_y}{E}\right) \tag{7.3}$$

where ε is strain, σ is stress, E is the Young's modulus, ν is the Poisson's ratio and the suffixes x, y and z refer to the 3 Cartesian directions.

The non-axial stresses have a smaller effect on the axial strain than the axial stress, by a factor of the Poisson's ratio (therefore approximately 0.3). Applying a radial stress, however, would also change the hoop stress (in the simple case the hoop stress would be equal to the radial stress), so the change in length could be around 0.6 that of the change in length resulting from an equivalent axial stress.

The error resulting from only considering the axial stresses could therefore be significant and obviously would depend on the level of the radial stresses compared to

the axial ones. To evaluate the approximate degree of error a finite element assessment of the method was undertaken.

7.3 Investigation of method using Finite Element

The etching experiment was modelled using the finite element model described in Chapter 6. After the temperature load step to cool the wire from 577°C down to room temperature, the etching was modelling by killing elements from the outside of the wire. A single element wide ring of elements was killed on each load step to minimise errors associated with coarse load stepping. After the wire diameter was reduced to the desired amount, the axial strain was extracted from the results and then negative pressure was applied in stages to the top face of the model to simulate a tensile test in just the same way as was done in Chapter 6. The results were then used to derive the stress-strain curves of each of the radial zones of material that were etched away in the way described in Section 7.2. To check the accuracy of these derived curves, the actual stress-strain behaviour of each of the radial zones was obtained by analysing the stresses using the results of an F. E. simulation of a tensile test on the whole wire. The force in each of the radial zones was obtained using the Ansys Surface Operations command. The results are compared in Figure 7.3.

It can be seen that the error in the prediction of stress-strain curves and residual stresses using the etching method is significant for some parts of the wire, but is remarkably accurate for other parts. For example, the axial residual stress in the outer bronze layer (Ø1.4 to surface) is under predicted by about 30%. The predictions are most accurate in the regions of the wire containing the Nb_3Sn filaments embedded in the bronze matrix, i.e. Ø0.6 to Ø0.8, Ø0.8 to Ø1.0, Ø1.0 to Ø1.2 and Ø1.2 to Ø1.4.

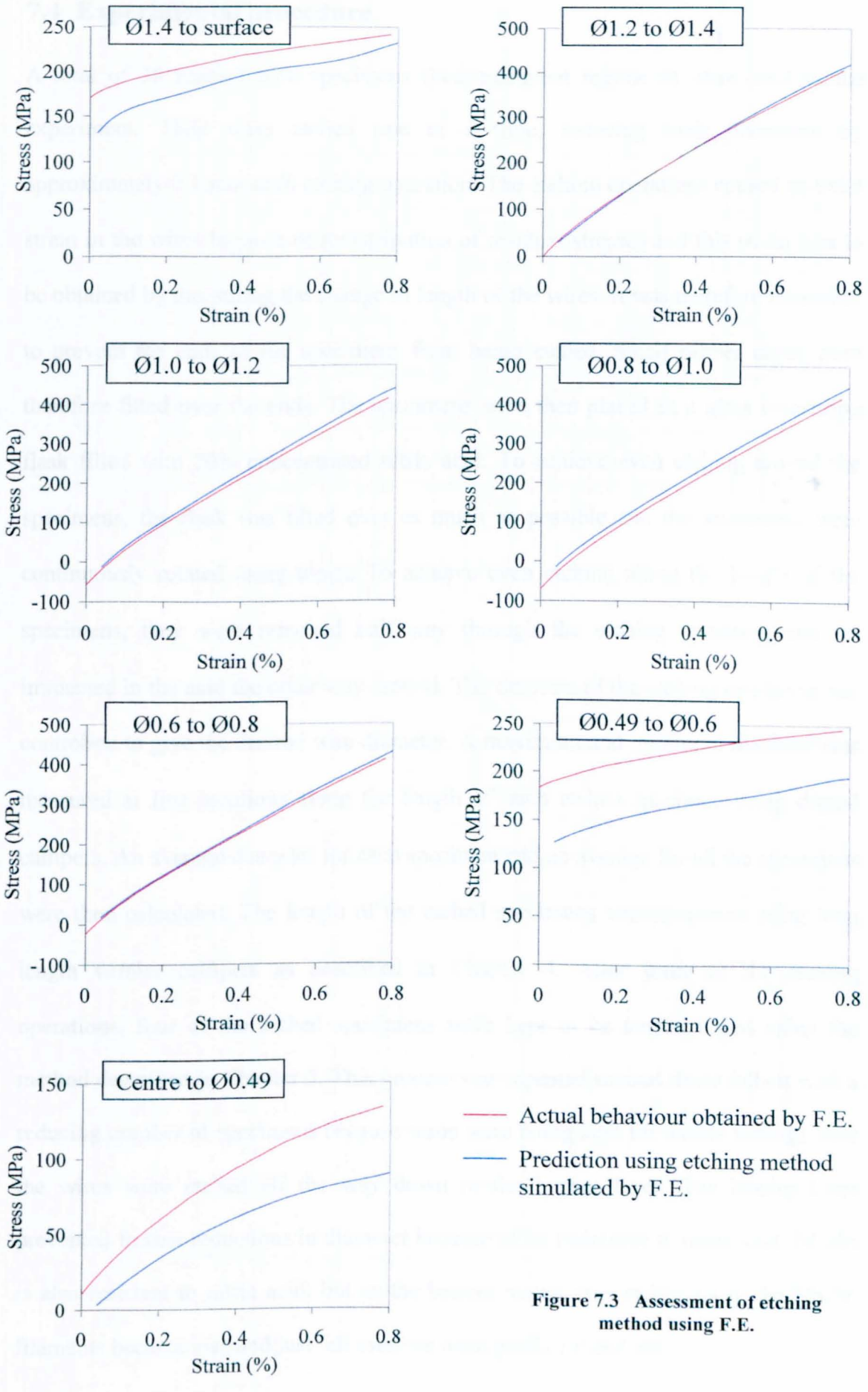

Figure 7.3 Assessment of etching method using F.E.

7.4 Experimental procedure

A total of 30 reacted wire specimens (heat-treatment regime 8) were used in the experiment. They were etched one at a time, reducing their diameters by approximately 0.1 mm each etching operation. The etching operations caused an axial strain in the wires because of redistribution of residual stresses and this strain was to be obtained by measuring the change in length of the wires. It was therefore necessary to prevent the ends of the specimens from being etched. Small rubber corks were therefore fitted over the ends. The specimens were then placed in a glass measuring flask filled with 20% concentrated nitric acid. To achieve even etching around the specimens, the flask was tilted over as much as possible and the specimens were continuously rotated using tongs. To achieve even etching along the length of the specimens, they were removed half way through the etching operation and re-immersed in the acid the other way around. The duration of the etching operation was controlled to give the desired wire diameter. A maximum and minimum diameter was measured at five locations along the length of each etched specimen using digital callipers. An average diameter for each specimen and an average for all the specimens were then calculated. The length of the etched specimens was measured using long length vernier callipers as described in Chapter 4. After some of the etching operations, four of the etched specimens were kept to be tensile tested using the method described in Chapter 5. This process was repeated several times (albeit with a reducing number of specimens because some were being kept for tensile testing) until the wires were etched all the way down to the barrier layer. The barrier layer prevented further reductions in diameter because of its resistance to nitric acid. Nb_3Sn is also resistant to nitric acid, but as the bronze matrix was etched away the Nb_3Sn filaments became lose and just fell away or were gently rubbed off.

7.5 Experimental results

7.5.1 Change in length

The results of the change in length measurements are shown in Figure 7.4. Each point shows the change in length of an individual wire specimen. The different colours and point types merely show the groups of specimens which were etched down to approximately the same target diameter. A best fit curve is also shown on the graph. There was quite a lot of scatter in the results, but the general trend was that the length increased as the outer layers were etched away, reaching a maximum with the diameter at about 1.0 mm, and then decreased as the diameter was reduced further.

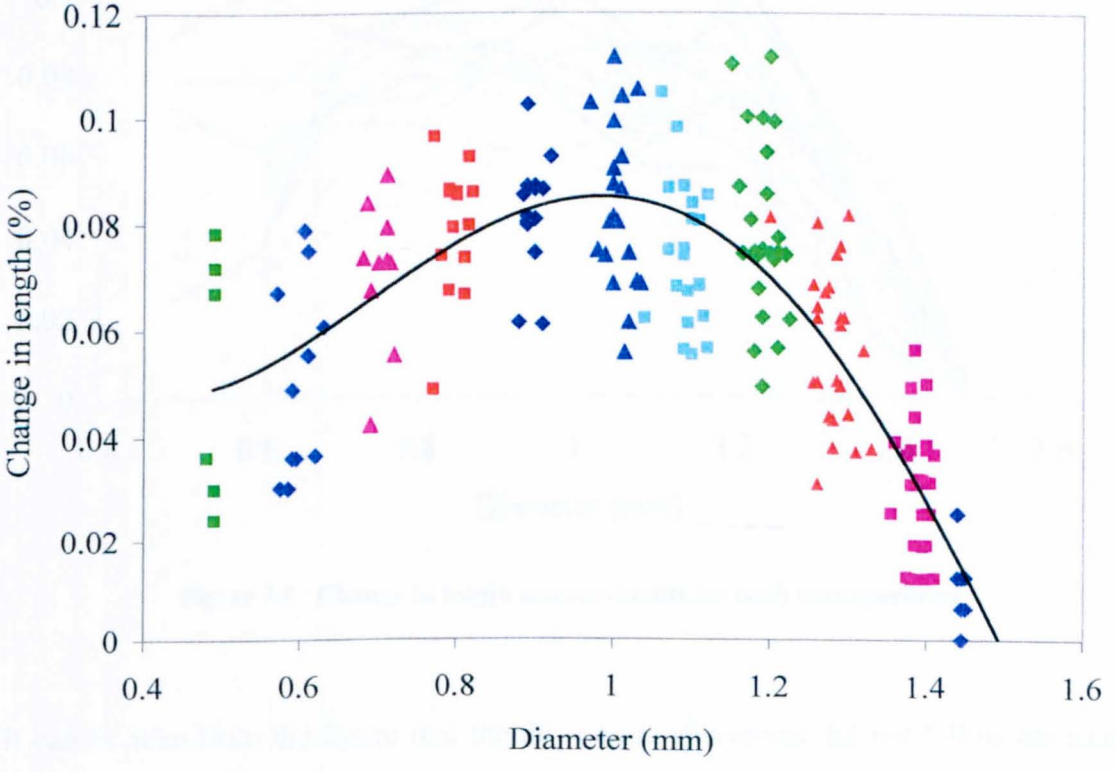

Figure 7.4 Change in length due to etching wires down to smaller diameters

There is some doubt about the results, however, particularly for the smaller diameters. The reason for this is that some significantly different results were obtained when three extra specimens were tested. These were specimens that had been kept for the tensile testing part of the experimental procedure, but were surplus to requirement. These specimens were then etched down to the smaller diameters and the changes in lengths were measured after each etching operation. The results from these specimens are shown in Figure 7.5 as bold lines to differentiate them from the other data.

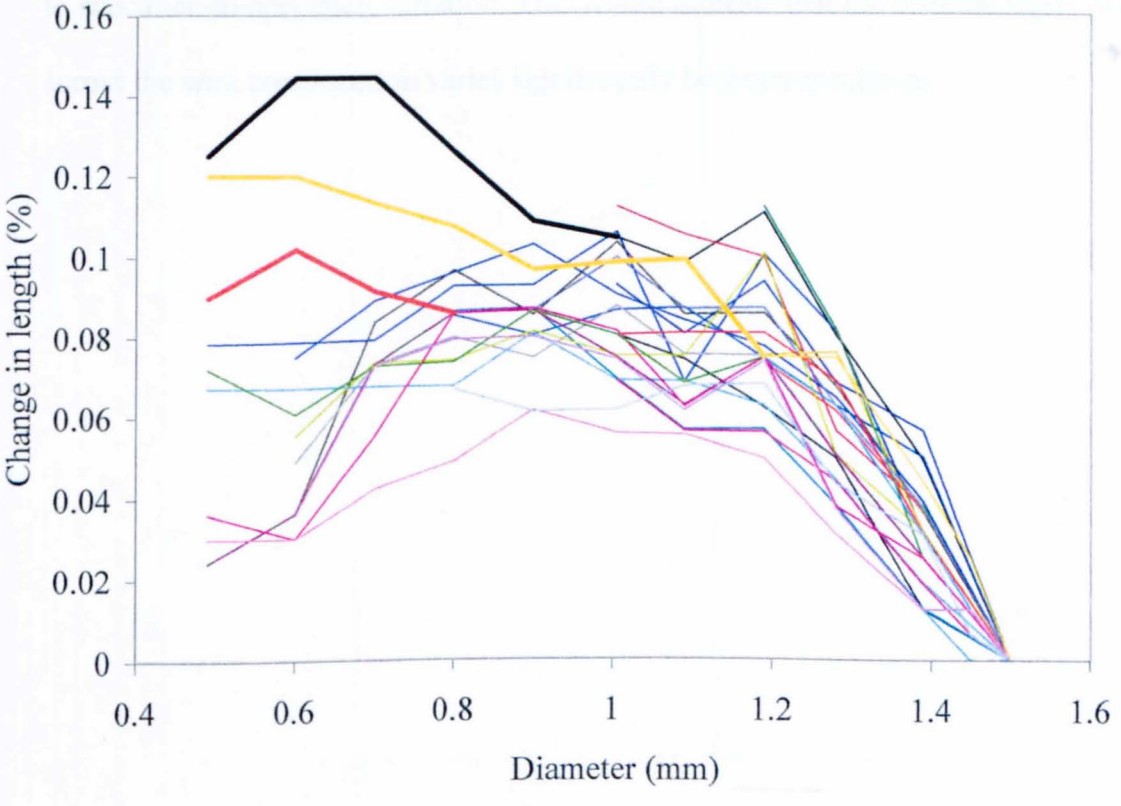

Figure 7.5 Change in length measurements for each wire specimen

It can be seen from the figure that the three extra specimens did not follow the same trend as the other specimens. A possible cause for the discrepancy is the time difference between testing the specimens. The bulk of the specimens were etched to the different diameters over a period of a few days with the length measurements

being made soon after each etching operation. The extra three specimens were given some of the etching operations at the same time as the other specimens, but were then kept for about 3 months before the etching operations were resumed. During this delay of 3 months it is possible that some stress relaxation had taken place. It had already been observed that some time dependent stress relaxation does indeed take place at room temperature. When the wires were straightened by hand to prepare them for heat-treatment it was found that the wires would regain some of their curvature if left for a few minutes. The figure also shows that the scatter in the results is mostly related to specimen-to-specimen variation. This would indicate that the residual stress profile across the wire cross-section varies significantly between specimens

7.5.2 Stress-strain behaviour of etched wires

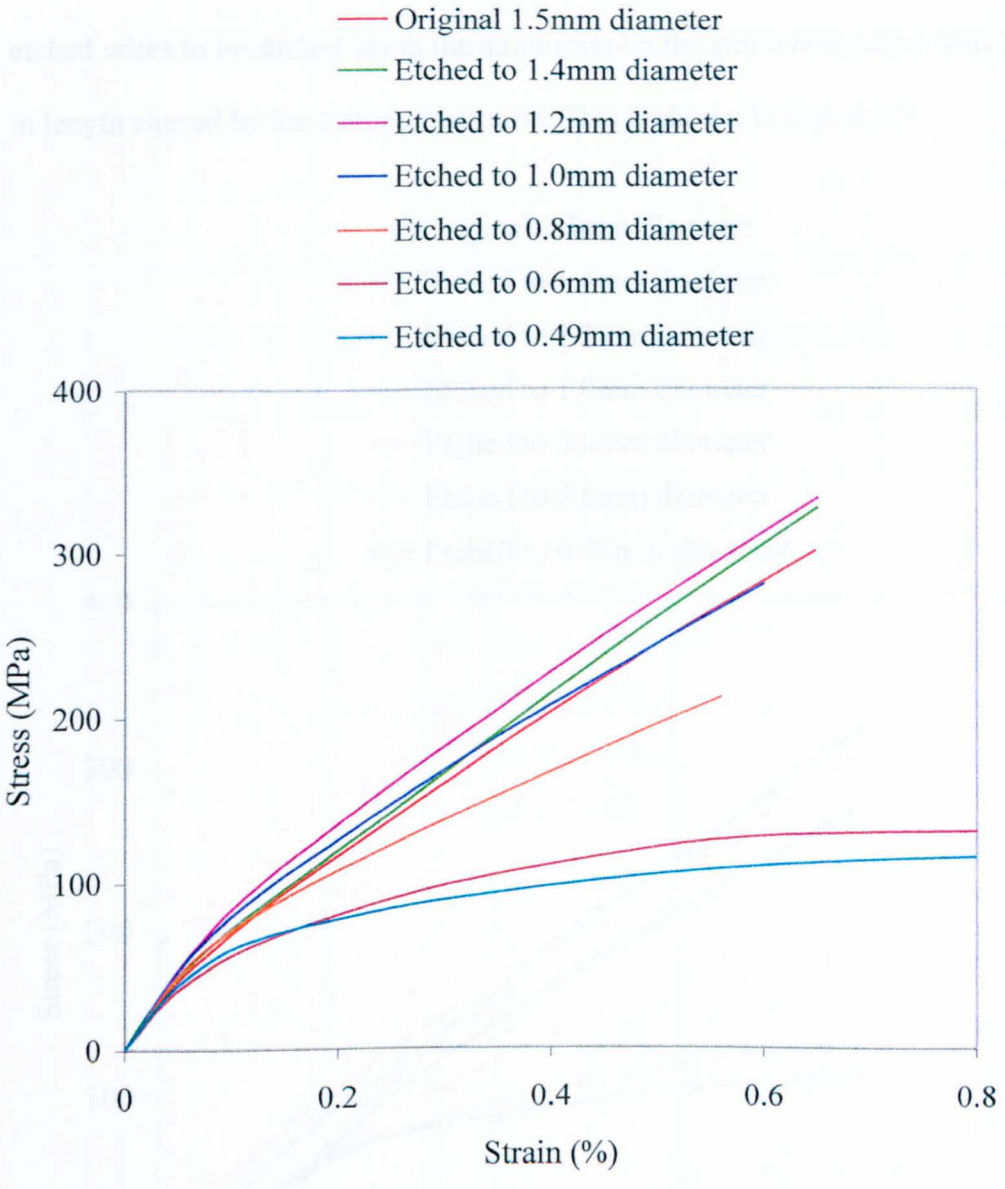

Figure 7.6 Stress-strain curves of wires after etching

Figure 7.6 shows the stress-strain curves that were obtained from the etched wire specimens. Each curve is an average of 4 tensile tests done on different specimens. For each individual test several loading and unloading cycles were performed in the same way as described in Chapter 5. To simplify the figure, however, the resulting hysteresis loops have been removed from the curves.

7.5.3 Derived residual stresses and stress-strain behaviour of radial zones

As described in Section 7.2, the method requires that the stress-strain curves for the etched wires to be shifted along the strain axis by the strain associated with the change in length caused by the etching operation. This is shown in Figure 7.7.

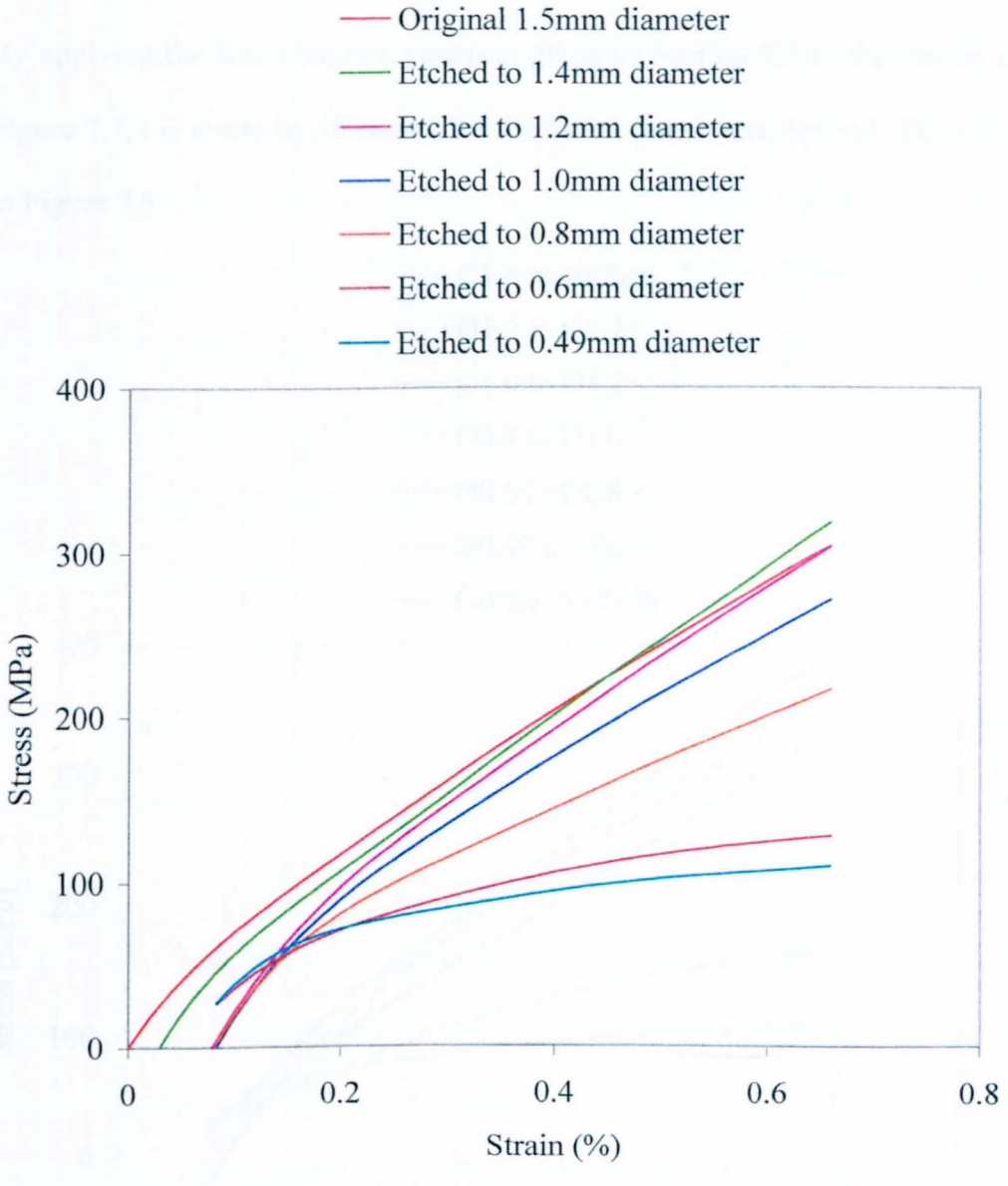

Figure 7.7 Stress-strain curves of etched wires with normalised strain

For some of the curves in Figure 7.7, the initial parts are not shown as they need to be disregarded. The reason for this is that the wires actually decrease in length for the etching operations that reduce the diameter below about 1 mm. Therefore, the wires

effectively behave as if being unloaded. During the subsequent tensile tests, the stress-strain behaviour does not return to the original loading curve until the strain exceeds that at which unloading began. The curves in the figure are only shown from this point.

By applying the force balance equation given in Section 7.2 to the curves shown in Figure 7.7, the stress-strain curves for the radial zones were derived. These are shown in Figure 7.8.

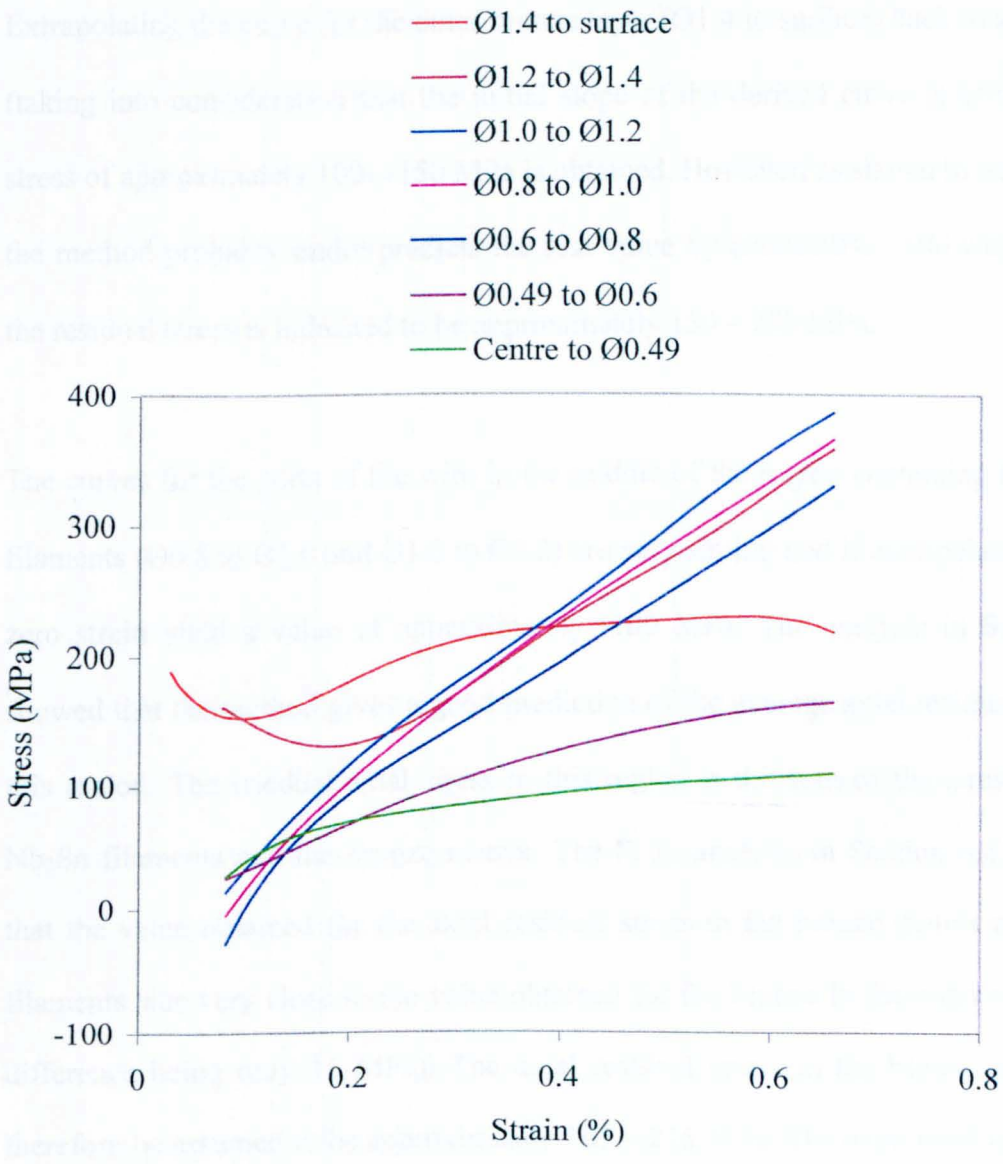

Figure 7.8 Experimentally derived stress-strain curves of radial zones

The derived stress-strain curves for the outer two radial zones, Ø1.4 to surface and Ø1.2 to Ø1.4, clearly show some error because of the negative slope at the start of the curves. This is probably due to error in the measured stress-strain curves in this strain region. The measured stress-strain curves are an average of the results from 4 specimens and because there was significant variation between these, some degree of error is inevitable. The axial residual stresses in each of the radial zones can be obtained by extrapolating the curves back to zero strain. It can be seen from the figure that accurate extrapolation is difficult, but approximate values can be obtained. Extrapolating the curve for the outer bronze layer (Ø1.4 to surface) back to zero strain (taking into consideration that the initial slope of the derived curve is erroneous), a stress of approximately 100 – 150 MPa is obtained. However, as shown in Section 7.3, the method probably under predicts the real value by about 30%. Allowing for this, the residual stress is indicated to be approximately 150 – 200 MPa.

The curves for the parts of the wire in the middle of the region containing the Nb_3Sn filaments (Ø0.8 to Ø1.0 and Ø1.0 to Ø1.2) are very similar and if extrapolated back to zero strain yield a value of approximately -100 MPa. The analysis in Section 7.3 showed that the method gives a good prediction of the average axial residual stress in this region. The residual axial stress in this region is the sum of the stresses in the Nb_3Sn filaments and the bronze matrix. The F. E. analysis in Section 6.6.3 showed that the value obtained for the axial residual stress in the bronze matrix around the filaments was very close to the value obtained for the bronze in the outer region (the difference being only 15 MPa). The axial residual stress in the bronze matrix can therefore be assumed to be approximately 165 – 215 MPa. The axial residual stress in the Nb_3Sn filaments can therefore be calculated as follows:

$$\sigma_T A_T = \sigma_f A_f + \sigma_m A_m \tag{7.4}$$

$$\Rightarrow \quad \sigma_f = \frac{\sigma_T A_T - \sigma_m A_m}{A_f} \tag{7.5}$$

where σ_T and A_T are the stress in and the area of the of the region as a whole, σ_f and A_f are the stress in and the total area of the filaments, and σ_m and A_{Tm} are the stress in and the area of the bronze matrix excluding the filaments. The areas are calculated from the measurements of the wire cross-section, i.e. diameter to inner and outer edge of filaments region is 0.58mm and 1.34mm respectively, filament diameter is 0.0047mm and the total number of filaments is 22866. The residual compressive stress in the filaments comes to 600 to 694 MPa when using 165 to 215 MPa for the residual tensile stress in the bronze matrix.

7.6 Comparison between F. E. and experimental results

7.6.1 Change in length

Figure 7.9 compares the F. E. and experimental results for the change in length resulting from removal of outer layers by etching. The results agree very well over the small range from 1.5mm diameter down to about 1.35mm, but for reductions in diameter beyond that there is a big difference in the results. In the F. E. analysis, the length begins to decrease after the etched surface reaches the filaments. Experimentally it was found that the length continued to increase until the diameter was reduced to approximately 1mm, well into the region containing the filaments. The reason for this is unknown, although it may be partly due to stress relaxation taking

place after the etching operations. The results presented in Section 7.5.1 indicate that such stress relaxation did takes place.

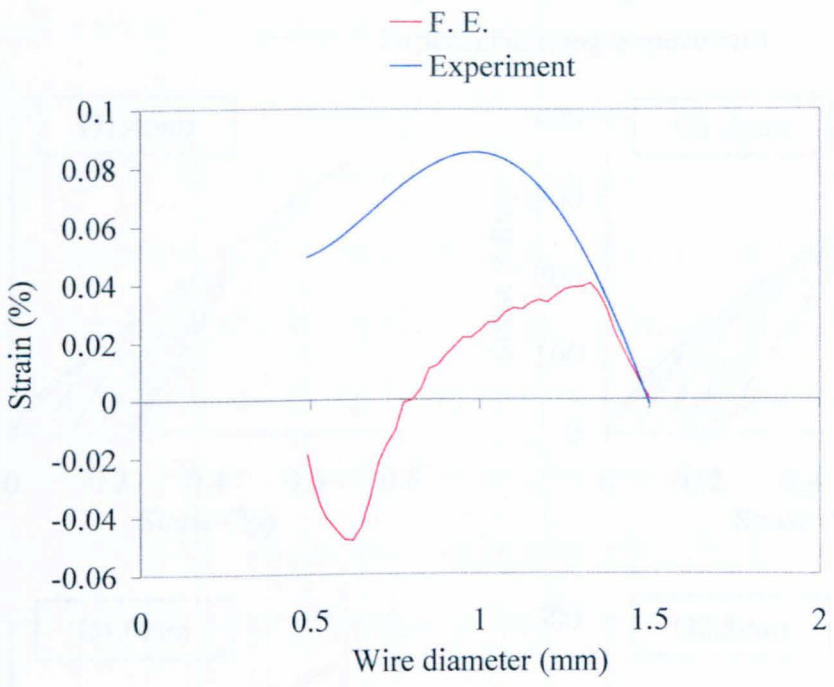

Figure 7.9 Change in length due to etching: F.E. and experiment compared

7.6.2 Stress-strain behaviour of etched wires

Figure 7.10 shows the stress-strain curves of the etched wires obtained experimentally and by F. E. modelling. For the experimental data, a stress-strain curve obtained from an individual wire specimen is shown on each graph along with the curve representing the average of the 4 specimens that were tested. This is so that the hysteresis loops can be compared (the curve representing the average does not include the hysteresis loops). The figure shows that the results compare reasonably well for all sizes except the smallest 0.49mm diameter. For the 1.4mm diameter wire, the results are in very close agreement. There are some differences in the sizes of the hysteresis loops. For the 1.2, 1.0 and 0.8mm diameter wires, the experimental hysteresis loops are narrower than those obtained from the F. E. analysis. For the 0.6 and 0.49mm diameter wires, the opposite is the case.

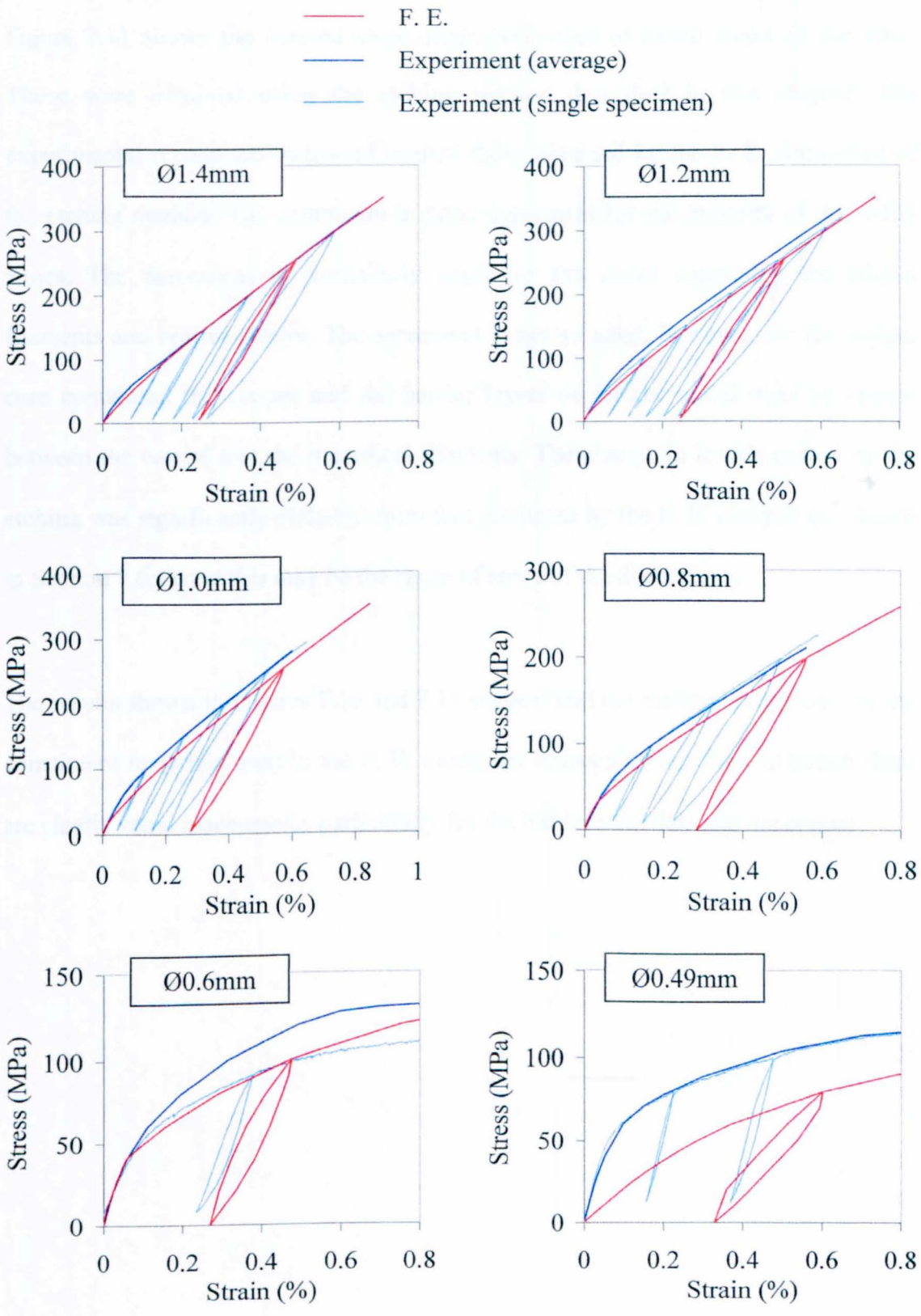

Figure 7.10 Stress-strain curves of etched wires: F.E. and experiment compared

7.6.3 Derived residual stresses and stress-strain behaviour of radial zones

Figure 7.11 shows the derived stress-strain behaviour of radial zones of the wire. These were obtained using the etching method described in this chapter. The experimental results are compared against those obtained by the F. E. simulation of the etching method. The results are in good agreement for the majority of the radial zones. The agreement is particularly good for the zones containing the Nb_3Sn filaments and bronze matrix. The agreement is not so good, however, for the central core containing the copper and the barrier layers or for the radial band of bronze between the barrier and the innermost filaments. The change in length caused by the etching was significantly different from that predicted by the F. E. analysis (as shown in Section 7.6.1) and this may be the cause of some of the discrepancy.

The results shown in Figures 7.10 and 7.11 suggest that the material properties for the constituent materials used in the F. E. model are reasonably accurate, although there are clearly some inaccuracies particularly for the barrier materials and the copper.

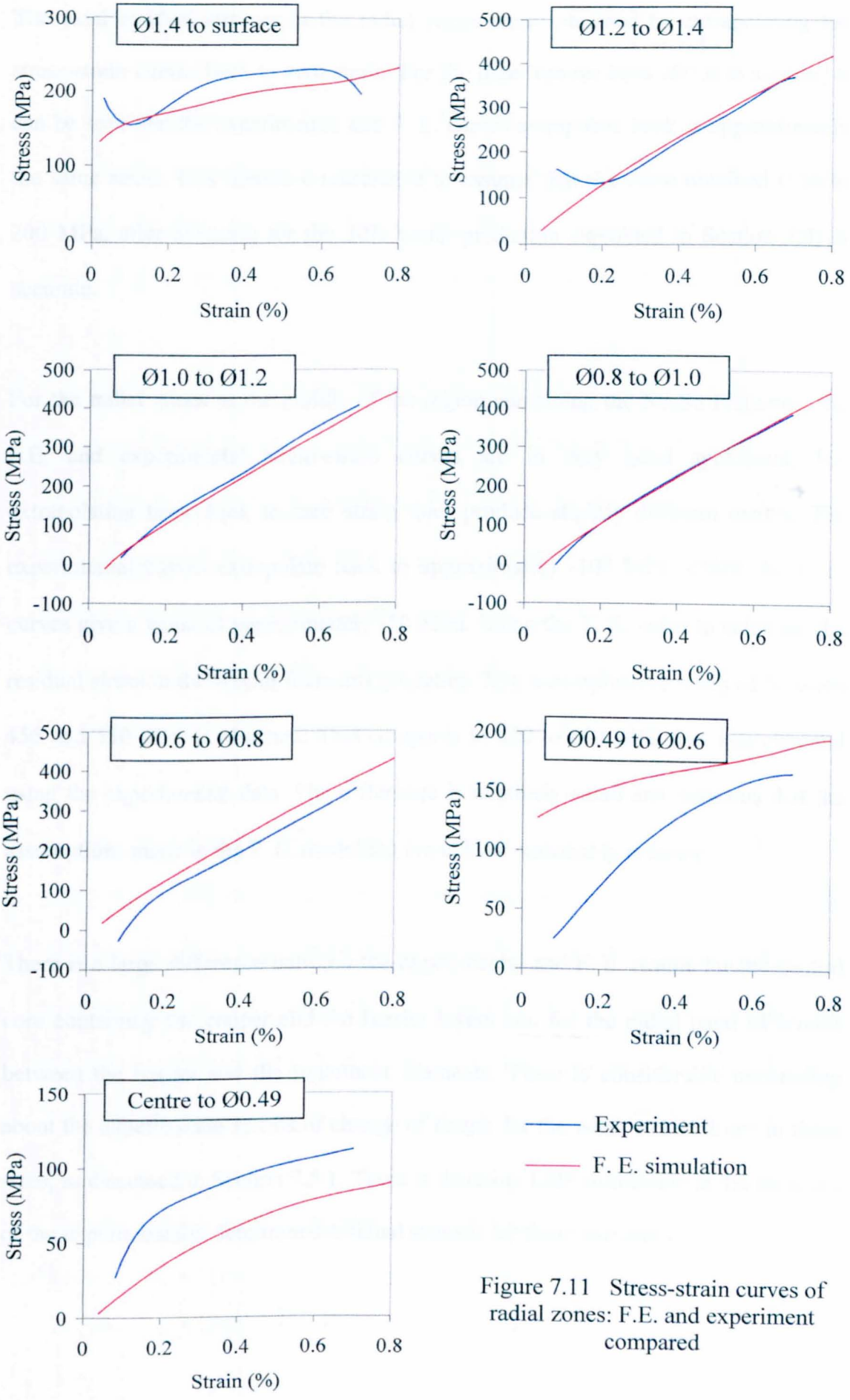

Figure 7.11 Stress-strain curves of radial zones: F.E. and experiment compared

The axial residual stresses in the radial zones werre obtained by extrapolating the stress-strain curves back to zero strain. For the outer bronze layer (Ø1.4 to surface) it can be seen that the experimental and F. E. curves extrapolate back to approximately the same stress. It is therefore reasonable to assume that the value obtained (150 to 200 MPa, after allowing for the 30% under-prediction explained in Section 7.3) is accurate.

For the radial zones in the middle of the region containing the Nb_3Sn filaments, the F.E. and experimental stress-strain curves are in very good agreement, but extrapolating them back to zero strain does produce slightly different results. The experimental curves extrapolate back to approximately -100 MPa, whilst the F. E. curves give a value of approximately -50 MPa. Using the F. E. value to calculate the residual stress in the Nb_3Sn filaments (equation 7.5), a compressive stress of between 456 and 550 MPa is obtained. This compares to 600 to 694 MPa that was obtained using the experimental data. The difference is relatively small and indicates that the assumptions made in the F. E. modelling are at least reasonably accurate.

There is a large difference between the experimental and F. E. results for the central core containing the copper and the barrier layers and for the radial band of bronze between the barrier and the innermost filaments. There is considerable uncertainty about the experimental results of change of length for the wires etched down to these sizes, as discussed in Section 7.5.1. There is therefore little confidence in the accuracy of the experimentally determined residual stresses for these two areas.

7.7 Discussion and conclusions

1. An experimental method has been proposed for providing data to validate F. E. models of superconducting wires and to measure axial residual stresses. The method involves etching away material from the surface of wire specimens, measuring the change in length and the stress-strain curves of the etched wires.

2. The method only takes axial stresses into account and will therefore produce inaccurate results if there are significant non-axial stresses present. An assessment of the errors was made by simulating the etching method using the F. E. model described in Chapter 6. The error between the actual stress-strain behaviour within radial zones and the behaviour derived by the etching method was relatively small for the majority of the radial zones. By having knowledge of this error, however, the experimental results can be compensated to increase the accuracy.

3. Etching away material from the outside of wire specimens produces a change in length that is related to the axial residual stress that was present in the material etched away. The experimental results partially agree with the change in length predicted by the F. E. simulation. The agreement was good with only small amounts of material being etched away, but the agreement did not hold with further etching. This shows that there are some deficiencies with the F. E. model.

4. The experimental results exhibited a large amount of scatter and appeared to be dependent on the time period between the etching operations. This suggested that some time dependent stress relaxation was taking place at room temperature. The

F. E. model described in Chapter 6 only allows for stress-relief at high temperatures and so may not be adequate for modelling this behaviour.

5. The measured stress-strain curves of wires etched down to a range of diameters have been compared with those obtained by F. E. simulation using the model presented in Chapter 6. Also the derived stress-strain curves of radial zones of material within the wire have been compared with those obtained by the F. E. simulation. Generally, the results compare well giving validation for the assumptions made in the modelling, particularly the material properties of the constituent materials. There were some differences, however, suggesting that the F. E. model is not accurate in some respects. In particular, the measured and F. E. stress-strain curves of wires etched down to the barrier layer are significantly different. This suggests that the material properties of the copper core and the barrier layers have not been represented accurately.

6. The value for the tensile axial residual stress in the outer bronze layer that was obtained using the experimental method was approximately 150 to 200 MPa. This is in agreement with the value produced by the F. E. analysis in Chapter 6 (170MPa).

7. Using the experimental data, the compressive residual stress in the Nb_3Sn filaments was calculated to be in the region of 600 to 694 MPa. The figure obtained from the F. E. analysis in Chapter 6 was 547 MPa. The difference is relatively small and so provides further experimental evidence of the validity of the F. E. model.

CHAPTER 8

Conclusions and recommendations for future work

8.1 Conclusions

The magnetic field strength that can be generated by superconducting magnets made with Nb_3Sn multi-filamentary composite wire is dependent on the mechanical as well as the superconducting properties of the wires. The wires can be subjected to high levels of stress, particularly in large or high field magnets. The amount of strain that is produced by this stress is dependent on the mechanical properties of the wires, and the strain state of the superconducting Nb_3Sn within the wires strongly influences the current carrying capacity and therefore the maximum magnetic field strength. This thesis presents a finite element model of a superconducting wire for modelling the mechanical behaviour and also the results of comprehensive experimental measurements of the mechanical properties made on particular superconducting wire manufactured by Oxford Instruments. The F. E. model was optimised and validated using the results of tensile tests carried out at room temperature and 77 K. A very good match was achieved between the F. E. and experimental results for stress-strain behaviour at both temperatures. Extra validation was provided by data obtained from a novel experimental method that involved etching away concentric layers from the outside of wire specimens, measuring the axial strain caused by the redistribution of residual stresses and measuring the change in the stress-strain behaviour. More details of the findings of the thesis are given below.

For the experimental work, it was necessary to have wire specimens that had been given a reaction heat-treatment process. Specialised inert atmosphere heat-treatment apparatus was designed and built for this purpose and this was used to prepare specimens with a range of different heat-treatments. In practice, the reaction heat-

treatment is usually given after the wire has been wound onto the magnet coil. Changes in wire dimensions that occur as a result of the heat-treatment can affect the performance of the magnet by causing the wire to become loose or by changing the axial and contact stresses. The changes in wire dimensions of the heat-treated wire specimens were measured. Specifically, specimen volume and length measurements were made from which specimen diameter was calculated. The average diameters of the Nb3Sn/Nb filaments within the wires were also measured. In general, wire length, diameter and volume, as well as filament diameter, all generally increase as a result of the heat-treatment. The implications of these dimensional changes for magnet manufacture were discussed in Chapter 4.

Obtaining accurate experimental measurements of the mechanical properties of superconducting wires is made difficult by the small diameter of the wires and their low yield strength. A tensile testing method was developed for this thesis that enabled reliable results to be obtained. The effect of the reaction heat-treatment process on the mechanical properties was investigated by testing wires given a range of different heat-treatments. To the knowledge of the author, this is the first time such a study has been carried out. The results indicated that significant changes in mechanical properties are caused by the heat-treatment. However, the mechanical properties of wires given short heat-treatments were very similar to those given very long ones. Therefore, altering the heat-treatment duration within the limits required to produce reasonable superconducting properties, would have an insignificant effect on the mechanical properties (at least for the particular wire investigated for this thesis).

A finite element model was developed to model the mechanical behaviour. This involved modelling the thermal residual stresses that develop as the wire is cooled from the heat-treatment temperature. These stresses are relatively large because of the big difference in the coefficients of thermal expansion of the different constituent materials of the wire. The stress-strain behaviour at room temperature and 77 K was obtained by simulating tensile tests. Loading and unloading cycles were included in the simulation to obtain hysteresis loops. Due to computational constraints it was not possible to model the true geometry of the composite wire with 22866 filaments within it. The volume fractions of the different components were accurately reproduced in the models, but the wire was modelled as having a reduced number of filaments: 6, 30 and 618 filaments in different models. The simulated stress-strain behaviour was the same for all three models and therefore it is reasonable to conclude that for the purposes of modelling overall stress-strain behaviour it is not necessary to model the true number of filaments: it is sufficient to model a smaller number of filaments, but with larger diameters to maintain the correct volume fraction.

The material properties of the constituent materials were required as an input for the F. E. models. There was some uncertainty, however, about the values of some of these properties. Where available, the data was taken from the literature, but because properties were required over a wide temperature range (approximately 4 to 1000 K) and because some of the materials don't exist in the same form outside of the composite wire, this was not possible in all cases. Material testing was not feasible either for the same reasons. For the main uncertainties, analyses were run using a range of estimated values that were based on the available data. Some of the uncertainties were found to have no significant effect on the stress-strain behaviour of

the wire as a whole and so were of little importance in modelling that behaviour. For other uncertainties, "best match" values were obtained by analysing the F. E. generated stress-strain curves and comparing them with the experimental results. It was possible to do this because of the unique effect that these uncertainties had on the stress-strain curves. For example, the work hardening rate of the bronze was the only uncertainty investigated that had any significant effect on the width of the hysteresis loops. For three of the uncertainties investigated, it was not possible to obtain "best match" values independently because they all had similar effects on the stress-strain curve. For two of these, however, the level of uncertainty was relatively low and so best estimate values were used. These were the grain size and tin content of the bronze, which were used in the expressions to generate the stress-strain curves of the bronze. A "best match" value could then be obtained for the last remaining uncertainty: how much stress-relief occurs during the cool-down at the end of the heat-treatment process. By assigning values to the uncertain material properties in this way very good agreement was achieved between the F. E. and experimental stress-strain curves at room and 77 K. This provided some limited validation of the F. E. model, but could not be considered proper validation because of the way that some of the assumptions made in the model were optimised to provide the best possible match with experiment.

To provide further validation of the F. E. model, an experiment was devised to measure thermal residual stresses as well as material properties of different parts of the wire. The experiment involved etching away concentric layers of material from the outside of wire specimens by immersing them in nitric acid. The residual stresses in the wire redistribute to maintain equilibrium as material containing residual stresses is

etched away. This resulted in a change in length of the wire specimen that could be measured. Using the change in length measurements and by also measuring the stress-strain curves of the etched wires, it was possible to calculate the axial residual stresses in different radial zones, i.e. the concentric rings that were etched away and the remaining core. It was also possible to derive the stress-strain curves of the material in each radial zone. The analysis only considers axial stresses, however, and does not take transverse stresses into account. F. E. analysis was carried out to investigate the error, which was generally shown to be relatively small. This error was only of consequence for the calculations of residual stress and derived stress-strain curves. It had no bearing on using the measured data to validate the F. E. model. Using the F. E. model, the etching experiment was simulated to obtain predictions for the change in length and for the stress-strain curves of etched wires. Generally, the F. E. and experimental results were in agreement, but there were some significant differences. The main differences were in the change in length measurements. For only small amounts of material having been etched away (down to diameter 1.4 mm) there was good agreement. This indicated that the residual stress in the outer bronze layer of the wire as measured in the experiment and as predicted by the F. E. model was reasonably accurate. The results did not agree, however, for further reductions in diameter. This indicated that there are some deficiencies with the F. E. model. One deficiency that the results pointed to was in the way that stress-relief is modelled. The model allows for stress-relief in only a simplistic way: full stress-relief is allowed to take place above a certain temperature (577°C was the value used), but none below it. The results indicated, however, that some stress-relief occurs at room temperature, although stresses are not completely relieved. More sophisticated modelling would therefore be required to adequately model the stress-relief behaviour. The results for

the stress-strain behaviour of etched wires indicated that the constituent material properties used in the F. E. model were generally reasonably accurate. The exception was the material properties for the copper core and/or barrier, which were not of great importance because of their small effect on the overall mechanical properties due to the low strength of the copper and the low volume fraction of the barrier.

8.2 Recommendations for future work

This thesis has demonstrated that the mechanical properties of superconducting wire can be accurately modelled using the finite element method, there is however scope for further work in the areas highlighted below:

a) Apply the F. E. model to other wires with different diameters and internal structures. The results should be checked against experimental measurements and the model improved upon if necessary.

b) Extend the F. E. model to give stress-strain behaviour at 4 K. This will require determination of constituent material properties down to 4 K. In particular, the work hardening rate of bronze with low tin content and small grain size is not known with any certainty. Also, the low temperature elastic modulus of Nb_3Sn is not known with certainty and, moreover, the literature suggests it is non-linear with stress. The validity of the model should be checked with experimental measurements.

c) Endeavour to fill the gaps in the knowledge of the mechanical properties of the constituent materials. As well as the work hardening rate of bronze and the low temperature elastic modulus of Nb_3Sn mentioned above, the properties of the niobium and tantalum of the barrier are also uncertain. Another area of uncertainty was the validity of the kinematic hardening rule to describe the stress-strain behaviour when loading is not uni-directional.

d) Investigate the stress-relief that takes place as wires cool down from the heat-treatment temperature. Also, investigate if any stress-relief takes place after wires are etched down to smaller diameters. If necessary, modify the etching experimental method to take account of this and improve the F. E. model to handle stress-relief more realistically.

e) Investigate whether the twist of superconducting wires has any influence on the mechanical properties.

APPENDIX A

Ellingham Diagram

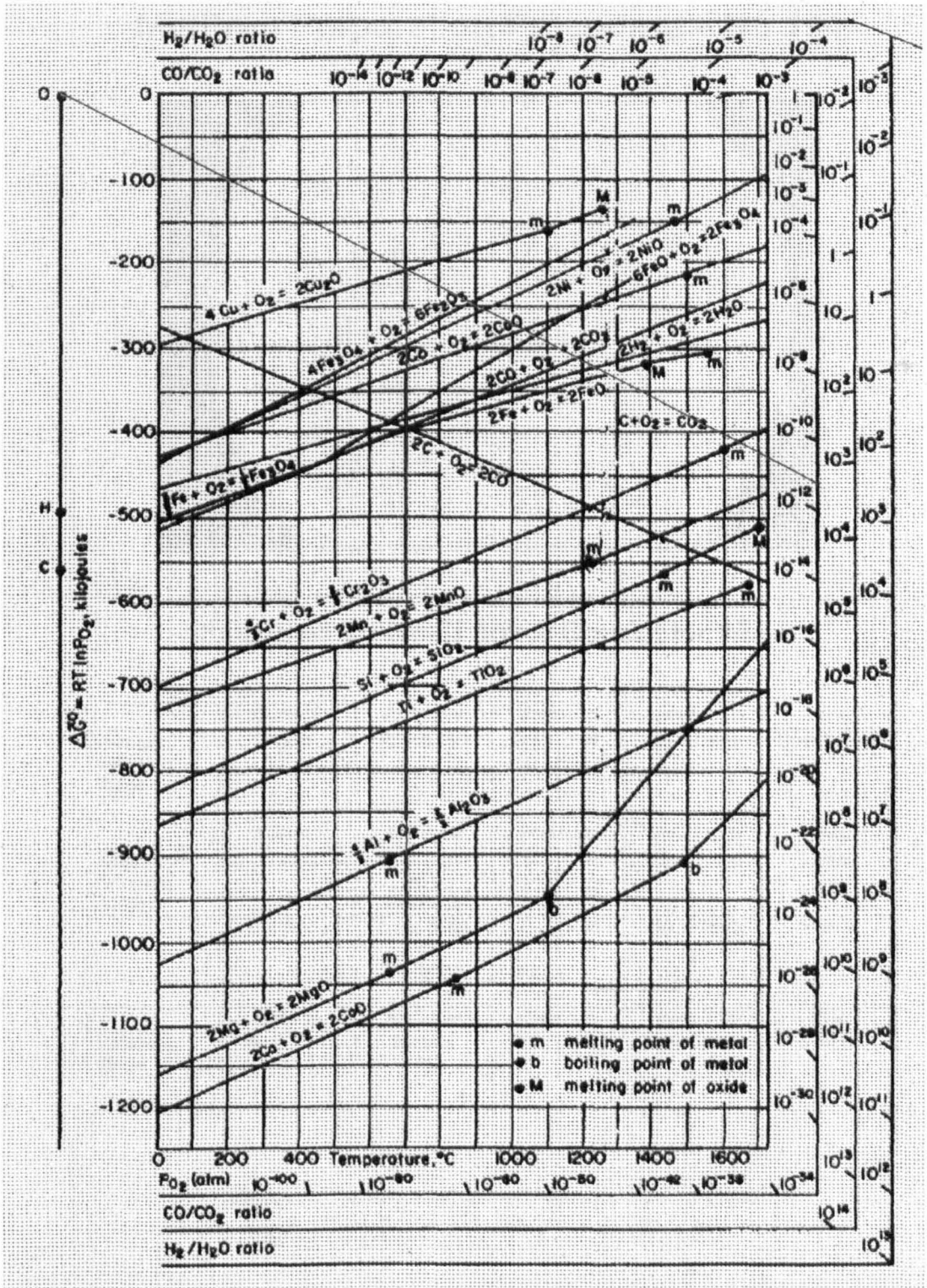

Figure 9–3. Ellingham diagram for some oxides; Richardson nomographic scales are included. (Adapted from D. R. Gaskell, *Introduction to Metallurgical Thermodynamics*, 2nd ed., Hemisphere Publishing, New York, 1981.)

APPENDIX B

MetPrep Preparation Procedure – No 194

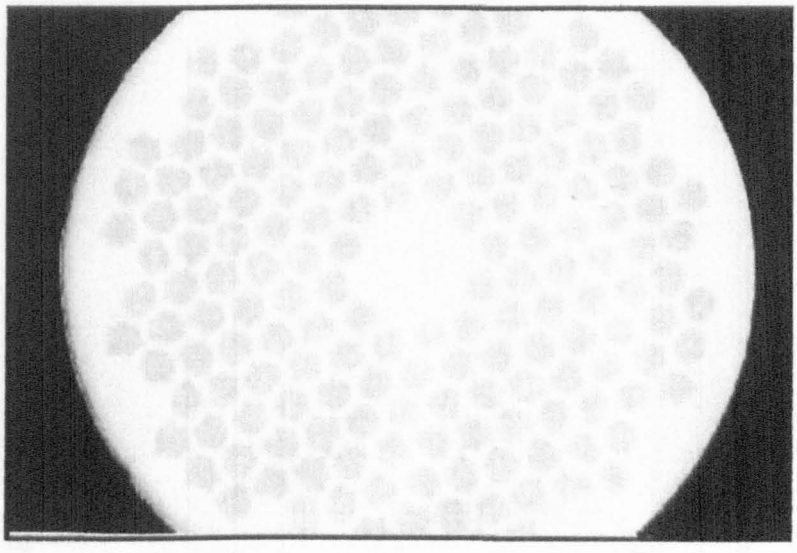

Multicored Cu-Nb-Ti Super Conductor Wires

	Surface	Abrasive	Pressure		Speed – Dir	Time
Primary Grinding Stage	Paper	P240g SiC	Psi	N	150 – Comp	Until Planar
			5	25		

	Surface	Abrasive	Pressure		Speed – Dir	Time
Additional Grinding Stages	Planocloth H	9 µm (WB) PCD Diamond	Psi	N	250 – Comp	5 mins
			5	25		
	Chrysalis	3 µm (WB) PCD Diamond	5	25	250 – Comp	4 mins

	Surface	Abrasive	Pressure		Speed – Dir	Time
Polishing Stage	Multicloth	0.06µm Silco	Psi	N	80 – Comp	3 mins
			3	15		

MetPrep Ltd, Curriers Close, Charter Avenue, Coventry. CV4 8AW
Tel: +44 (0) 24 7642 1222 Fax: +44 (0) 24 7642 1192
Website: www.metprep.co.uk Email: sales@metprep.co.uk

APPENDIX C

Engineering Drawings of Heat-treatment Apparatus

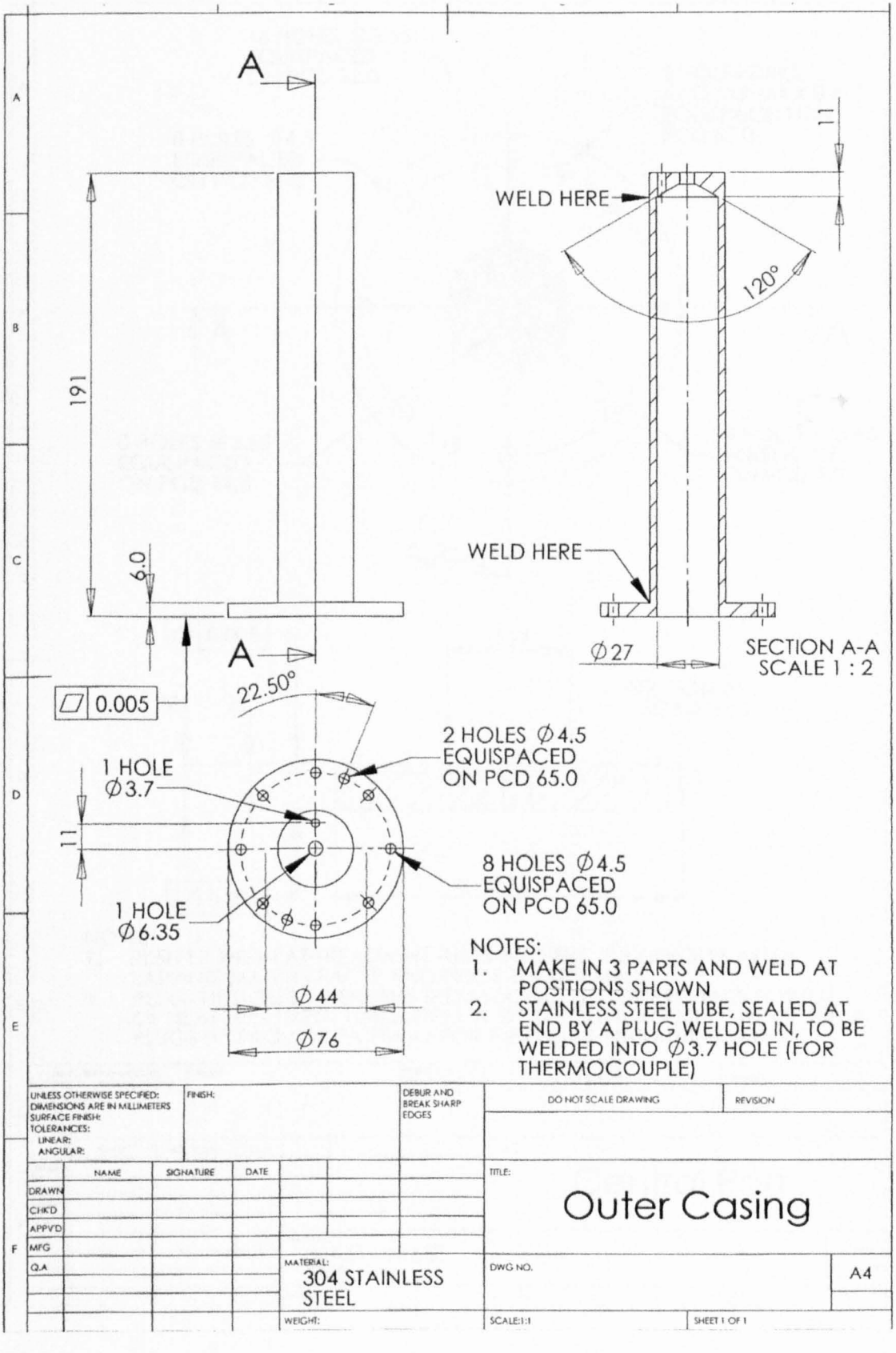

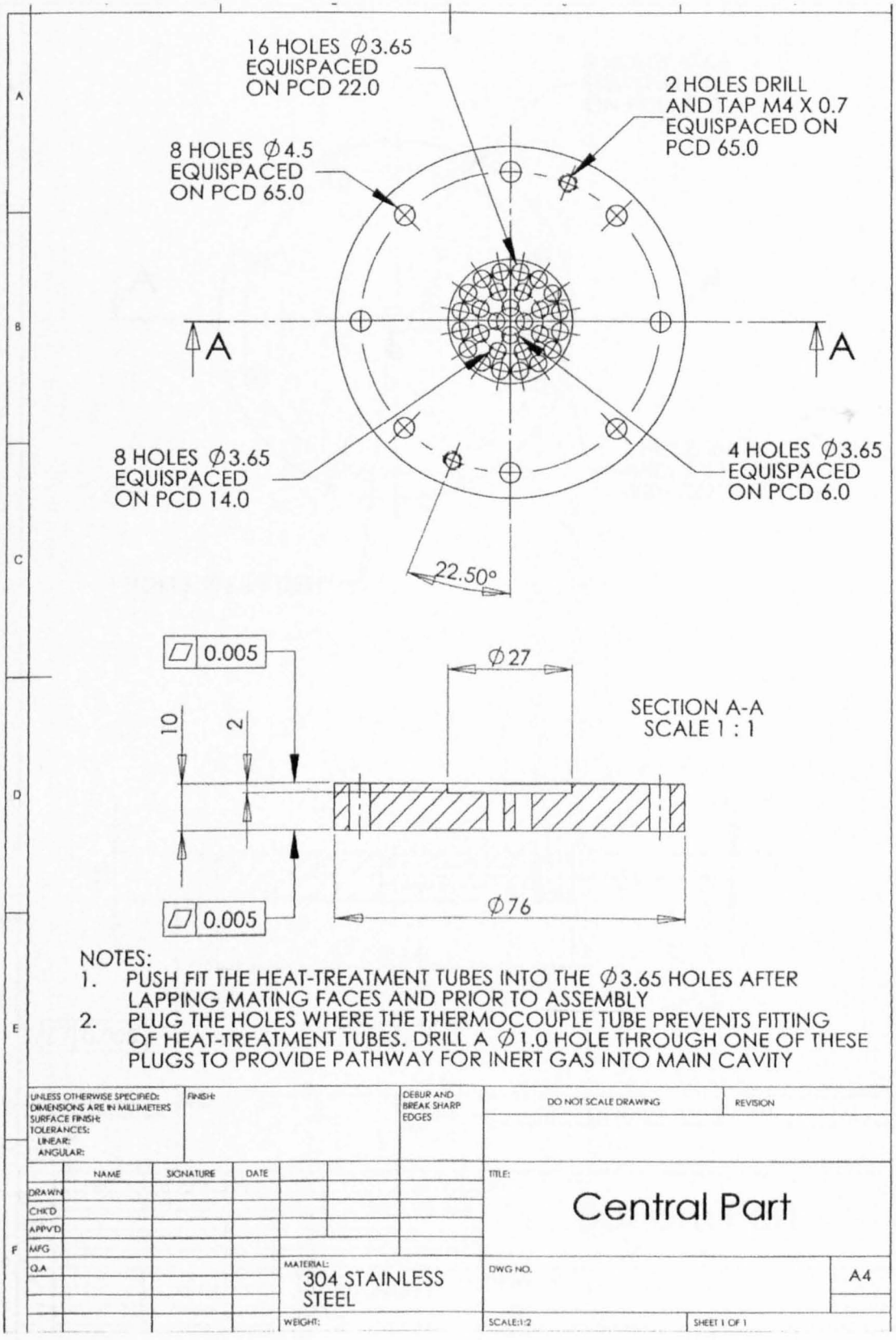
16 HOLES Ø3.65
EQUISPACED
ON PCD 22.0
2 HOLES DRILL
AND TAP M4 X 0.7
EQUISPACED ON
PCD 65.0
8 HOLES Ø4.5
EQUISPACED
ON PCD 65.0
A
A
8 HOLES Ø3.65
EQUISPACED
ON PCD 14.0
4 HOLES Ø3.65
EQUISPACED
ON PCD 6.0
22.50°
0.005
Ø27
10
2
SECTION A-A
SCALE 1 : 1
Ø76
0.005
NOTES:
1. PUSH FIT THE HEAT-TREATMENT TUBES INTO THE Ø3.65 HOLES AFTER LAPPING MATING FACES AND PRIOR TO ASSEMBLY
2. PLUG THE HOLES WHERE THE THERMOCOUPLE TUBE PREVENTS FITTING OF HEAT-TREATMENT TUBES. DRILL A Ø1.0 HOLE THROUGH ONE OF THESE PLUGS TO PROVIDE PATHWAY FOR INERT GAS INTO MAIN CAVITY
UNLESS OTHERWISE SPECIFIED:
DIMENSIONS ARE IN MILLIMETERS
SURFACE FINISH:
TOLERANCES:
LINEAR:
ANGULAR:
FINISH:
DEBUR AND BREAK SHARP EDGES
DO NOT SCALE DRAWING
REVISION
NAME
SIGNATURE
DATE
DRAWN
CHK'D
APP'VD
MFG
Q.A
TITLE:
Central Part
MATERIAL:
304 STAINLESS STEEL
DWG NO.
A4
WEIGHT:
SCALE:1:2
SHEET 1 OF 1

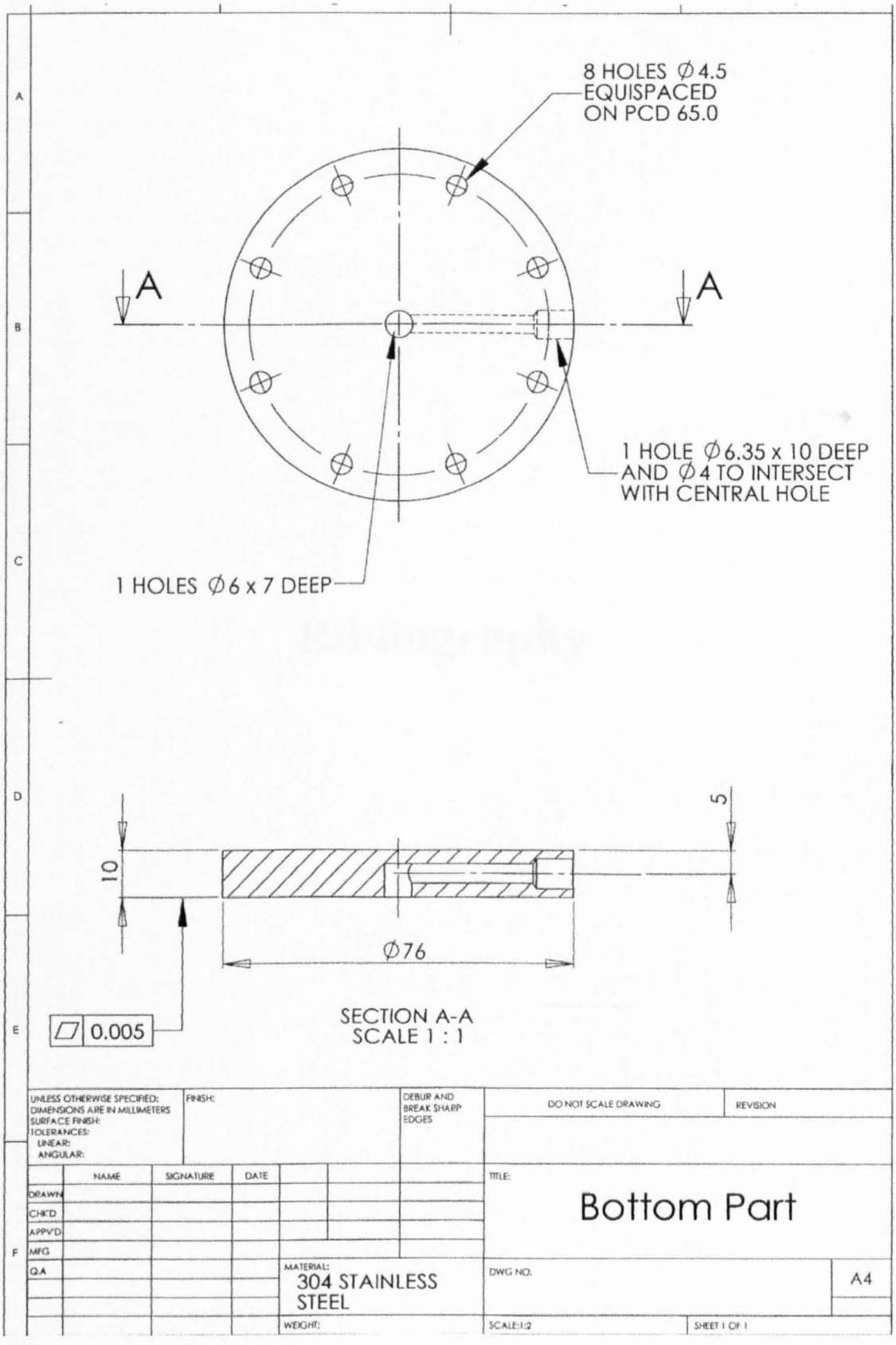
8 HOLES Ø4.5
EQUISPACED
ON PCD 65.0
A
A
1 HOLE Ø6.35 x 10 DEEP
AND Ø4 TO INTERSECT
WITH CENTRAL HOLE
1 HOLES Ø6 x 7 DEEP
10
5
Ø76
0.005
SECTION A-A
SCALE 1 : 1
UNLESS OTHERWISE SPECIFIED:
DIMENSIONS ARE IN MILLIMETERS
SURFACE FINISH:
TOLERANCES:
LINEAR:
ANGULAR:
FINISH:
DEBUR AND
BREAK SHARP
EDGES
DO NOT SCALE DRAWING
REVISION
NAME
SIGNATURE
DATE
DRAWN
CHK'D
APPV'D
MFG
Q.A
TITLE:
Bottom Part
MATERIAL:
304 STAINLESS
STEEL
DWG NO.
A4
WEIGHT:
SCALE:1:2
SHEET 1 OF 1

Bibliography

References

Ahoranta, M., Lehtonen, J., Tarhasaari, T. and Weiss, K. (2008). "Modelling of local strain and stress relaxation in bronze processed Nb3sSn wires", *Superconductor Science and Technology*, 21(2), 025005.

Alsharo'a, M., Barzi, E., Bossert, M., Johnson, R. P., Turrioni, D., Yamada, R. and Zlobin, A. V. (2008). "Optimization of brittle superconducting Nb3Sn strand designs", *IEEE Transactions on Applied Superconductivity*, 18(2), 1496-1499.

Andreev, N., Barzi, E., Chichili, D. R., Mattafirri, S. and Zlobin, A. V. (2002). "Volume expansion of Nb-Sn strands and cables during heat treatment", *CP614, Advances in Cryogenic Engineering: Proceedings of the International Cryogenic Materials Conference 2001 – ICMC*, 48, 941-948.

Ansys (1998), Structural Analysis Guide (Release 5.5), SAS IP Inc.

Ashby, M. F. and Jones, D. R. H. (1980). "Engineering materials: an introduction to their properties and applications", Pergamon International Library, ISBN 0-08-026138-8.

Awaji, S., Oguro, H., Nishijima, G., Watanabe, K., Harjo, S., Kamiyama, T. and Katagiri, K. (2005). "Prebending effects in bronze route Nb3Sn wires". *Superconductor Science and Technology*, 18(12) S313-S318.

Awaji, S., Oguro, H., Nishijima, G., Badica, P., Watanabe, K., Harjo, S., Kamiyama, T. and Katagiri, K. (2006). "Neutron diffraction study on prebending effects for bronze route Nb3Sn wires without reinforcement", *IEEE Transactions on Applied Superconductivity*, 16(2), 1228 - 1231.

Awaji, S., Watanabe, K. and Kazumune, K. (2003). "Improvement of mechanical and superconducting properties in CuNb/$(Nb,Ti)_3Ti$ wires by applying bending strain at room temperature", *Superconductor Science and Technology*, 16, 733-738.

Balankin, A. (1988). "Elastic properties of superconductors with A15-type structure", *Soviet Journal of Low Temperature Physics*, 14(4), 187-191.

Boso, D. P., Lefik, M. and Schrefler, B. A. (2005). "Multiscale analysis of the influence of the triplet helicoidal geometry on the strain state of a Nb3Sn based strand for ITER coils", *Cryogenics*, 45(9), 589-605.

Boso, D. P., Lefik, M. and Schrefler, B. A. (2006). "Homogenisation methods for the thermo-mechanical analysis of Nb3Sn strand", *Cryogenics*, 46(6), 420-431.

Bray, S. and Ekin, J. (1997). "Tensile measurements of the modulus of elasticity of Nb_3Sn at room temperature and 4 K", *IEEE Transactions on Applied Superconductivity*, 7(2), 1451-1454.

Bruzek, C. E., Sulten, P., Sirot, E., Kohler, C., Mocaer, P., Peltier, F. and Grunblatt, G. (1997). "Effect of heat treatments on superconducting properties of Nb_3Sn strands developed at GEC ALSTHOM", *IEEE Transactions On Applied Superconductivity*, 7(2), 1041-1044.

Bussière, J. F., Welch, D. O. and Suenaga, M. (1980). "Young's modulus of polycrystalline Nb_3Sn between 4.2 and 300 K", *Journal of Applied Physics*, 51(2), 1024-1030.

Bussière, J., Faucher, B., Snead, C. Jr. and Welch, D. (1981). "Internal friction and elastic softening in polycrystalline Nb_3Sn", *Physical Review B*, 24(7), 4087-4090.

Bussière, J., Faucher, B., Snead, C. Jr. and Suenaga, M. (1982). "Effects of ternary additions on Young's modulus and the martensitic transformation of Nb_3Sn", *Advances in Cryogenic Engineering*, 28, 453-460.

Cave, J. R. and Weir, C. A. F. (1983). "Cracking and layer growth in Nb3Sn bronze route material", *IEEE Transactions on Magnetics*, 19(3), 1120-1123.

Choy, K. L., Durodola, J. F., Derby, B. and Ruiz, C. (1995). "Effect of TiB2, TiC and TiN protective coatings on tensile strength and fracture behaviour of SiC monofilament fibres", *Composites*, 26(8), 531-539

Cogan, S. F., Holmes, D. S., Puffer, I. M., Eagar, T. W. and Rose, R. M. (1979). "On the micromechanics of multifilamentary superconducting composites", *IEEE Transactions on Magnetics*, 15(1), 684-686.

Cogan, S. F., Klein, J. D., Kwon, S., Landis, H. and Rose, R. M. (1983). "On the mechanical properties of Sn-core processed Nb_3Sn filamentary composites", *IEEE Transactions on Magn*etics, 19(3), 917-919.

Easton, D. S. and Kroeger, D. M. (1979). "Kirkendall voids - a detriment to Nb3Sn superconductors", *IEEE Transactions on Magnetics*, 15(1), 178-181.

Easton, D. S., Kroeger, D. M, Specking, W. and Koch, C. C. (1980). "A prediction of the stress state in Nb_3Sn superconducting composites", *Journal of Applied Physics*, 51(5), 2748-2757.

Ekin, J. (1976). "Effect of stress on the critical current of Nb_3Sn multifilamentary composite wire", *Applied Physics Letters*, 29(3), 216-219.

Ekin, J. (1979). "Strain dependence of the critical current and critical field in multifilamentary Nb_3Sn composites", *IEEE Transactions on Magnetics*, 15(1), 197-200.

Ekin, J. (1980). "Strain scaling law for flux pinning in practical superconductors. Part 1: Basic relationship and application to Nb_3Sn conductors", *Cryogenics*, 20(12), 611-624.

Ekin, J. (1987). "Effect of transverse compressive stress on the critical current and upper critical field of Nb_3Sn", *Journal of Applied Physics*, 62(12), 4829-4834.

Ekin, J. W., Bray, S. L. and Bahn, W. L. (1991). "Effect of transverse stress on the critical current of bronze process and internal-tin Nb_3Sn", *Journal of Applied Physics*, 69(8), 4436-4438.

Ekin, J. W. (1995). "Stress/strain effects on critical current", *Cryogenics*, 35, VAMAS Supplement S25-S28.

Ekin, J. W., Cheggour, N., Abrecht, M., Clickner, C., Field, M., Hong, S., Parrell, J. and Zhang, Y. (2005). "Compressive pre-strain in high-niobium-fraction Nb3Sn superconductors", *Ieee Transactions on Applied Superconductivity*, 15(2), 3560-3563.

Ellingham, H. J. T. (1944). "Reducibility of oxides and sulphides in metallurgical processes", Journal of the Society of Chemical Industry (London), 63(5), 125-133

Entwistle, K. M. and Myerscough, P. (1983). "The measurement of the axial internal stress in steel wire", *International Journal of Mechanical Sciences*, 25(11), 823-831.

Farinon, S., Boutboul, T., Devred, A., Fabbricatore, P., Leroy, D. and Oberli, L. (2007). "Finite element model to study the deformations of Nb3Sn wires for the next european dipole (NED)", *IEEE Transactions on Applied Superconductivity*, 17(2), 1136 – 1139.

Fillunger, H., Foitl, M., Hense, K., Kajgana, I., Kasztler, A., Kirchmayr, H., Lackner, R., Leoni, J., Maix, R., Matthias, T. and Fidler, J. (2002). "Influence of the annealing time of internal tin Nb_3Sn strands on the critical current and the magnetization losses", *Physica C*, vol. 372-376, 1758-1761.

Flükiger, R., Schauer, W., Specking, W., Schmidt, B. and Springer, E. (1981). "Low temperature phase transformation in Nb_3Sn multifilamentary wires and the strain dependence of their critical current density", *IEEE Transactions on Magnetics*, 17(5), 2285-2288.

Flükiger, R. (1982). "Martensitic transformations and their effects on superconductivity in A15 superconductors", *Journal de Physique*, Colloque C4, Supplément au n° 12, Tome 43, 357-362.

Flükiger, R., Uglietti, D., Abächerli, V. and Seeber, B. (2005). "Asymmetric behaviour of $Jc(\varepsilon)$ in Nb3Sn wires and correlation with the stress induced elastic tetragonal distortion", *Superconductor Science and Technology*, 18, S416-S423.

Goddard, R., Chen, J, McClellan, E. and Han, K. (2005). "Microanalysis of Nb3Sn Superconducting Wire Using the Environmental Scanning Electron Microscope (ESEM)", *Microscopy and Microanalysis*, 11(Supplement 2), 424-425.

Goldacker, W. and Flükiger, R. (1984). "Direct observation of crystallographical changes at 10 K caused by the application of varying stresses to Nb_3Sn wires", *Journal de Physique*, Colloque C1, Supplément au n° 1, Tome 45, 387-390.

Harvey, D. A., Fellows, N. A., Durodola, J. F., Vázquez-Navarro, M. D. and Twin, A. (2005). "Tensile testing of superconducting wires", *Revista Mexicana de Física*, 51(Suplemento 1), 51-55

Harvey, D. A., Fellows, N. A., Durodola, J. F., Twin, A. (2005). "Influence of the heat-treatment process on the mechanical properties and dimensions of multi-filamentary composite Nb_3Sn superconducting wires", *Advances in experimental Mechanics IV: Applied Mechanics and Materials Vols. 3 - 4*, 141-148

Harvey, D. A., Fellows, N. A., Durodola, J. F. and Twin, A. (2006). "The influence of the reaction heat-treatment process on the mechanical properties of multi-

filamentary composite Nb_3Sn superconducting wires at 77 and 300 K", *Superconductor Science and Technology*, 19(1), 79-84

Hense, K., Fillunger, H., Kajgana, I., Kirchmayr, H., Lackner, R., Maix, R. K. and Muller, M. (2003). "Optimisation of the reaction heat treatment cycle of internal tin and bronze Nb_3Sn strands for ITER", *Fusion Engineering And Design*, 66(8), 1103-1107.

Hoard, R. W., Scanlan, R. M. and Hirzel, D. G. (1980). "MAXIMSUPER: A computer program to assist in the design of multifilamentary superconducting filaments", *Advances in Cryogenic Engineering*, 26, 578-588.

Hojo, M., Matsuoka, T., Nakamura, M., Tanaka, M., Adachi, T., Ochiai, S. and Miyashita, K. (2004). "Investigation of mechanical behavior of copper in Nb3Sn superconducting composite wire", *Physica C*, 412-414(2), 1261-1266.

Hojo, M., Matsuoka, T., Hashimoto, M., Tanaka, M., Sugano, M., Ochiai, S. and Miyashita, K. (2006). "Direct measurement of elastic modulus of Nb3Sn using extracted filaments from superconducting composite wire and resin impregnation method", *Physica C*, 445-448, 814-818.

Iwaki, G., Kimura, M., Moriai, H., Asano, K., Watanabe, K. and Motokawa, M. (2000). "High strength $(Nb,Ti)_3Sn$ superconducting wire reinforced by Nb/Cu composite", *Advances in Cryogenic Engineering*, 46(B), 981-988.

Iwaki, G., Sato, J., Inaba, S. and Kikuchi, K. (2002). "Development of bronze-processed Nb_3Sn superconducting wires for high field magnets", *IEEE Transactions on Applied Superconductivity*, 12(1), 1045-1048.

Jewell, M. C., Lee, P. J. and Larbalestier, D. C. (2003). "The influence of Nb_3Sn strand geometry on filament breakage under bend strain as revealed by metallography", *Superconductor Science and Technology*, 16(9), 1005-1011.

Katagiri, K., Watanabe, K., Kuroda, T., Kasaba, K., Noto, K., Okada, T. and Kohno, O. (1996). "Axial tensile strain / transverse compressive stress characteristics in high strength Nb_3Sn superconducting wires", *Science Reports of the Research Institutes Tohoku University Series A*, 42(2), 381-388.

Katagiri, K., Kasaba, K., Hojo, M., Osamura, K., Sugano, M., Kimura, A. and Ogata, T. (2001). "Tensile testing methods of Cu/Nb_3Sn superconducting wires at room temperature", *Physica C*, 357, 1302-1305.

Kondoh, J., Tateishi, H., Umeda, M., Arai, K., Agatsuma, K., Gotoh, K. and Saitoh, T. (2001). "Mechanical properties of a niobium-tin superconductor reinforced by tantalum cores", *IEEE Transactions on Applied Superconductivity*, 11(1), 3635-3638.

Kumakura, H., Tachikawa, K., Snead, C. Jr. and Suenaga, M. (1985). "Studies on Young's modulus and internal friction in alloyed Nb_3Sn : effects of alloying additions on the martensitic transformation and superconducting properties", *Journal of the Japan Institute of Metals*, 49(9), 792-800.

Lanteigne, J., Roberge, R., LeHuy, H., Fihey, J. L. and Foner, S. (1981). "Origin of the improved resistance to strain of in situ Nb3Sn multifilamentary composites", *IEEE Transactions on Magnetics*, 17(1), 265-269.

Larbalestier, D., Madsen, P., Lee, J., Wilson, M. and Charlesworth, J. (1975). "Multifilamentary niobium tin magnet conductors," *IEEE Transactions on Magnetics*, 11(2), 247-250.

Larbalestier, D. C., Magraw J. E. and Wilson M. N. (1977). "The influence of tensile stress on the critical current of filamentary Nb3Sn." *IEEE Transactions on Magnetics*, 13(1), 462-465.

LeHuy, H., Bussière, J. and Berry, B. (1983). "Effect of interstitial hydrogen on Young's modulus and martensitic transformation of Nb_3Sn", *IEEE Transactions on Magnetics*, 19(3), 893-896.

Luhman, T., Suenaga, M., Welch, D. O. (1979). "Degradation mechanism of Nb3Sn composite wires under tensile strain at 4.2K." *IEEE Transactions on Magnetics*, 15(1), 699-702.

Markiewicz, W. D. and Goddard, R. E. (2002). "Bronze tin content and grain size in Nb_3Sn composite superconductors", *IEEE Transactions on Applied Superconductivity*, 12(1), 1063-1066.

Markiewicz, W. D. (2004). "Invariant formulation of the strain dependence of the critical temperature Tc of Nb3Sn in a three term approximation", *Cryogenics*, 44(12), 895-908.

Markiewicz, W. D. (2004). "Elastic stiffness model for the critical temperature T-c of Nb3Sn including strain dependence", *Cryogenics*, 44(11), 767-782.

McDonald, W. K., Curtis, C. W., Scanlon, R. M., Larbalestier, D. C., Marken, K., and Smather, D. B. (1983). "Manufacture and evaluation of Nb3Sn conductors

fabricated by the MJR method", *IEEE Transactions on Magnetics*, 19(3), 1124-1127.

McDougall, I. L. (1975). "The mechanical properties of filamentary niobium tin composites", *IEEE Transactions on Magnetics*, 11(5), 1467-1469.

Mitchell, N. (2005). "Modeling of the effect of Nb3Sn strand composition on thermal strains and superconducting performance", *IEEE Transactions on Applied Superconductivity*, 15(2), 3572-3576.

Mitchell, N. (2005). "Finite element simulations of elasto-plastic processes in Nb3Sn strands", *Cryogenics*, 45(7), 501-515.

Murase, S., Okamoto, H., Wakasa, T., Tsukii, T. and Shimamoto, S. (2003). "Three-directional analysis of thermally-induced strains for Nb_3Sn and oxide composite superconductors". *IEEE Transactions on Applied Superconductivity*, 13(2), 3386-3389.

Murase, S. and Okamoto, H. (2004). "FEM analysis of three directional strain states under applied tensile stress for various composite superconductors." *IEEE Transactions on Applied Superconductivity*, 14(2), 1130-1133.

Naus, M., Lee, P. and Larbalestier, D. (2000). "The interdiffusion of Cu and Sn in internal Nb_3Sn superconductors", *IEEE Transactions on Applied Superconductivity*, 10(1), 983-987.

Nishijima, G., Watanabe, K., Araya, T., Katagiri, K., Kasaba, K and Miyoshi, K. (2005). "Effect of transverse compressive stress on internal reinforced Nb3Sn superconducting wires and coils", *Cryogenics*, 45, 653-658.

Nyilas, A., Osamura, K. and Sugano, M. (2003). "Mechanical and physical properties of Bi-2223 and Nb_3Sn superconducting materials between 300 K and 7 K", *Superconductor Science and Technology*, 16, 1036-1042.

Nyilas, A. (2005). "Strain sensing systems tailored for tensile measurement of fragile wires", *MEM'05: the 3rd international workshop on mechano-electromagnetic properties of composite superconductors*, Kyoto, Japan, Institute of Physics.

Ochiai, S., Osamura, K. and Uehara, T. (1986). "Room-temperature tensile behaviour of bronze-processed multi-filamentary Nb_3Sn superconducting materials", *Journal of Materials Science*, 21, 1027-1036.

Ochiai, S., Uehara, T., Hojo, M. and Osamura, K. (1986). "Tensile strength and flux pinning force of superconducting Nb_3Sn compound as a function of grain size", *Journal of Materials Science*, 21, 1020-1026.

Ochiai, S., Osamura, K. and Uehara, T. (1987). "Grain size and its relation to tensile strength of Nb_3Sn compound in bronze-processed multi-filamentary superconducting materials", *Journal of Materials Science*, 22, 2163-2168.

Ochiai, S., Osamura, K. and Ryoji, M. (1988). "Tensile strength of bronze-processed Nb_3Sn compound with titanium addition", *Transactions of the Iron and Steel Institute of Japan*, 28(11), 973-977.

Ochiai, S., Osamura, K. and Maekawa, M. (1991). "Comparison of mechanical and superconducting properties of titanium-added Nb_3Sn composite wire with those of non-added ones", *Superconductor Science and Technology*, 4, 262-269.

Ochiai, S. and Osamura, K. (1992). "Influence of cyclic loading at room-temperature on the critical current at 4.2 K of Nb_3Sn superconducting composite wire", *Cryogenics*, 32(6), 584-590.

Ochiai, S., Osamura, K. and Watanabe, K. (1993). "Estimation of strength distribution of Nb_3Sn in multifilamentary composite wire from change in superconducting current due to preloading", *Journal of Applied Physics*, 74(1), 440-445.

Ochiai, S., Nishino, S., Hojo, M., Osamura, K. and Watanabe, K. (1994). "Nb_3Sn tensile strength and its distribution estimated from change in superconducting critical current of preloaded multifilamentary composite wire", *Cryogenics*, 35(1), 55-60.

Ochiai, S., Nishino, S., Hojo, M. and Watanabe, K. (1995). "Relation of the strength distribution of Nb3Sn to the critical current of a pre-stressed multifilamentary composite superconductor", *Superconductor Science and Technology*, 8(12), 863-869.

Osamura, K., Nyilas, A., Thoener, M., Seeber, B., Flükiger, R., Ilyin, Y., Nijhuis, A., Ekin, J., Clickner, C., Walsh, R. P., Toplosky, V., Shin, H., Katagiri, K., Ochiai, S., Hojo, M., Kubo, Y. and Miyashita, K. (2008). "International round robin test for mechanical properties of Nb3Sn superconductive wires at room temperature", *Superconductor Science and Technology*, 21(4), 045006.

Peng, X., Sumption, M. D. and Collings, E. W. (2005). "Finite element analysis of drawing of multifilamentary wires", *IEEE Transactions on Applied Superconductivity*, 15(2), 3426-3429.

Poirier, M., Plamondon, R., Cheeke, J. and Bussière, J. (1984). "Elastic constants of polycrystalline Nb_3Sn between 4.2 and 300 K", *Journal of Applied Physics*, 55(9), 3327-3332.

Poirier, M., Laroche, F. and Martin, M. (1985). "Elastic behavior of polycrystalline Nb_3Sn at low temperatures", *Applied Physics Letters*, 47(2), 92-94.

Roberge, R., LeHuy, H. and Foner, S. (1985). "Martensitic phase transformation in Nb_3Sn – X-ray observations", *IEEE Transactions on Magnetics*, 21(2), 811-814.

Ross, C. T. F. (1987). "Advanced Applied Stress Analysis", Ellis Horwood Ltd., ISBN 0130161632.

Rupp, G. (1979). "Stress induced normal-superconducting transition in multifilamentary Nb3Sn conductors." *IEEE Transactions on Magnetics*, 15(1), 189-192.

Rupp, G. (1981). "Self-healing effect in strained multifilamentary Nb_3Sn conductors", *Cryogenics*, 21(10), 619-621.

Sakai, S., Osamura, K., Hojo, M., Ogata, T. and Shimada, M. (1996). "Standardization of the method for the room temperature tensile test of Cu/Nb-Ti composite superconductors", *Proceedings of the 16th ICEC/ICMC*, 1791-1794.

Sakamoto, H., Endoh, S., Nagasu, Y., Wada, K., Kimura, A., Meguro, S., Awaji, S., Watanabe, K. and Motokawa, M. (2002). "$(Nb,Ti)_3Sn$ superconducting wire with CuNb reinforcing stabilizer", *IEEE Transactions on Applied Superconductivity*, 12(1), 1067-1070.

Scanlan, R. M., Fietz, W. A. and Koch, E. F. (1975). "Flux pinning centers in superconducting Nb_3Sn", *Journal of Applied Physics*, 46(5), 2244-2249.

Schauer, W. and Schelb, W. (1981). "Improvement of Nb3sn High-Field Critical Current by a 2-Stage Reaction", *IEEE Transactions on Magnetics*, 17(1), 374-377.

Schelb, W. (1981). "Electron-microscopic examination of multifilamentary bronze-processed Nb3Sn", *Journal of Materials Science*, 16(9), 2575-2582.

Simon, N. J., Drexler, E. S. and Reed R. P. (1992). "Properties of copper and copper alloys at cryogenic temperatures", NIST Monograph 177.

Snead, C. Jr., Kumakura, H. and Suenaga, M. (1983). "Effect of disorder on the martensitic phase transformation in Nb_3Sn", *Applied Physics Letters*, 43(3), 311-313.

Suenaga, M., Sampson, W. and Luhman, T. (1981). "Fabrication techniques and properties of multifilamentary Nb3Sn conductors", *IEEE Transactions on Magnetics*, 17(1), 646-653.

Taillard, R., Verwaerde, C., Bruzek, C. E. and Sulten, P. (1997). "Heat treatments, microstructure and properties of internal-tin Nb_3Sn", *IEEE Transactions on Applied Superconductivity*, 7(2), 1504-1507.

Tan, K. S., Hopkins, S. C., Glowacki, B. A., Majoros, M. and Astill, D. (2004). "In situ resistance measurements of bronze process Nb-Sn-Cu-Ta multifilamentary composite conductors during reactive diffusion", *Superconductor Science & Technology* 17(4): 663-670.

Tang, X. D., Chan, D. Q., Li, M. S. and Zhu, D. S. (1981). "The effect of heat-treatment on practical multifilamentary Nb3sn conductor", *IEEE Transactions on Magnetics*, 17(1), 674-676.

van den Eijnden, N. C., Nijhuis, A., Ilyin, Y., Wessel, W. A. J. and ten Kate, H. H. J. (2005). "Axial tensile stress–strain characterization of ITER model coil type Nb_3Sn strands in TARSIS", *Superconuctor Science and Technology*, 18, 1523-1532.

Vorobiova, A., Shikov, A., Nikulin, A., Silaev, A., Golikov, I., Davudov, I. and Izmailova, T. (1996). "Investigation on mechanical properties of Nb3Sn multifilamentary wires", *IEEE Transactions on Magnetics* 32(4), 2913-2916.

West, A. W. and Rawlings, R. D. "A transmission electron microscopy investigation of filamentary superconducting composites", *Journal of Materials Science*, 12, 1862-1868.

Watanabe, K., Katagiri, K., Noto, K., Awaji, S., Goto, K., Sadakata, N., Saito, T. and Kohno, O. (1995). "Residual strain estimation in multifilamentary Nb3Sn wires with CuNb reinforcement", *IEEE Transactions on Applied Superconductivity*, 5(2), 1905-1908.

Wright, R. and Dixon, G. (1988). "The elastic modulus and flow stress of Nb_3Sn at

elevated temperatures", *Metallurgical Transactions A*, 19A, 1127-1129.

Zanino, R., Boso, D. P., Lefik, M., Ribani, P. L., Savoldi Richard, L. and Schrefler, B. A. (2008). "Analysis of bending effects on performance degradation of ITER-relevant Nb3Sn strand using the THELMA code", *IEEE Transactions on Applied Superconductivity*, 18(2), 1067-1071.

Articles published in the course of the research

(i) Harvey, D. A., Fellows, N. A., Durodola, J. F., Vázquez-Navarro, M. D. and Twin, A. (2005). "Tensile testing of superconducting wires", *Revista Mexicana de Física*, 51(Suplemento 1), 51-55

(ii) Harvey, D. A., Fellows, N. A., Durodola, J. F., Twin, A. (2005). "Influence of the heat-treatment process on the mechanical properties and dimensions of multi-filamentary composite Nb_3Sn superconducting wires", *Advances in experimental Mechanics IV: Applied Mechanics and Materials Vols. 3 - 4*, 141-148

(iii) Harvey, D. A., Fellows, N. A., Durodola, J. F. and Twin, A. (2006). "The influence of the reaction heat-treatment process on the mechanical properties of multi-filamentary composite Nb_3Sn superconducting wires at 77 and 300 K", *Superconductor Science and Technology*, 19(1), 79-84

PAGES NOT SCANNED AT THE REQUEST OF THE UNIVERSITY

SEE ORIGINAL COPY OF THE THESIS FOR THIS MATERIAL